LOW ALTITUDE RADAR WAVE PROPAGATION MODELLING

A THESIS SUBMITTED TO
THE GRADUATE SCHOOL OF NATURAL AND APPLIED SCIENCES
OF
MIDDLE EAST TECHNICAL UNIVERSITY

BY

ORHAN ŞENGÜL

IN PARTIAL FULFILLMENT OF THE REQUIREMENTS FOR THE DEGREE
OF
DOCTOR OF PHILOSOPHY
IN
ELECTRICAL AND ELECTRONICS ENGINEERING

MAY 2007

Approval of the Graduate School of Natural and Applied Sciences

Prof. Dr. Canan ÖZGEN
Director

I certify that this thesis satisfies all the requirements as a thesis for the degree of Doctor of Philosophy.

Prof. Dr. İsmet ERKMEN
Head of Department

This is to certify that we have read this thesis and that in our opinion it is fully adequate, in scope and quality, as a thesis for the degree of Doctor of Philosophy.

Assoc. Prof.Dr. Sencer KOÇ
Co-Supervisor

Prof. Dr. Altunkan HIZAL
Supervisor

Examining Committee Members (first name belongs to the chairperson of the jury and the second name belongs to supervisor)

Prof. Dr. Fatih CANATAN	(METU,EE)	
Prof. Dr. Altunkan HIZAL	(METU,EE)	
Prof. Dr. Gülbin Dural	(METU,EE)	
Prof. Dr. Erdem YAZGAN	(Hacettepe Üniv.,EE)	
Assoc.Prof. Dr. S. Sencer KOÇ	(METU,EE)	

I hereby declare that all information in this document has been obtained and presented in accordance with academic rules and ethical conduct. I also declare that, as required by these rules and conduct, I have fully cited and referenced all material and results that are not original to this work.

Name, Last name : ORHAN ŞENGÜL

Signature :

ABSTRACT

LOW ALTITUDE RADAR WAVE PROPAGATION MODELLING

Şengül, Orhan
Ph.D., Department of Electrical and Electronics Engineering
Supervisor : Prof.. Dr. Altunkan HIZAL
Co-Supervisor : Assoc. Dr. S. Sencer KOÇ

May 2007, 88 pages

In this PhD thesis, propagation aspects of low altitude radar performance have been modeled using geometrical optics. Both the path propagation factor and the radar clutter have been modeled. Such models already exist at various complexity levels, such as round earth specular reflection combined with knife edge hill diffraction [SEKE:IEEE,Ap-34,No:8,1980] and round earth and slant plateau reflection combined with hill diffraction [RADCAL: 1988-2000,EE,METU]. In the proposed model we have considered an extension to RADCAL's model to include convex and concave slant plateaus between hills and depressions (troughs). This propagation model uses a reflection model based on the Geometrical Theory of Reflection for the convex and concave surfaces. Also, back scattering from surface (clutter) is formulated for the new model of the terrain profile. The effects of the features of the terrain profile on the path propagation factor have been investigated. A real terrain data have been smoothed on the basis of the above study. In order to verify the formulation, the Divergence and Convergence Factors associated with the convex and concave plateaus, respectively are inserted into the RADCAL program. The chosen terrains have convex or concave plateaus in the model. The output of the RADCAL is compared with measured values and other propagation algorithms such as Forward-Backward Spectrally Accelerated (FBSA) [FBSA:IEEE Vol.53, No:9,2005] and Parabolic Equation Method [TPEM:IEEE Vol.42,No:1,1994]. Moreover, as the RADCAL Propagation model is based on the ray optics, the results are also compared with another ray optics based propagation model. For this purpose the results of SEKE [Lincoln Lab.] propagation model are used. SEKE model has been used to compute path loss for different types of terrain as a function of receiving antenna height at a fixed distance between transmit and receive

antennas. For Beiseker W35 Terrain profile, the results of RADCAL, SEKE and measurements are compared. All results are in good agreement with those of RADCAL.

Keywords: Propagation modeling, convex and concave surface, path propagation factor, detectability factor, ground clutter

ÖZ

ALÇAK İRTİFA RADAR DALGASI YAYILIM MODELLEMESİ

Şengül, Orhan
Doktora, Elektrik ve Elektronik Mühendisliği Bölümü
Tez Yöneticisi : Prof. Dr. Altunkan HIZAL
Ortak-Tez Yöneticisi : Doç. Dr. S. Sencer KOÇ

Mayıs 2007, 88 sayfa

Bu doktora tezi çalışmasında, alçak irtifa radarların performanslarının geometrik optik esasları kullanılarak yayılım yönünden modellenmesi yapılmıştır. Hem yol yayılım faktörü hem de radar yansıması modellenmiştir. Bıçak sırtı tepe saçılmaları ile birleşmiş olan yuvarlanmış yüzeylerden yansımalar [SEKE: IEEE, AP-34, No:8,1980] ve bıçak sırtı tepe saçılmaları ile birleşmiş olan yuvarlanmış yüzeyler ve eğik platolardan olan yansımaların [RADCAL: 1988-2000,EE,METU] modellendiği farklı kompleks seviyelerde daha önceden yapılmış böyle modeller vardır. Önerilen bu modelde RADCAL modelinin uzantısı olarak dağların ve vadilerin arasındaki dışbükey ve içbükey eğik platoları göz önünde bulundurulmuştur. Bu yayılım modeli dışbükey ve içbükey yüzeyler için geometrik saçınım teorisini temel alan bir saçılma modelini (GTD) temel alan bir modeli kullanılmıştır. Buna ek olarak bu yeni arazi profile için araziden (yer yansıması) gelen geri saçınımlar hesaplanmıştır. Gerçek arazi profili özelliklerinin yol yayılım faktörü üzerindeki etkileri araştırılmıştır. Gerçek arazi verileri yukarıdaki çalışmalar temel alınarak düzleştirilmiştir. Formülleri doğrulamak için dışbükey ve içbükey yüzeylerden olan dağılma ve toplam faktörleri RADCAL programının içerisine eklenmiştir. Modelde seçilen araziler içbükey ve dışbükey platolar içermektedir. RADCAL sonuçları ölçülen değerler ve İleri Geri Hızlandırılmış Spektrallar (FBSA) [FBSA:IEEE Vol.53, Issue 9,2005] ve Parabolik Eşitlik Metodu [TPEM:IEEE Vol. 42, No:1,1994] gibi diğer yayılım algoritmaları ile karşılaştırılmıştır. Hatta RADCAL Yayılım Modeli ışın optiği teorisine dayandığı için onun sonuçları diğer ışın optik temelli yayılım modelleri ile de karşılaştırılmıştır. Bu amaçla SEKE (Lincoln Lab.) Yayılım Modeli kullanılmıştır. SEKE Modeli değişik arazi tipleri için gönderici ve alıcı arasında ki mesafe sabit kalırken alıcı antenin yüksekliğine bağlı olarak yol kaybını hesaplamaktadır. Beiseker W35 Arazi modeli için RADCAL, SEKE ve ölçülen değerler karşılaştırılmıştır. Tüm sonuçlar RADCAL'ın sonuçları ile iyi uyumludur.

Anahtar Kelimeler: Yayılım modellemesi, içbükey ve dışbükey yüzeyler, yol yayılım faktörü, tespit faktörü, yer karışıklığı, radar simülasyonu

To my wife and daughter

ACKNOWLEDGEMENTS

I would like to express my gratitude to Prof. Dr. Altunkan HIZAL for his precious supervision, helpful guidance and frank interest throughout all the phases of this study. This thesis bears valuable importance to me for the fact that I had found the chance to work with him.

I would also like to acknowledge all of my committee members, Prof. Dr. Erdem Yazgan, Prof. Dr.Fatih Canatan and Assoc. Prof. Dr. Sencer KOÇ for very constructive suggestion during the course of the thesis.

TABLE OF CONTENTS

LIST OF ABBREVIATIONS

RADAR:	**RAdio Detection And Ranging**	**MTI:**	**Moving Target ındıcator**
RCS:	**Radar Cros-Section**	**LOS:**	**Line Of Sight**
HF:	**High Frequency**	**VHF:**	**Very High Frequency**
GO:	**Geometrical optics**	**GTD:**	**Geometrical theory of diffraction**
D:	**Divergence Factor**	**CF:**	**Convergence Factor**
EM:	**Electromagnetic**	**SEKE:**	**Spherical Earth Knife Edge**
IE:	**Integral equation**	**UTD:**	**Uniform theory of diffraction**
TPEM:	**Terrain Parabolic Equation Model**	**PE:**	**Parabolic Equation**
FFTS:	**Fast Fourier Transform**	**PO:**	**Physical optics**
UHF:	**Ultra High Frequency**	a_e :	**Effective Earth Radius**
IEEE:	**Institute of Electrical and Electronics Engineers**	**FBSA:**	**Spectrally Accelerated Forward Backward**

LIST OF FIGURES

FIGURES:

LIST OF TABLES

TABLES:

CHAPTER 1

INTRODUCTION

1.1 Introduction

RADAR (RAdio Detection And Ranging) is an electromagnetic remote sensing instrument, which operates by transmitting a particular type of waveform and detecting the echo signal. Radar is used to extend the capability of one's sense for observing the outside environment and gathers information from objects, which are generally called "targets". The usual parameters extracted from a radar can be range of target, azimuth and elevation bearings of target and radial velocity of target. Signal processing of these parameters obtained from a target can lead to identification of a target. Moreover, amplitude and phase of the echo signal can be recorded for imaging of a target.

The major user of radar has been military, which is also contributor of the cost of almost all its development, although there are lots of civilian areas where a radar application is used. Typical examples are; Air Traffic Control, Aircraft Navigation, Ship Safety, Space, Remote Sensing, Law Enforcement and Military.

When a radar is to be used in an application, the user must concern with the radar system with regard to receiver and transmitter, the propagation path between the radar and target and also characteristics of the target. The prediction of radar performance requires a detailed examination of all these factors that build up the radar system. Radar simulation programs help not only the radar system designer but also the radar system user to enhance the performance of radar.

The following factors are effective in determining the radar performance:

(i) The technical characteristics of the radar equipment: Maximum transmitter power, IF filtering characteristics, antenna parameters, pulse repetition frequency, pulse repetition interval, pulse compression and integration, receiver noise figure, radar's one way and two way plumbing loses, frequency agility bandwidth, type of radar (MTI, pulsed doppler, etc.) and all the transmitter and receiver features of radar are to be considered.

(ii) The layout of the propagation path: The layout of the propagation path is affected by attenuation of radar waves due to atmospheric conditions; attenuation caused by meteorological effects, like rain, snow, hail; reflection from ground (land or sea); diffraction of radar waves from obstructions along the ray paths; obstruction of direct or reflected ray by plateaus and hills; properties of land and sea; bending of radar rays due to tropospheric refraction and earth's curvature. These factors have considerable influence on the radar performance. Moreover clutter due to rain, ground and jamming causes target signal to noise ratio to decrease; hence, the false alarm rate of the radar increases. Therefore clutter effects should also be analyzed and included in the performance calculations.

(iii) Target types and properties: Target Radar Cross-Section (RCS) fluctuations, dimensions, material properties, swerling case number, etc. all affect the target interception capability of radar.

The propagation of a radio wave through propagation path is affected by various mechanisms which degrades the originality of the received signal. Accurate prediction of these effects is essential in the design and development of a radar system. These effects can include reflection, shadowing and diffraction caused by obstacles along the propagation path, such as hills or mountains in a rural area, or buildings in a more urban environment. Reflections off obstacles or the ground cause multi-path effects and the radio signal can be significantly attenuated by various environmental factors such as ionospheric effects, propagation through vegetation, such as in a forest environment, or reflection from an impedance transition such as a river or land/sea interface. When line-of-sight (LOS) propagation is not present, these environmental mechanisms have the dominate effect on the originality of the received signal through dispersive effects, fading, and signal attenuation.

Accurate prediction of these propagation effects allow the system engineer to address the trade-off between radiated power and signal processing by developing an optimum system configuration in terms of modulation schemes, coding and bandwidth, antenna design, and power. Current techniques commonly applied to characterizing the communications channel are highly heuristic in nature and not generally applicable. It is the intent of this work to define a new method for the accurate and general prediction of radio wave propagation by application of ray theory, and within this framework to develop electromagnetic models of convex and concave surface which represent various scattering and diffraction mechanisms in the propagation environment.

1.2 Scope and Objective

The basic motivating factor behind this work is the need for development of an accurate and general propagation model. In order to predict a radar system performance, all these considerations should be suitably modeled and formulated. The propagation model should predict the path propagation losses performance.Consequently the method should be simple, accurate and very fast.

Numerous methods for predicting field strength at high frequencies over irregular terrain have been presented in the literature . Evaluating radar performance at a given site requires estimation of the path propagation factor for the specific propagation path due to the combined effects of reflection and diffraction.

The most widely used propagation model based on ray optics is that known as SEKE [4] . It is a site-specific propagation model for general terrain, makes use of the original Lincoln Laboratory geometrical optics models for rough reflecting terrain, low altitude spherical earth propagation for level terrain, and low altitude multiple knife edge diffraction for hilly non-reflecting terrain.

Another propagation model RADCAL [1,2] is a simulation program of a radar system that is comprised of radar, propagation environment, and target. This simulation program models the propagation medium (land, sea, rain, atmosphere, hills, etc.), radar transmitter-receiver characteristics, clutter, and target. The propagation model used in RADCAL concerns the round earth and slant plateau reflections combined with hill diffractions. It considers contributions of specular reflections from flat (round earth) and slant plateaus between diffracting hills and nondiffracting depressions. It checks obstructions of incident, reflected and diffracted rays by flat plateaus and considers Knife-edge diffraction from rounded hilltops at oblique incidence. RADCAL also concerns, clutter backscattering from ground (land or sea); properties of land and sea; bending of radar rays due to tropospheric refraction and earth's curvature. The five-ray propagation model for reflection and diffraction can be used to find the path propagation factor. This model includes knife-edge diffraction and ground reflection simultaneously. In the new version of RADCAL, terrain will be modeled as convex and concave plateaus together with flat slant plateaus joining hills and depressions. (See Figure 1-1)

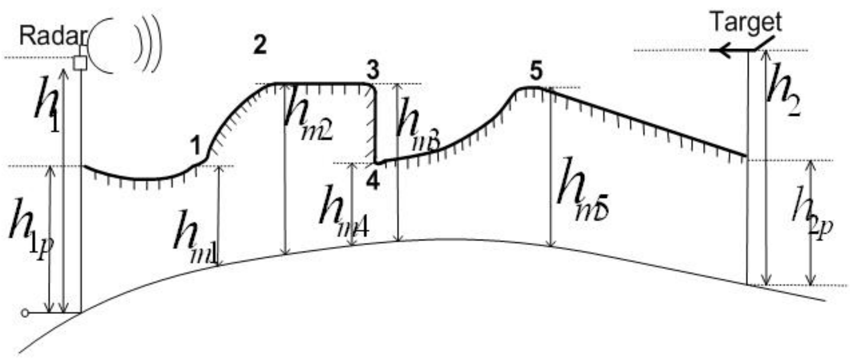

Figure 1-1 Geometry describing new RADCAL terrain Model

There is also full wave integral equation formulations for the propagation factor which are suitable for HF and VHF [7]. Another propagation model is the parabolic equation model which is also suitable for HF and VHF [8]. For microwave frequencies GO is more appropriate due to its simplicity and fast calculation. It reflects the specular reflection and hill diffraction effects which are dominant in the microwave propagation over irregular terrain. This type of fast algorithms in microwave radar propagation are very valuable as they can be embedded into real time simulation programs.

Efficient and accurate high frequency diffraction analysis techniques have been of interest for many years. One of the techniques that have been widely used in the propagation model is ray optics. One of the techniques capable of predicting the far zone field is the Keller's Geometrical theory of diffraction (GTD) [9]. When its deficiencies at shadow and reflection boundaries were removed by the uniform geometrical theory of diffraction [10] and the uniform asymptotic theory [11], GTD has become an even more effective tool because of its accuracy and simplicity. In this thesis GO (ray optic) is used to find the Divergence Factor (well known) and Convergence Factor (defined here). However, the singularities of GTD at caustics still exist.

GO method is the best candidate for this purpose previous method exist and in this thesis we improve GO techniques suitable for a complicated irregular terrain. The GO model used here consists of modeling the terrain by round earth plateaus, slant flat plateaus, convex and concave plateaus between hills and depression. Multiple hill top diffraction combined with reflections from plateaus are considered.

1.3 Relevant Assumptions & Definitions

In this section relevant assumptions, definitions, and conventions are given. Unless otherwise indicated they are valid throughout the thesis.

In this thesis, in all derivation and calculation we assume that radius of convex or concave slant plateaus (R_0), the distance from the source of the incident or reflected ray to the reflection point (R_1) and the distance from reflection point to observation point (R_2) are much greater than the wavelength (λ).

$$R_0 >> \lambda \quad \text{and } R_1 >> \lambda \text{ and } R_2 >> \lambda \tag{1.1}$$

Therefore we can accept that the area of reflection is smooth. Since we assume that radius of convex or concave slant plateaus are very high ($R_0 >> R_1 R_2$), we shall consider this surface as a circle.

Also we assume that the distance from reflection point to observation point (R_2) is less then the distance from reflection point to caustic point ($R_{CAUSTIC}$).

$$R_2 < R_{CAUSTIC} \tag{1.2}$$

For concave plateaus for low grazing angles the reflected rays form caustic surface is quite close to the specular point then divergences again. The Convergent Factor is valid if the field point is sufficiently away (roughly more than 10λ) from the caustic surface.
Finally the height of the source point and the observation point from the surface of the earth must be much greater than the wavelength (λ):

$$h_1 >> \lambda \text{ and } h_2 >> \lambda \tag{1.3}$$

otherwise Whispering Gallery(Surface wave) Mode may occur and our derivation is not valid.

1.4 Outline

In the chapters that follow the development of the new propagation model including the results and applications are presented.

Evaluating radar performance at a given site requires estimation of the path propagation factor for the specific propagation path due to the combined effects of reflection and diffraction. The propagation models for predicting field strength at high frequencies over irregular terrain have been presented in Chapter II.

Another problem of significant interest is the propagation of radio waves over convex or concave obstacles encountered in the propagation environment such as hills, mountains, or wiley. Current methods applied to this problem include knife-edge diffraction and GTD methods for both wedge and convex surfaces.

In Chapter 3, a model is presented which calculates the reflection from a convex or a concave surface. A study concerning the effects of fine details of terrain is also studied. This work reveals the significant features of a terrain and suggest ways of smoothing a very detailed tarrain profile.

In Chapter 4, numerical and geometrical verification of the present method are given.

In Chapter 5 this thesis work is summarized and conclusions are drawn as well as suggestions for future work.

CHAPTER 2

RADIO WAVE PROPAGATION MODELS

2.1 Introduction

Maxwell's equations formulated in 1873 define EM phenomena. Although it had been more than a century since its establishment, people try to found more efficient and powerfull numeric or analytical solutions for specific problems. Now engineers and researchers worldwide use analytical or numeric methods to obtain solutions for EM wave propagation, radiation, guiding and scattering. In this chapter, we present a brief history of propagation models. Then, we present detailed information about RADCAL in which the present model is implemented.

2.1 Propagation Models

Many models currently exist that use a combination of spherical earth diffraction, multiple knife-edge diffraction, wedge diffraction, and geometrical optics to arrive at a solution for the field for a given transmitter/receiver geometry and a specified terrain path.

Commonly used methods of propagation models can be broken down into two areas, empirical models, which are highly heuristic in nature, and simplified analytic models.

The empirical models are constructed from measured data and are not directly connected to the theory of the physical processes involved. This limits them to very specific enviromental conditions at the time the measurements were made as well as measurement system attributes (frequency, bandwidth, and polarization). An example of a commonly used empirical model for urban environments is the Okumura model [2]. This model uses simple algebraic equations to calculate mean path-loss for fixed frequency, observation distance, and transmitter/receiver height. It does not account for coherence bandwidth, fading, or depolarization effects. In addition it fails if the antenna heights or orientations are changed.

Analytic models, while attempting to account for the interaction of the various mechanisms which effect propagation, are simplified to a degree as to make them fast for most practical applications. An example of this is the Longley-Rice irregular terrain model [3]. It uses Geometrical Optics (GO) and ray-tracing to account for reflected fields and knife-edge or Kirchhoff diffraction to account for path obstacles.

There are also full wave integral equation formulations for the propagation factor which are suitable for HF and VHF [7]. Another propagation model is the parabolic equation model which is also suitable for HF and VHF [8]. For microwave frequencies GO is more appropriate due to its simplicity and fast calculation. It reflects the specular reflection and hill diffraction effects which are dominant in the microwave propagation over irregular terrain. This type of fast algorithms in microwave radar propagation are very valuable as they can be embedded into real time simulation programs.

Efficient and accurate high frequency diffraction analysis techniques have been of interest for many years. One of the techniques that have been widely used in the propagation model is ray optics. One of the techniques capable of predicting the far zone field is the Keller's Geometrical theory of diffraction (GTD) [9]. When its deficiencies at shadow and reflection boundaries were removed by the uniform geometrical theory of diffraction [10] and the uniform asymptotic theory [11], GTD has become an even more effective tool because of its accuracy and simplicity. In this thesis, GO (ray optic) is used to find the Divergence Factor to account for ray spread from a convex surface during reflection and the Convergence Factor to account ray collimation from concave surface during reflection. However, the singularities of GTD at caustics still exist.

In the following section we present other propagation models (SEKE, FBSA,TPEM) and detailed information about RADCAL in which present model is included.

2.2 SEKE: A Computer Model For Low Altitude Radar Propagation Over Irregular Terrain

SEKE (Spherical Earth Knife Edge) [4] is a computer model for low altitude radar propagation over irregular terrain. It is a new site-specific propagation model for general terrain, makes use of the original Lincoln Laboratory models geometrical optics (GOPT) for rough reflecting terrain, low altitude propagation spherical earth (LAPSE) for level terrain, and low altitude propagation knife edges (LAPKE) for hilly non-reflecting terrain to compute multipath, spherical earth diffraction, and multiple knife-edge diffraction losses. The proper algorithm is selected based on terrain geometry, antenna and target heights, and frequency:

SEKE predicts the one-way propagation factor over composite terrain by selecting, based on terrain geometry, one algorithm or combinations of the algorithms designed to compute specular reflection, spherical earth diffraction, and multiple knife-edge diffraction losses. It makes use of the Lincoln Laboratory models GOPT or GEOSE (the part of LAPSE that computes specular reflection loss) for multipath, SPH35 (the part of LAPSE that computes spherical earth diffraction loss) for spherical earth diffraction, and KEDEY (a new modified version of LAPKE) for multiple knife-edge diffraction loss computations.

The model SEKE is based on the assumption that the propagation loss over any path at the microwave frequencies of interest (VHF to X-band) can be approximated by one of the multipath, multiple knife-edge diffraction, or spherical earth diffraction losses alone or a weighted average of these three basic losses. The model uses as subroutines the algorithms that have been developed previously at Lincoln Laboratory for smooth sphere reflections (GEOSE), multispecular reflections (GOPT), multiple knife-edge diffraction (KEDEY), and spherical earth diffraction (SPH35). The proper algorithm is selected based on the terrain elevation data for the propagation path, the altitude and range of the target, and the radar frequency. Figure 2-1 summarizes the guidelines of the model.

SEKE was discussed for four categories of terrain:

- Level reflective terrain,
- Intermediate rolling farmland,
- Rough reflective terrain,
- Rough forested terrain.

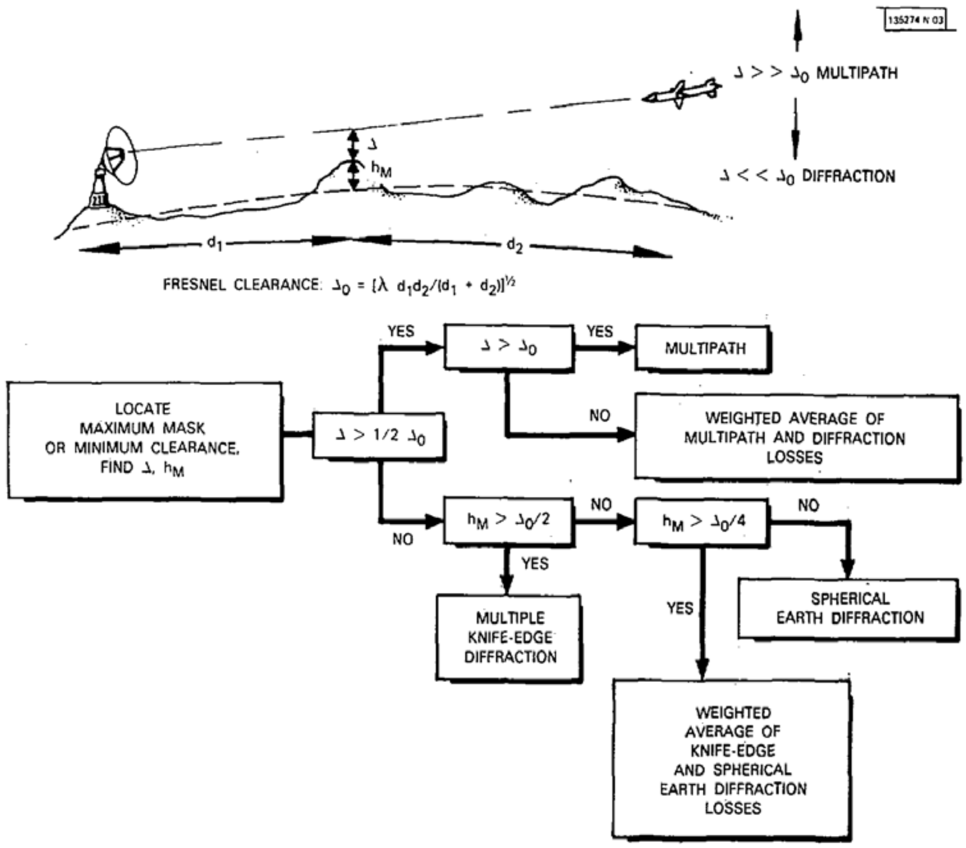

Figure 2-1 : Guidelines of the SEKE propagation model

An example of the output plot of the program SEKE for the Intermediate rolling farmland is shown in Figure 2-2 below.

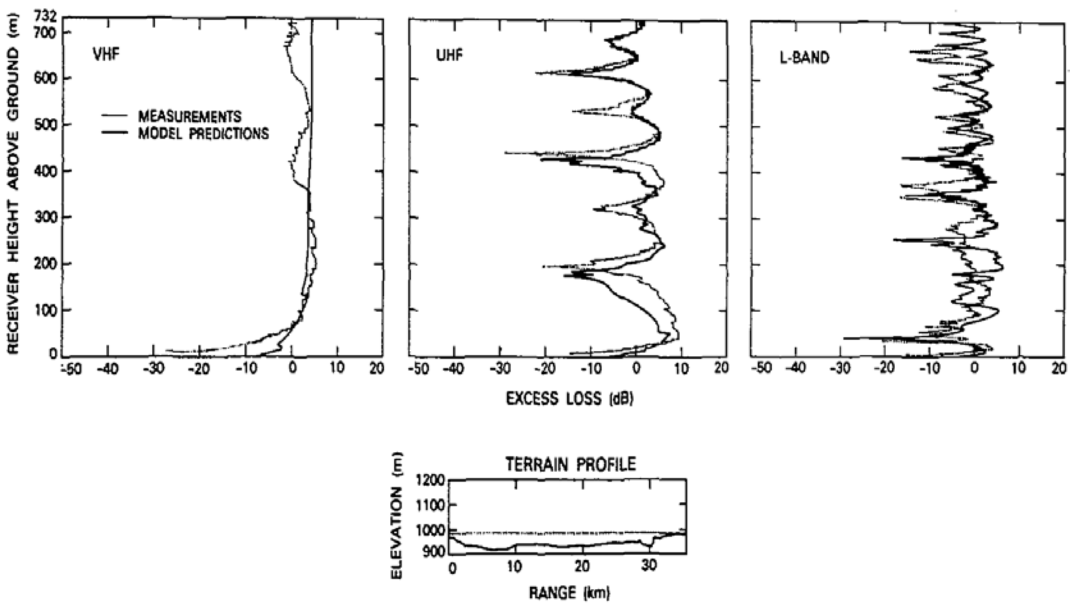

Figure 2-2 : One-way propagation loss as a function of receiver altitude

The model was tested at VHF frequencies through X band over many paths for which propagation data were available. For all the paths considered, the proper algorithm was selected by the program, and good agreement with the measurements was generally achieved.

SEKE model was compared with two other general site-specific models, Longley-Rice [3] and terrain integrated rough earth model (TIREM) [4], which was also work directly on digital terrain elevation data, in terms of their expected performance. It was found that the SEKE models generally performed better. Also, the model was tested over many types of terrain at frequencies ranging from X-band to VHF, and the results were generally in good correlation with the measurements.

2.3 Spectrally Accelerated Forward Backward Model

Spectrally Accelerated Forward Backward (FBSA) [46] is a fast integral equation solution. FBSA results are obtained for propagation over large scale terrain profiles and compared with measurements to assess the accuracy of FBSA.

Most of the automated propagation prediction tools for coverage analysis over geometrical databases use empirical models with or without semi-empirical multiple knife-edge diffraction (MD) losses in order to predict field strengths over terrain profiles. These empirical models which are described by equations or curves derived from statistical analysis of a large number of measured data, are simple and do not require details of the terrain. Therefore, they are easy and fast to apply. However, they cannot provide a very accurate estimation of the scattered field or the path loss for an arbitrary environment.

Furthermore, the good agreement between the FBSA and measured results confirm the consistency of the method to be used for a section of the three-dimensional (3-D) environment, though the FBSA is based on the two-dimensional (2-D) Green’s function. Use of other 2-D Green’s function based integral equations for 3-D environments has been presented in the literature before [47]–[54]. They have chosen the FBSA among these methods, because of its O(N) computational cost, to examine the propagation models over electrically large terrain profiles.

In the following paragraphs first the integral equation (IE) formulation and its solution using the FBSA is briefly discussed. Then numerical results are presented.

The scattered field over an electrically large rough terrain profile which is illuminated by an incident electromagnetic field $\{\{E^{inc}(p), H^{inc}(p)\}(p = \hat{x}x + \hat{z}z)$ is computed using an IE based method to be used as a reference solution. Figure 2-3 illustrates such a rough surface that is characterized with the curve C defined by $z = f(x)$, along the x-axis.

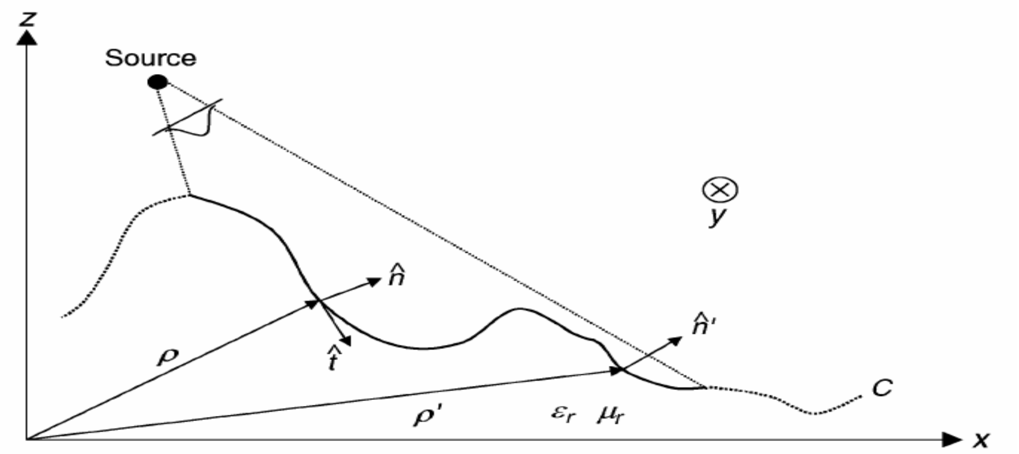

Figure 2-3 : Generic terrain profile.

Considering the terrain as an imperfect conductor $(\varepsilon_r(p), \mu_r(p))$ and using the Impedance boundary conditions (IBC) [55], an electric field integral equation (EFIE) for a transverse magnetic (TM_y) polarization can be written in terms of the equivalent electric current density J_y on the surface and a magnetic field integral equation (MFIE) for the transverse electric (TE_y) polarization case can be obtained in terms of the tangential induced current J_t [46].

Instead of the direct solution of the system, which requires $O(N^3)$ operations, the FBSA ($O(N)$) is used in order to find the unknown current coefficients for electrically very large terrains.

In order to assess the accuracy of the FBSA as well as to demonstrate its consistency with measurements, comparisons of FBSA results with measurements are shown in Figures 2-4 and Figures 2-5. The terrain profiles are from Denmark with lengths up to 8 km. The height variations are of the order 20–50 m. Measured data were obtained byHviid et al. [47] using a dipole with a transmitted power of 10 W and a gain of 8 dBi. The transmitter height is 10.4 m. The receiver antenna is $\lambda/4$ monopole on top of a van with a height of 2.4 m. Having no exact information about the vegetation and electrical properties of terrains, the surface impedances are taken as $\eta_s = 20.2 + j8.1\ \Omega$ in order to handle some small forests and other land cover data along the profiles [14]. Also shown in the figures are the computations of Hviid et al. [14] with a different terrain based integral equation method. This method neglects the backscattering, has a computational cost of $O(N^2)$, assumes perfect magnetic conductor terrain, and it can only handle the TM polarization case. They have taken the segment length $\lambda/10$, and the strong region length, $L_s = (z_{\max} - z_{\min})/4$, is calculated as 13λ and 6λ, respectively, for the terrain profiles in Figure 2-4(a) and Figure 2-5(a).

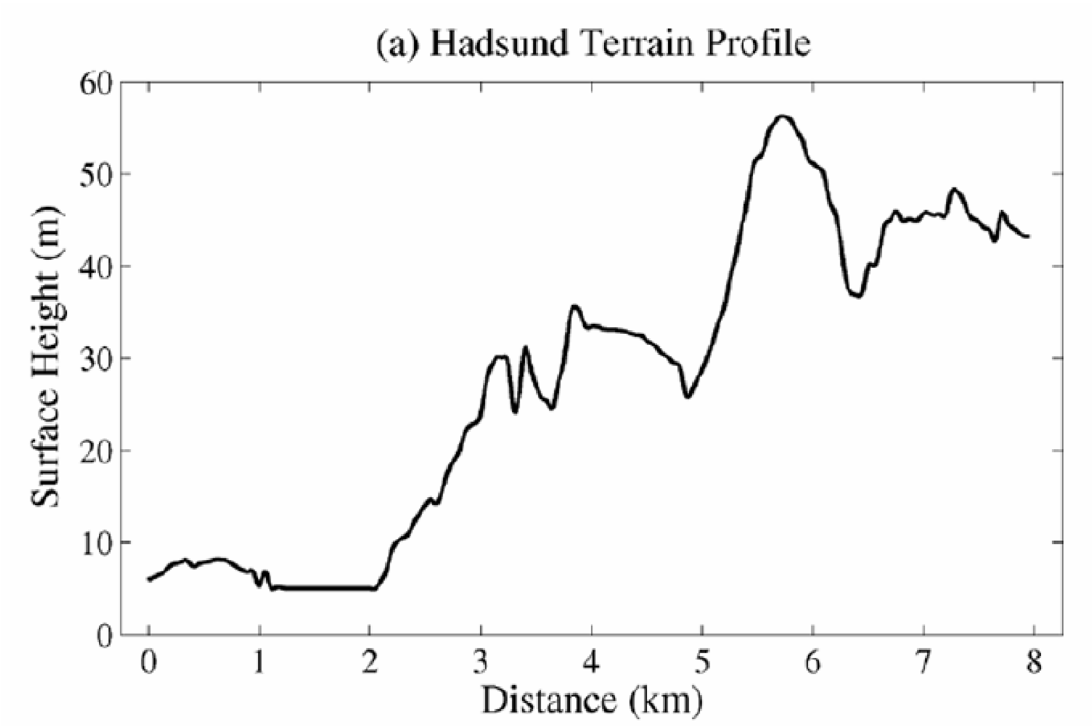

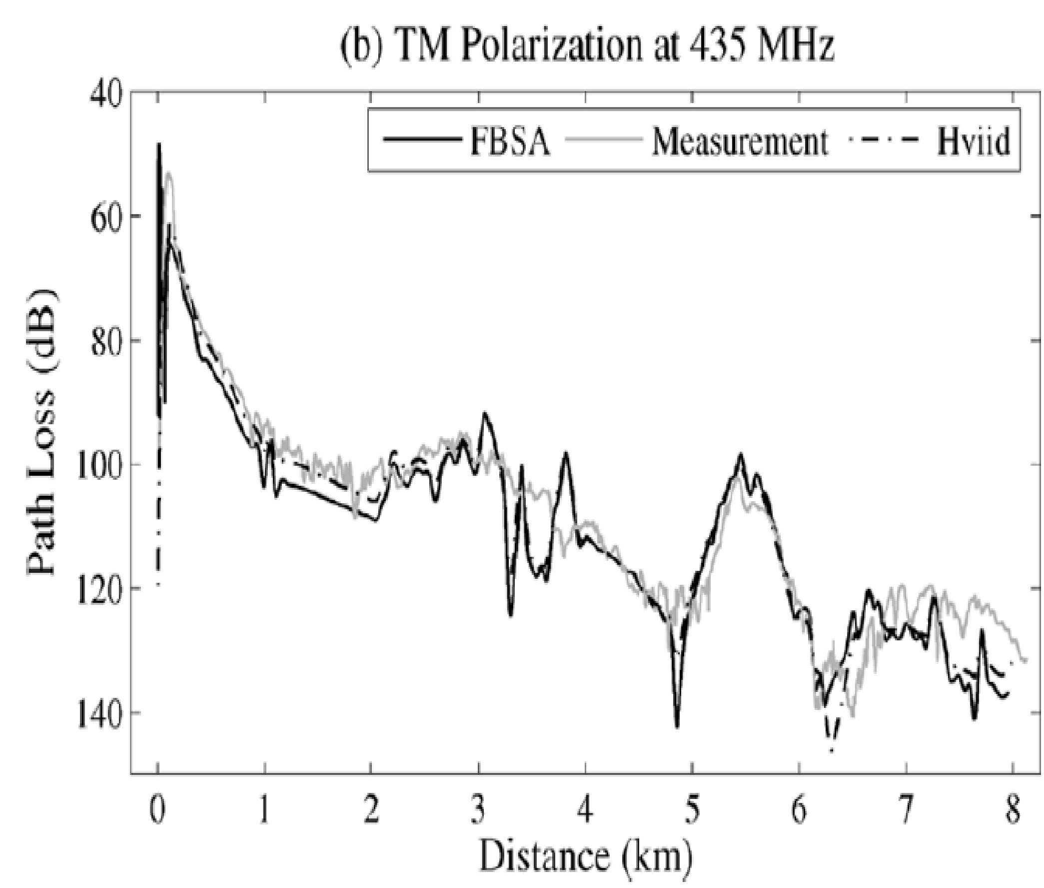

Figure 2-4 : Path loss over Hadsund terrain profile. (a) Profile geometry.(b) TM polarization at 435 MHz. $Distance = 7950m$, $\Delta x = 0.1\lambda$, $N = 115275$, $N_q = 117$, $L_s = 13\lambda$.

In Figure 2-4(b), the results are presented over Hadsund terrain profile at 435 MHz operating frequency, while the comparisons over Jerslev profile for 970 MHz are shown in Figure 2-4(b). Both figures show the very good agreement of the FBSA results with the measurements and the other IE method.

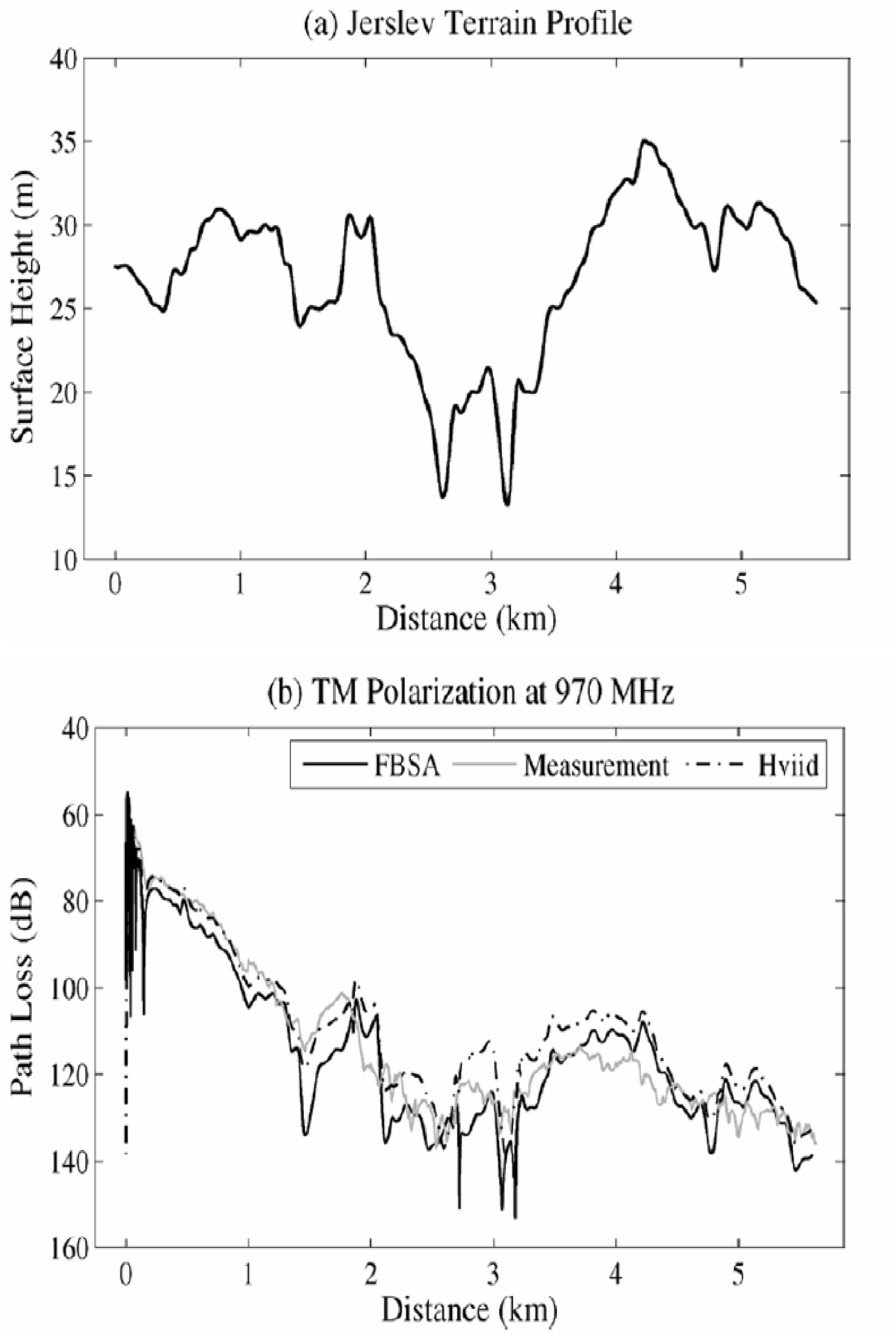

Figure 2-5 : Path loss over Jerslev terrain profile. (a) Profile geometry. (b) TM polarization at 970 MHz. $Dis\tan ce = 5600m$, $\Delta x = 0.1\lambda$, $N = 185066$, $N_q = 124$, $L_s = 6\lambda$ 6 .

2.4 Terrain Parabolic Equation Model

For many years now, the parabolic equation (PE)[60] method has been used to model radiowave propagation in the troposphere for over-ocean paths . The biggest advantage to use the PE method is that it gives a full-wave solution for the field in the presence of range-dependent environments. Two methods may be used to solve the PE. One uses finite-difference techniques, and the other uses the split-step Fourier algorithm.

Terrain Parabolic Equation Model (TPEM) is based on a modification to the smooth earth Parabolic Equation (PE) and uses the split-step Fourier algorithm.This is a numerically efficient model because of the use of fast Fourier transforms (FFTS) in its implementation. Since only a minor modification to the smooth earth PE is required to include terrain effects, a brief description of the derivation and implementation will be given in following paragraph.

In the following formulation, the atmosphere is assumed to vary in range and height only, making the field equations independent of azimuth. Also, there is an assumed time dependence of e^{-iwt} in the field components. They begin with the parabolic wave equation for a flat earth.

The field from either a horizontal or vertical electrical dipole source satisfies the same parabolic differential equation. The type of source one wants to model determines the boundary condition that is applied at the earth's surface. For the present, only horizontal polarization will be addressed.

A transformation is made according to the method first presented by Beilis and Tappert [58], in which they used this technique to model rough surface scattering for underwater acoustic fields. The original coordinate system is transformed such that a simpler boundary condition is obtained in the new coordinate system and a new PE is derived.

With this simpler boundary condition the problem becomes easier to solve and, in fact, can be solved by the same split-step PE algorithm. For the implementation of the smooth earth PE and further details on the TPEM, the reader is referred to [59].

In order to assess the accuracy of the TPEM all measurement and prediction results will be displayed as height vs. one-way propagation factor (field strength relative to free space) in dB.

Propagation measurements were made over several sites in Canada by Lincoln Laboratory [4]. Comparisons will be presented for one site in particular, the Beiseker area in Alberta, Canada. The terrain is considered to be intermediate rolling farmland with negligible vegetation. A standard atmosphere of 118 M-unitsh for TPEM was used and a 4/3 earth radius factor was used for SEKE. Figure 2-6 shows the 55 km north terrain profile (Beiseker N55) along with the height-gain plot comparing SEKE, TPEM, and the propagation measurements. The frequency is 435 MHz, the transmitter height is 18.3 m above the ground, and the receiver range is 54.5 km. For this case TPEM and SEKE agree fairly well with the measured data. Figure 2-7 shows the same comparison for a frequency of 167 MHz along the 35 km west path (Beiseker W35). Here, both TPEM and SEKE agree well with the data, however, TPEM is also able to capture the multipath pattern at the higher altitudes.

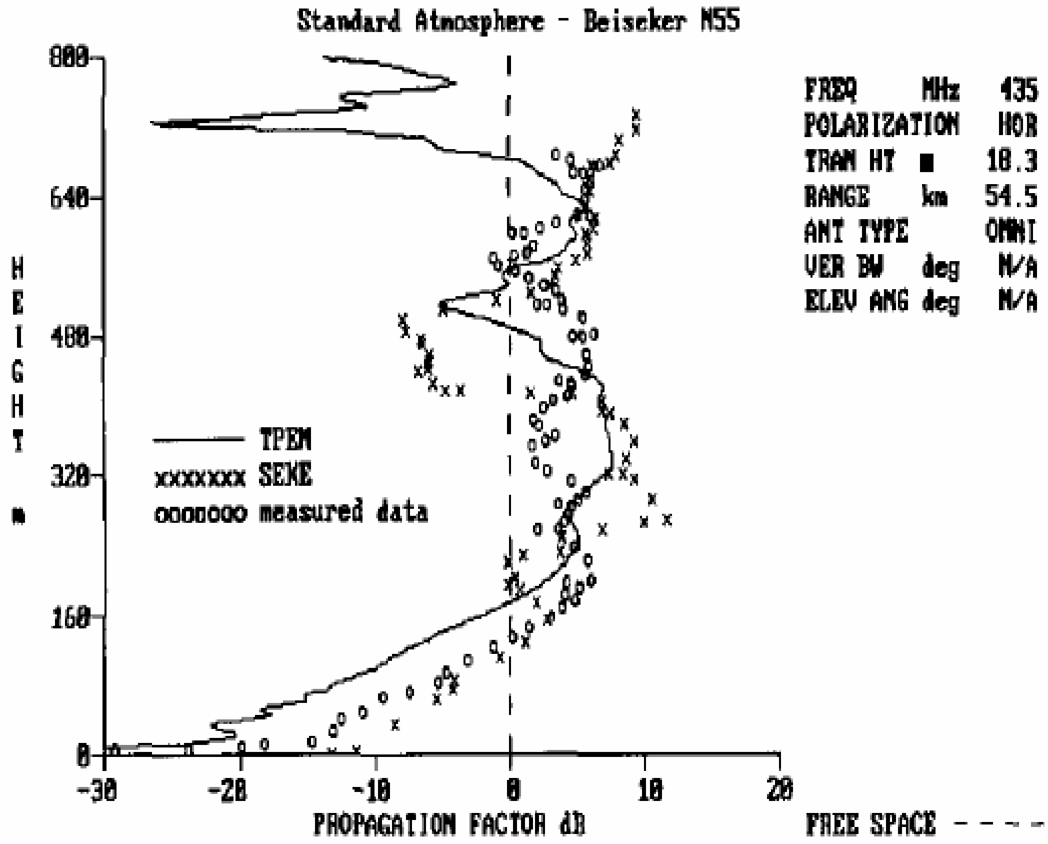

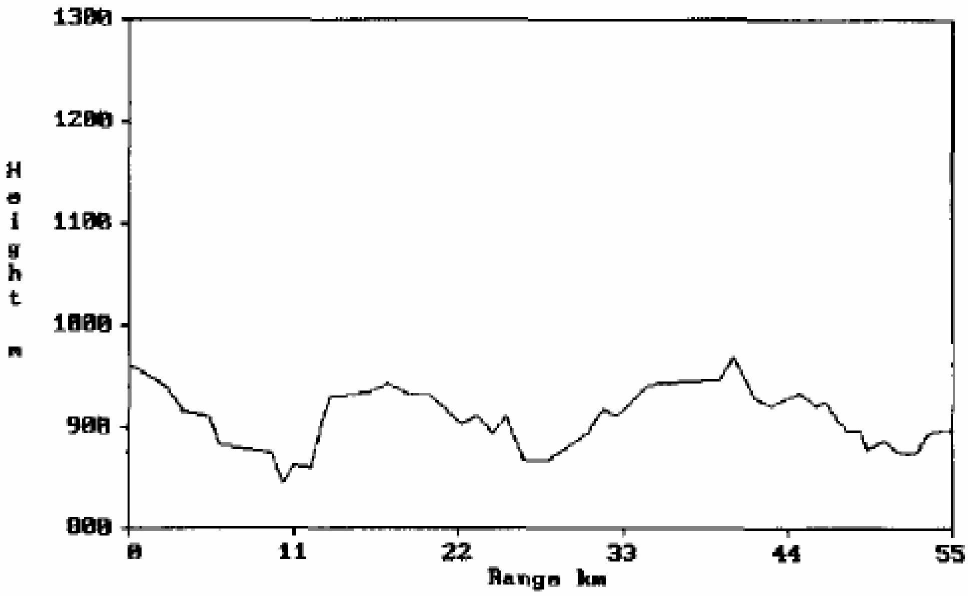

Figure 2-6 : Terrain profile for north (55 h) Beiseker path with height-gain plot showing TPEM, SEKE, and measured signal.

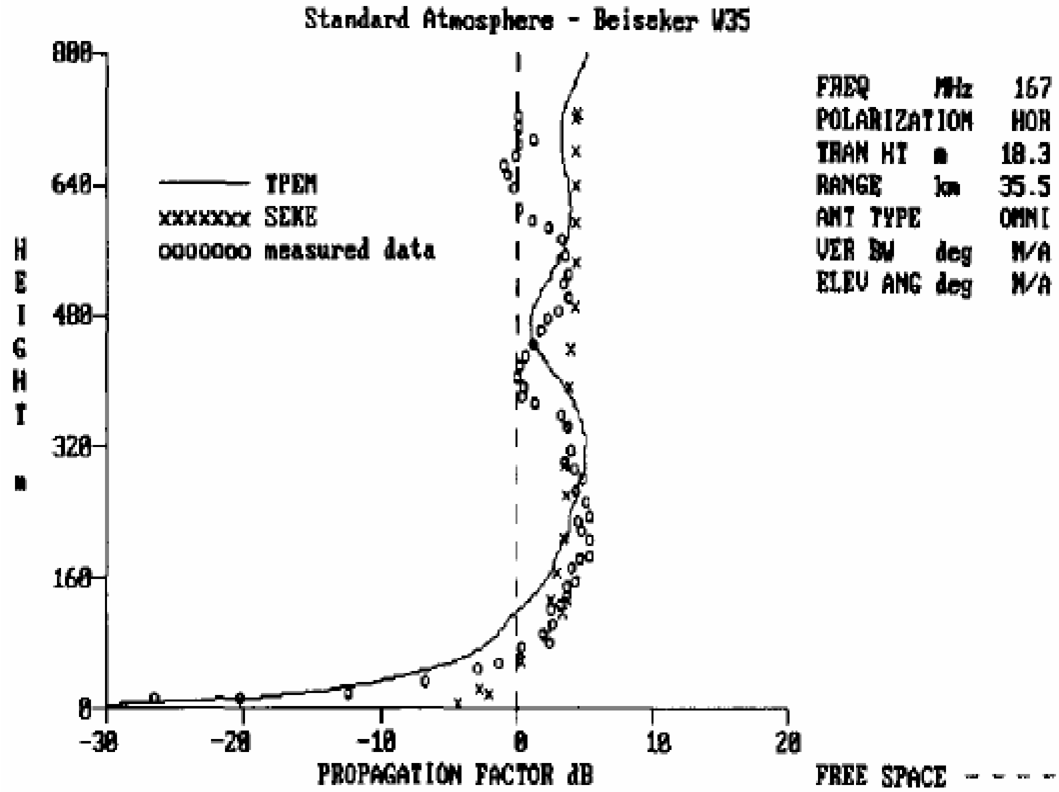

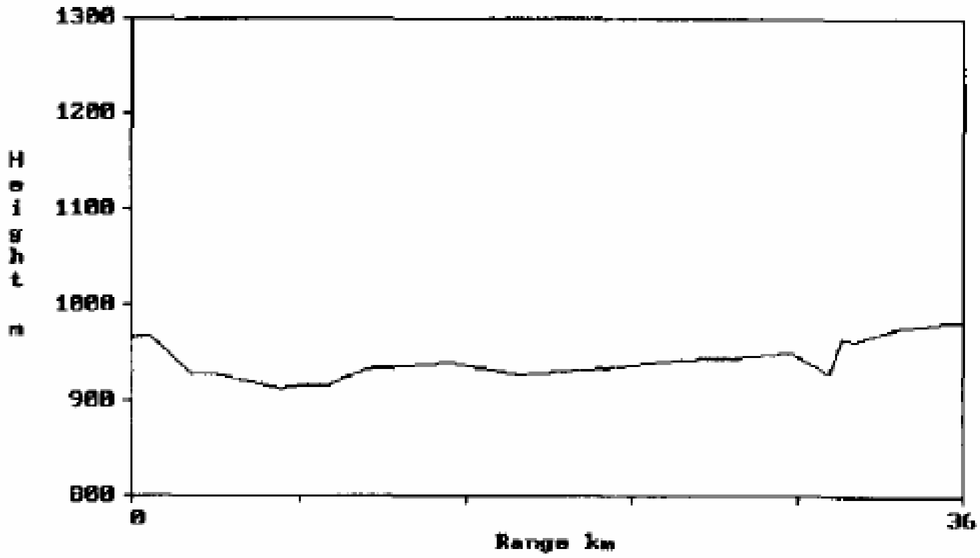

Figure 2-7 : Terrain profile for west (35 h) Beiseker path with height-gain plot showing TPEM, SEKE,and measured signal.

2.5 RADCAL

RADCAL is a simulation program of a complete radar system that is comprised of radar, propagation environment and target. This simulation program models the propagation medium (land, sea, rain, atmosphere, hills, etc.), radar transmitter-receiver characteristics and target, and evaluates all the related mathematical formulation. As an output of these processes, performance of the radar against the target is examined. This algorithmic work is also supplemented with a suitable user-interface and display capabilities in both Borland Pascal and Visual C++.

RADCAL propagation model concerns the round earth and slant plateau reflection combined with hill diffraction. It considers contributions of specular reflections from flat and slant plateaus between diffracting hills. It checks obstructions of incident and reflected rays by flat plateaus and considers Knife-edge diffraction from rounded hilltops at oblique incidence. RADCAL also concerns attenuation of radar waves due to atmospheric conditions; attenuation caused by meteorological effects, like rain, snow, hail; reflection from ground (land or sea); properties of land and sea; bending of radar rays due to tropospheric refraction and earth's curvature.

RADCAL calculates the path propagation factor which is defined as the ratio of the realized signal strength, at the target position conditions to that which would exist in free space. It expresses the effects of the interaction of the direct wave with the underlying surface of the earth and the atmospheric refraction. These effects include any reflected wave reaching the target from the surface, and the diffraction of the wave as it passes close to the surface. The five-ray propagation model for reflection and diffraction can be used to find the path propagation factor. This model includes knife-edge diffraction and ground reflection simultaneously.

The overall "path propagation factor" is obtained by complex addition of the five ray propagation factors. That is:

$$F_t = F_1 + F_2 + F_3 + F_4 + F_5 \qquad (2.1)$$

Each propagation factor can be calculated as follows:

2.5.1 RAY-1

This is the direct ray between the radar and the target. It takes into account the knife-edge diffraction, antenna field pattern function along the direct path, atmospheric lens effect loss, one way atmospheric attenuation, rain attenuation and diffraction zone path-gain-factor. It is described in Figure 2.8 and expressed by (2.2).

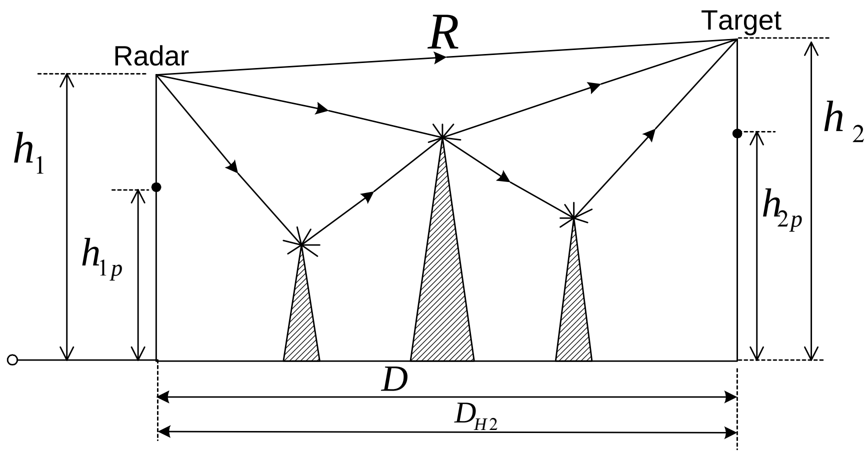

Figure 2.8 : Geometry Describing RAY-1.

$$F_1 = F_{KE1} \cdot f(\theta_1) \cdot L_l \cdot L_{AT} \cdot R_{Att1} \cdot A_{fdz} \tag{2.2}$$

where

F_{KE1} : Knife-Edge diffraction factor. (See Appendix A.1)

$f(\theta_1)$: Antenna field pattern function along the direct path. (See Appendix A.2)

L_l : Atmospheric lens effect loss for Ray-1. (See Appendix A.3)

L_{AT} : One way atmospheric attenuation from H_1 to H_2 along R. (See Appendix A.3)

R_{Att1} : Rain attenuation factor and is contributed to the Ray as L_r, the rain length for the path radar to target. (See Appendix A.8)

A_{fdz} : Diffraction zone path-gain-factor. (See Appendix A.4)

The value of F_1 is calculated by using the $Direct\_Ray(...)$ procedure.

2.5.2 RAY-2

This is the complex summation of the rays which emanate from radar and reflect from a flat or slant plateau and reach the target. It takes the knife-edge diffraction, antenna field pattern function along the direction of incidence, atmospheric lens effect loss, one way atmospheric attenuation, rain attenuation, divergence factor, available area for reflection, reflection coefficients, specular reflection and pulse extension into account. It is described in Figure 2.9 and expressed by (2.3).

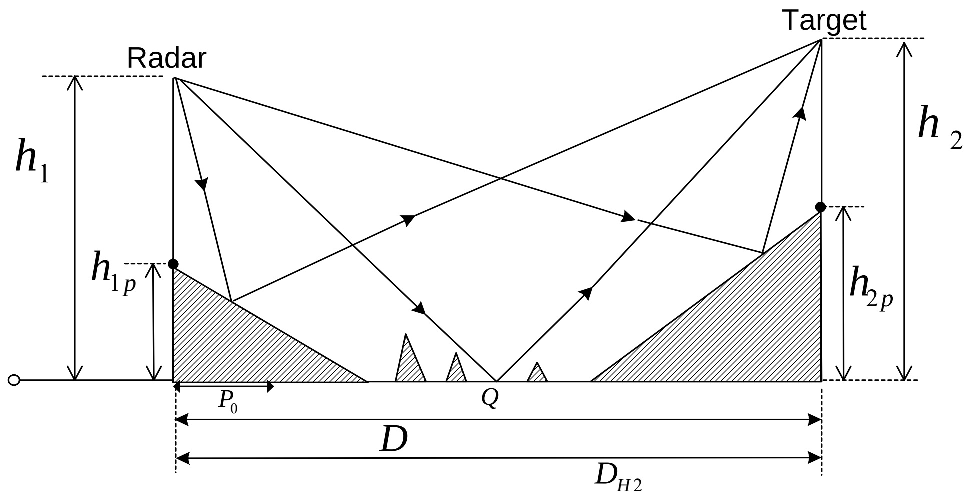

Figure 2.9 : Geometry Describing RAY-2.

$$F_1 = F_{KE21} \cdot F_{KE22} \cdot f(\theta_2) \cdot L_{l1} \cdot L_{AT1} \cdot L_{l2} \cdot L_{AT2} \cdot R_{Att2}$$
$$\cdot D_v \cdot W_r \cdot W_{ra} \cdot \text{Reflect} \cdot \rho \cdot \rho_s \cdot \rho_v \cdot e^{j\beta} \qquad (2.3)$$

where;

F_{KE21} : Knife-Edge diffraction factor from radar to specular reflection points. (See Appendix A.1)

F_{KE22} : Knife-Edge diffraction from specular reflection points to target. (See Appendix A.1)

$f(\theta_2)$: Antenna field pattern function along the specular reflection path. (See Appendix A.2)

L_{l1} : Atmospheric lens effect loss from radar to specular reflection points. (See Appendix A.3)

L_{AT1} : One way atmospheric attenuation from H_1 to specular reflection points. (See Appendix A.3)

L_{l2} : Atmospheric lens effect loss from specular reflection points to target. (See Appendix A.3)

L_{AT2} : One way atmospheric attenuation from specular reflection points to H_2. (See Appendix A.3)

R_{Att2} : Rain attenuation factor and is contributed to the Ray as L_r, the summation of rain lengths for the path radar to specular reflection points and specular reflection points to target. (See Appendix A.8)

D_v : The divergence factor due to the divergence of incident rays after reflection from round earth. The value of D_v is calculated in $Specular(\ )$ procedure. (See Appendix G.34)

W_r : Ratio of lateral 1st Fresnel zone radius for reflection to the radius of the available plain at the specular reflection point. (See Appendix A.5)

W_{ra} : Ratio of longitudinal 1st Fresnel zone radius for reflection to the radius of the available plain at the specular reflection point. (See Appendix A.5)

Reflect : The parameters which checks specular reflection occurs or not. (See Appendix G.34)

$\rho e^{j\beta}$: The reflection coefficient of the ground pertinent to the polarization of the transmitting antenna. (See Appendix A.6)

ρ_s : Rough surface specular reflection coefficient. (See Appendix A.6)

ρ_v : Vegetation reflection coefficient. (See Appendix A.6)

The value of F_2 is calculated by using the Specular_Reflection(...) procedure. This procedure also checks obstruction of incident rays from H_1 to the reflection point Q by convex masks or flat plateaus. It also checks obstruction of reflected rays from reflection point Q by convex masks or flat plateaus. (See Appendix A.7)

2.5.3 RAY-3

This ray is the complex summation of rays, which emanate from radar and diffract from a hill and then reflect from flat or slant plateau and reach the target. RAY-3 can be expressed in terms of RAY-1 and RAY-2. It is described in Figure 2.10 and expressed by (2.4).

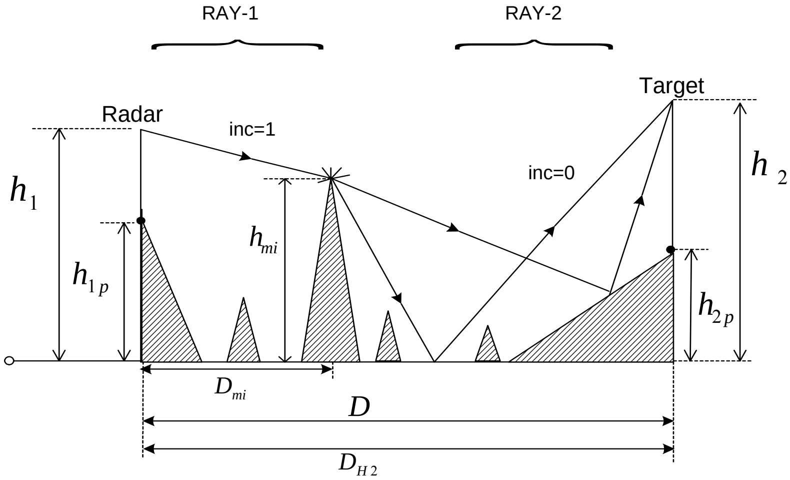

Figure 2.10 : Geometry Describing RAY-3.

The complex summation of RAY-1 and RAY-2 path propagation factors gives RAY-3 path propagation factor, F_{3i}, for any hill selected for diffraction. A phase correction term for RAY-3 should be added to the phase summation of rays. (See Appendix A.7) The procedure described here should be repeated for all the masks and the results should be added for calculating RAY-3:

$$F_3 = \sum_{i=1}^{N_m} F_{3i} \tag{2.4}$$

The value of F_3 is calculated by using the $Rays\_3\_4\_5(...)$ procedure.

2.5.4 RAY-4

This ray is the complex summation of rays which emanate from radar and reflect from a flat or slant plateau and then diffract from a hill and reach the target. RAY-4 can be expressed in terms of RAY-1 and RAY-2. It is described in Figure 2.11 and expressed by (2.5).

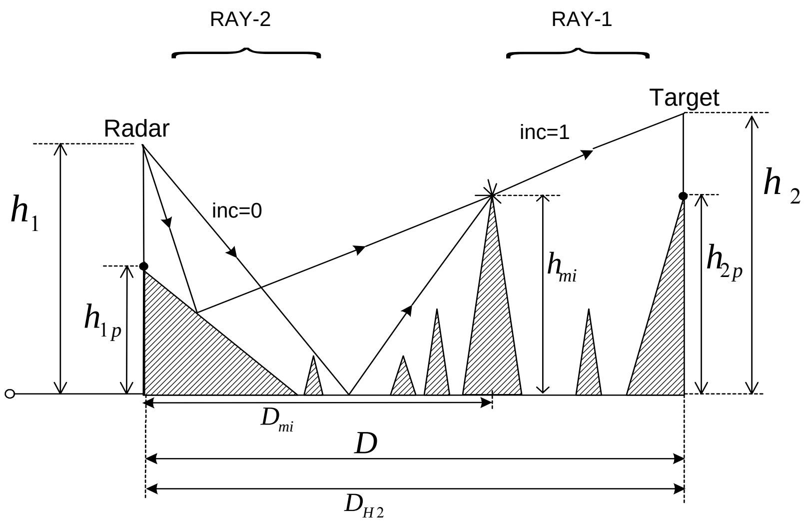

Figure 2.11 : Geometry Describing RAY-4.

The complex summation of RAY-2 and RAY-1 path propagation factors gives RAY-4 path propagation factor, F_{4i}, for any hill selected for diffraction. A phase correction term for RAY-4 should be added to the phase summation of rays. (See Appendix A.7) The procedure described here should be repeated for all the masks and the results should be added for calculating RAY-4:

$$F_4 = \sum_{i=1}^{N_m} F_{4i} \tag{2.5}$$

The value of F_4 is calculated by using the $Rays\_3\_4\_5(...)$ procedure.

2.5.5 RAY-5

This ray is the summation of rays, which emanate from radar and reflect from a flat or slant plateau, then diffract from a hill and then again reflect from a flat or slant plateau and reach the target. RAY-5 can be expressed in terms of RAY-2. It is described in Figure 2.12 and expressed by (2.6).

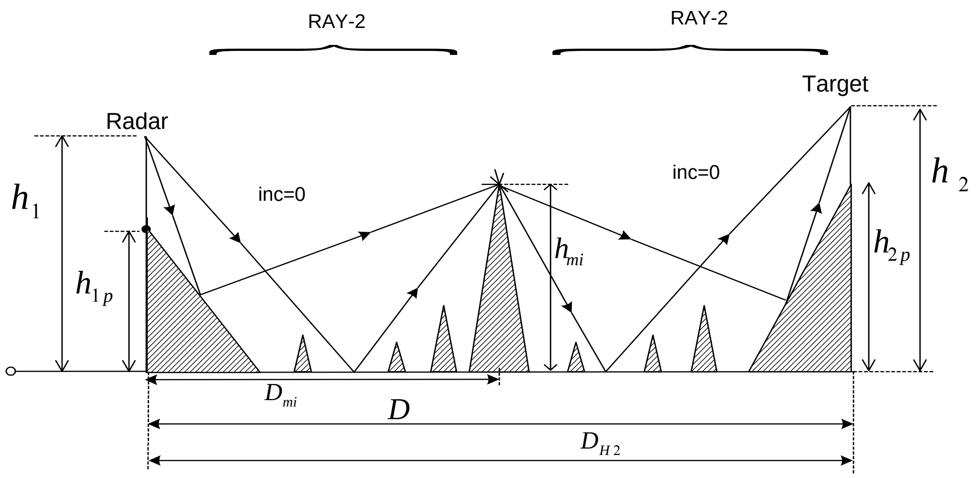

Figure 2.12 : Geometry Describing RAY-5.

The complex summation of two RAY-2 path propagation factors gives the RAY-5 path propagation factor, F_{5i}, for any hill selected for diffraction. A phase correction term for RAY-5 should be added to the phase summation of rays. (See Appendix A.7) The procedure described here should be repeated for all the masks and the results should be added for calculating RAY-5:

The value of F_5 is calculated by using the $Rays\_3\_4\_5(...)$ procedure.

$$F_5 = \sum_{i=1}^{N_m} F_{5i} \tag{2.6}$$

By introducing the "path propagation factor" in Eqn.(2.6) to the radar equation, then equation takes the form below.

$$\frac{S}{N_0} \propto F_t^{\,4} \qquad (2.7)$$

where F_t is the field path propagation factor.

This equation is going to be taken as general radar SNR equation from now on.

RADCAL calculates effective signal-to-noise ratio SNR_{eff} as a function of the geodesic distance "d" of the target from the location of the radar and detectability factor $D_x(n)$. Comparing SNR_{eff} to the detectability factor $D_x(n)$ gives the performance of the radar for a given P_d : probability of detection and P_{fa} : probability of false alarm and other parameters. When SNR_{eff} is greater than $D_x(n)$, the performance is better than specified in terms of P_d and P_{fa}.

For further details on the RADCAL, the reader is referred to [1],[2] and [3].

A typical example of geometry describing the terrain profile defined in RADCAL and the output plot of the program in Borland Pascal version of the RADCAL program are shown Figure 2-13 and Figure 2-14 respectively.

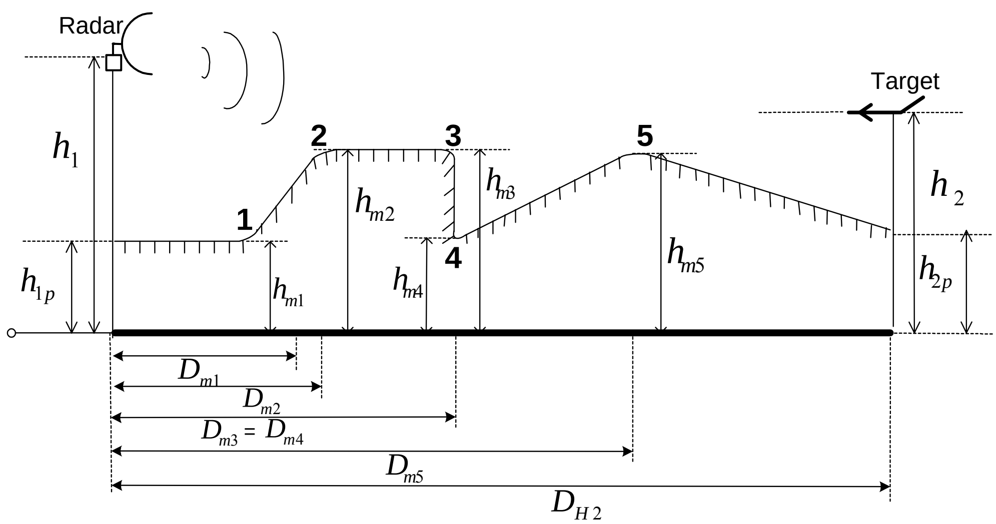

Figure 2-13 : An example Geometry Describing the Profile

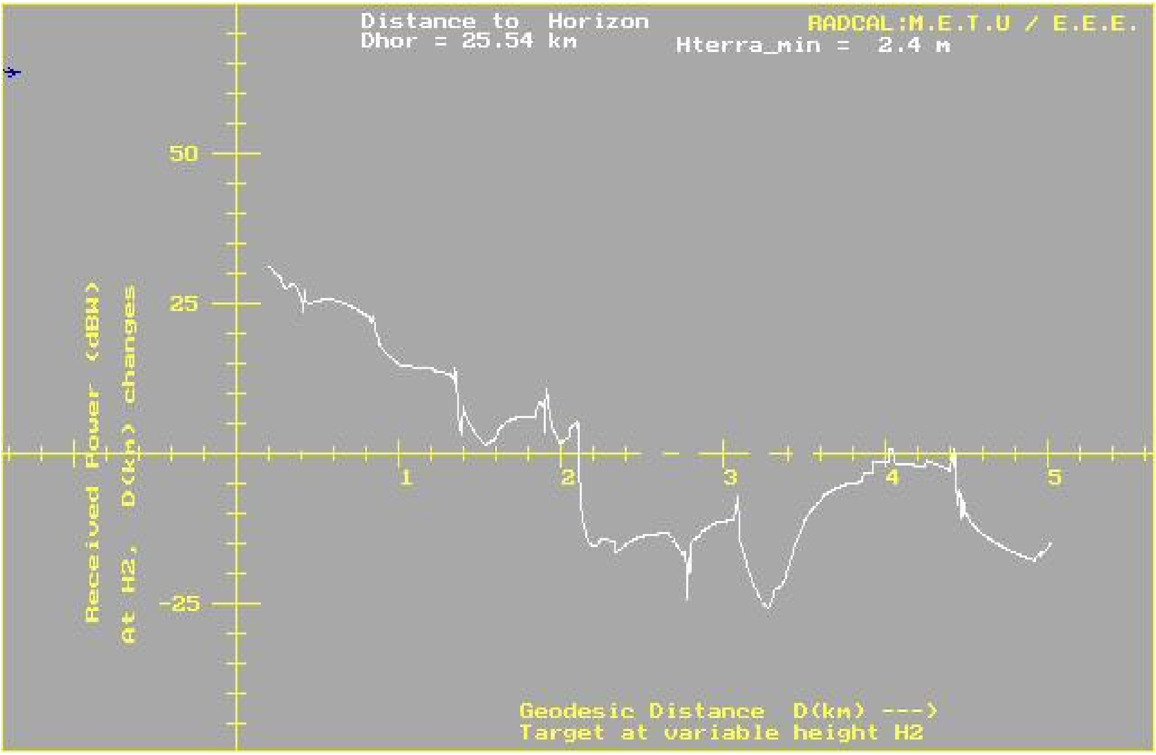

Figure 2-14 : The Output of Jerslev Terrain Profile Example

In the new version of RADCAL, terrain will be modeled by convex and concave Plateaus together with flat slant plateaus joining hills and depressions. (See Figure 2-15)

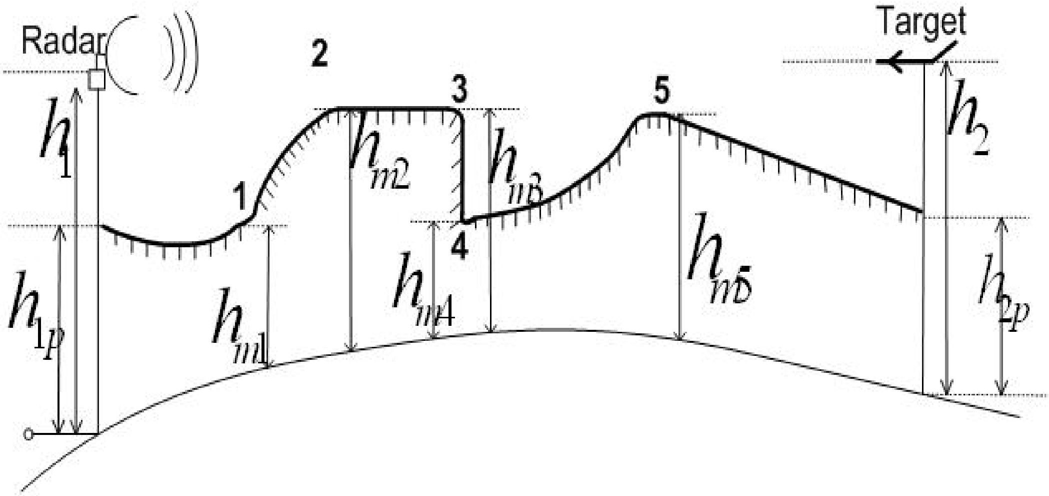

Figure 2-15 : Geometry describing new RADCAL terrain Model

CHAPTER 3

GEOMETRICAL OPTICS FORMULATION OF REFLECTIONS

3.1 Introduction

In a rural or semi-rural propagation environment, natural obstacles such as hills, mountains, or ridge lines can have a significant effect on the propagating radio wave. Many natural terrain features exhibit curved ridge lines in mountainous areas exhibit the features of a long curved cylinder which is essentially infinite in one dimension at high-frequencies. These lines may be the result of the natural formation of the mountain chain or a feature of erosion. Geologically recent mountain chains, while exhibiting sharp edged features, still have electrically large radii of curvature even at HF bands. This indicates that the radius of curvature must be accounted for, in diffraction calculations. In this chapter, we present a developed irregular terrain propagation model based on ray optics. The model consists of modeling the terrain by round earth plateaus, slant flat plateaus, convex and concave plateaus between hills and depression.

3.2 New Propagation Model

Rigourous high frequency approaches to problem of scattering from wedge type diffracting obstacles with curved surfaces involve infinite series and integrals[41] to [44]. And special functions [45][46]. Such techniques are not suitable in a real time propagation model and they require long computation time. However, the accuracy obtained is not justified as the terrain is irregular and cannot be modeled in fine detail. The proposed method use ray optics based on the Geometrical Theory of Reflection from the convex and concave surfaces to calculate Divergence Factor (well known) and Convergence Factor (defined here) from convex and concave surface respectively.

3.3 Divergence Factor

The classical Divergence Factor D is the quantity that represents the spherical shape of the earth in the weakening energy reflected from the surface in the interference region. Kerr D.E. [7] had derived the formula for D both by field strength formulas and by purely geometrical consideration. The geometrical derivation of the Divergence Factor D also suggested by that of Van der Pol and Bremmer [40], who derived the same result as part of an elaborate analysis of diffraction of the waves by a conducting sphere.

Using the same analogy and geometrical theory of diffraction we derive the Divergence Factor for a convex surface as follows;

Figure-3 shows a convex surface and an isotropic source at height r_1 from the centre of convex circle. It is desired to compare the density of the rays in a small cone reflected from the convex surface near the principal point of reflection with the density of the rays of the same cone would have if they were reflected from a plane reflector at the same point. The field strength is proportional to the square root of the ray density. More specifically, D is the square root of the ratio of cross section of the cone after reflection by a plane to reflection from convex surface.

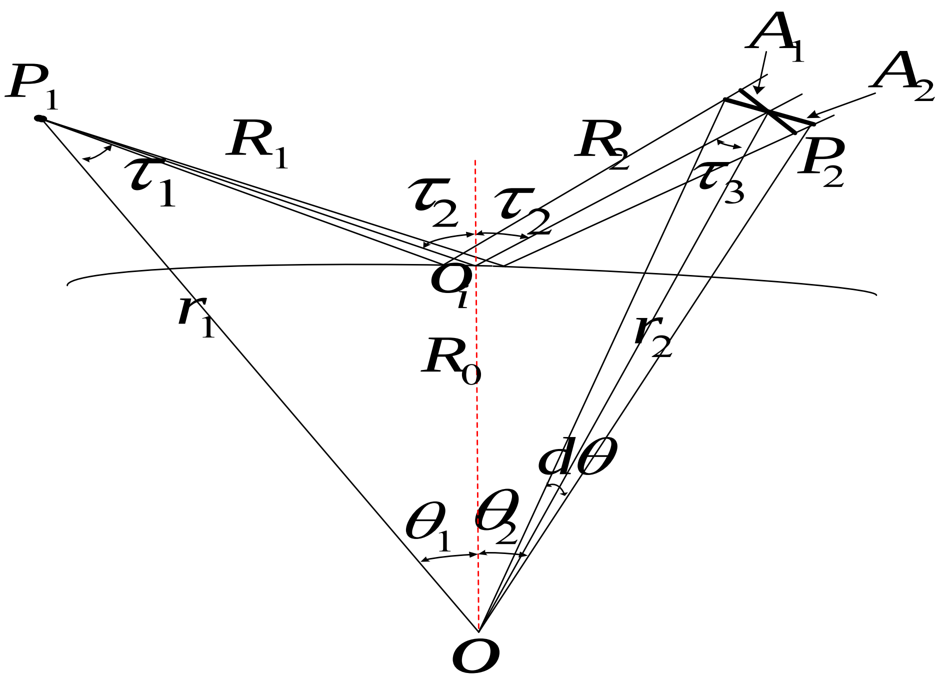

Figure 3-1 : Reflection from a Convex Surface

The cross section of the bundle of the rays leaving the source is $R^2.Sin\tau_1.d\tau_1.d\phi$ where ϕ measured perpendicular to the plane of the paper is R is slant range. After reflection from a plane its cross section would be $(R_1+R_2)^2 Sin\tau_1.d\tau_1.d\phi$, as the rays appear to have traveled a distance R_1+R_2 from the image of the source below the plane tangent at the point of reflection. (See Figure 3-2)

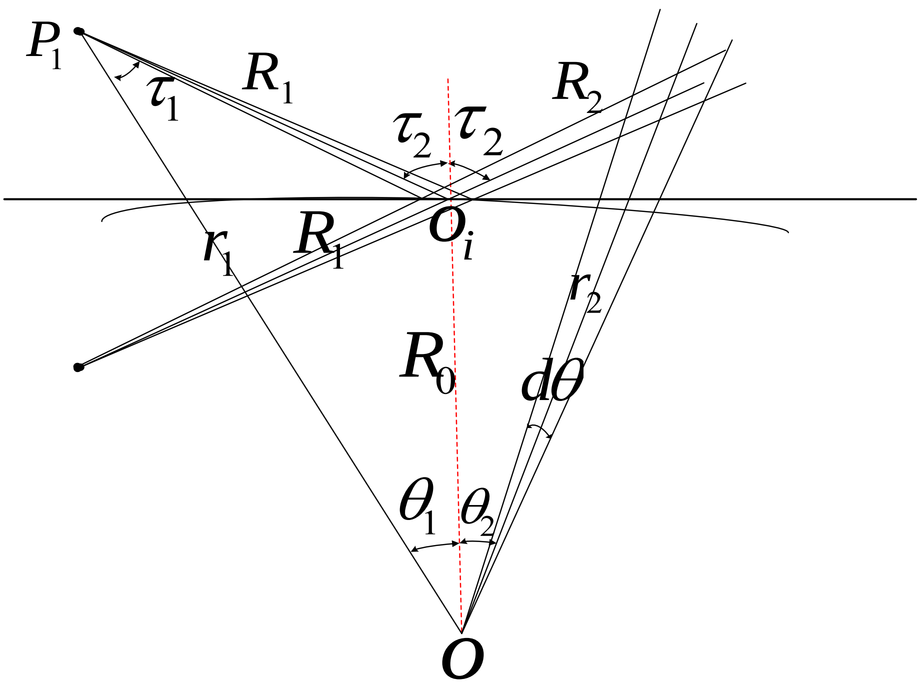

Figure 3-2 : Reflection from a Plane Surface

After reflection from the convex surface the cross section is A_1 of the Figure 3-2:. It is also equal to the $A_2.Cos\tau_3$, where $A_2 = r_2.Sin\,\theta.d\theta.d\phi$. The divergence factor is then given by

$$D = \sqrt{\frac{(R_1+R_2)^2.Sin\,\tau_1.d\tau_1.d\phi}{r_2^{\ 2}.Sin\,\theta.Cos\,\tau_3.d\theta.d\phi}}$$

$$D = \frac{R_1+R_2}{r_2}\sqrt{\frac{Sin\,\tau_1}{Sin\,\theta.Cos\,\tau_3.\frac{d\theta}{d\tau_1}}} \tag{3.1}$$

In order to obtain $d\theta / d\tau_1$, we require several relations that can be obtained from inspection of Figure 3-2:

$$R_0.Sin\,\tau_2 = r_1.Sin\,\tau_1 = r_2.Sin\,\tau_3 \tag{3.2}$$

$$R_1.Sin\tau_1 = R_0.Sin\theta_1 \quad R_2.Sin\tau_3 = R_0.Sin\theta_2 \tag{3.3}$$

$$R_1 = r_1.Cos\tau_1 - R_0.Cos\tau_2 \tag{3.4}$$

$$R_2 = r_2.Cos\tau_3 - R_0.Cos\tau_2 \tag{3.5}$$

$$R_1^{\ 2} = R_0^2 + r_1^2 - 2.R_0.r_1.Cos\theta_1 \tag{3.6}$$

$$R_2^{\ 2} = R_0^2 + r_2^2 - 2.R_0.r_2.Cos\theta_2 \tag{3.7}$$

By manipulating of (3.2) to (3.7) it is easy to show θ can be expressed in terms of $a, r_1, r_2 (z_1 \,\&\, z_2)$ and τ_1. As τ_1 is the only variable quantity, we can then write $d\theta = \frac{\partial\theta}{\partial\tau_1} d\tau_1$ where $\frac{\partial\theta}{\partial\tau_1}$ can be evaluated by differentiation of (3.6) and (3.7) wrt. τ_1 and use (3.3) yields

$$\frac{\partial (R_1)^2}{\partial\tau_1} = 2.R_1.\frac{\partial R_1}{\partial\tau_1} = 2.R_1.r_1.Sin\tau_1.\frac{\partial\theta_1}{\partial\tau_1} \tag{3.8}$$

$$\frac{\partial (R_2)^2}{\partial\tau_1} = 2.R_2.\frac{\partial R_2}{\partial\tau_1} = 2.R_2.r_2.Sin\tau_3.\frac{\partial\theta_2}{\partial\tau_1} \tag{3.9}$$

Then $\frac{\partial\theta}{\partial\tau_1}$ becomes

$$\frac{\partial\theta_1}{\partial\tau_1} + \frac{\partial\theta_2}{\partial\tau_1} = \frac{\partial\theta}{\partial\tau_1} = \frac{1}{r_1.Sin\tau_1}.\frac{\partial R_1}{\partial\tau_1} + \frac{1}{r_2.Sin\tau_3}.\frac{\partial R_2}{\partial\tau_2} \tag{3.10}$$

From (3.2) to (3.5) one can obtain $\frac{\partial R_1}{\partial \tau_1}$ and $\frac{\partial R_2}{\partial \tau_2}$

$$\frac{\partial R_1}{\partial \tau_1} = \frac{Sin\tau_2}{Cos\tau_2}.R_1 = R_1.Tan\tau_2 \tag{3.11}$$

$$\frac{\partial R_2}{\partial \tau_1} = R_2.Cot\tau_1.Tan\tau_2.Tan\tau_3 \tag{3.12}$$

Combination of (3.11) and (3.12) into (3.10) then $\frac{\partial \theta}{\partial \tau_1}$ becomes

$$\frac{\partial \theta}{\partial \tau_1} = \frac{r_2.R_1.Cos\tau_3 + r_1.R_2.Cos\tau_1}{R_0.r_2.Cos\tau_2.Cos\tau_3} \tag{3.13}$$

With the aid of (3.13) the expression Divergence Factor can be calculated as;

$$D = R_0.(R_1 + R_2).\sqrt{\frac{Sin\tau_2.Cos\tau_2}{r_1.r_2.Sin\theta.[2.R_1.R_2 + (R_1 + R_2).R_0.Cos\tau_2]}} \tag{3.14}$$

Kerr's Approximation!

The angle τ_2 is the complement of the grazing angle ψ_2, which is always very small in the region where Divergence Factor has an appreciable effect. Hence we write $Sin\tau_2 = Cos\psi_2 \approx 1$ and $Cos\tau_2 = Sin\psi_2$. Then if we make some simplification in (3.14) and assuming ranges are so small that $R_0.Sin\theta = R_0.\theta = R_1 + R_2$ Divergence Factor becomes;

$$D \approx \frac{1}{\sqrt{\frac{2.R_1.R_2}{R_0.(R_1 + R_2).Sin\ \tau_2} + 1}} \tag{3.15}$$

3.4 Convergence Factor

The Convergence Factor C is the quantity that in the interference region represents the concave parts of the earth in strengthening the energy reflected from the surface. It is meaningful to derive the formula for C from purely geometrical consideration like the Divergence Factor. For concave surfaces, the reflected rays converge and intersect. Such an intersection point is called a caustic point, and the locus of such points are called the caustic surface of the ray system. The amplitude in GO is infinite at caustic points (See Figure 3-3).

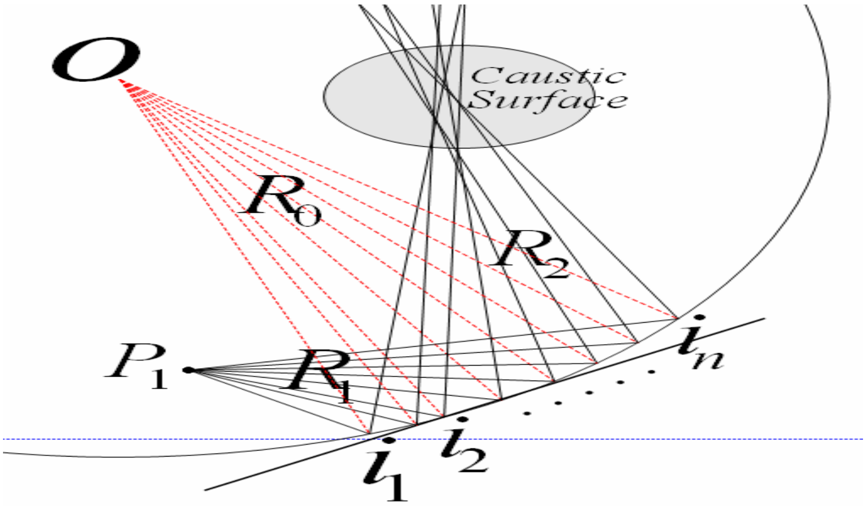

Figure 3-3 : Caustic Condition Geometry

The intensity of the light is increased near a caustic. Caustics can be produced by reflection, as here, or by refraction, in a variety of ways (See Figure 3-4).

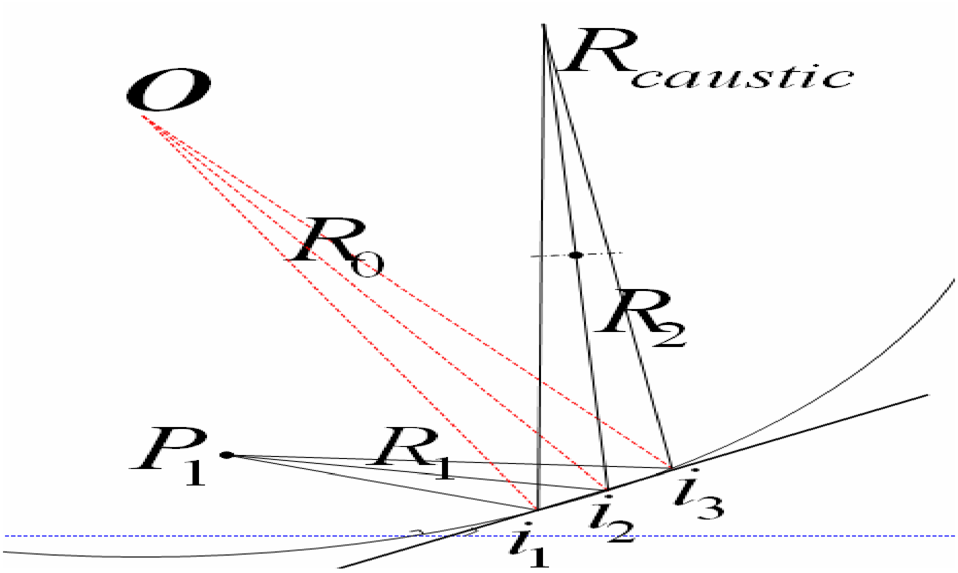

Figure 3-4 : Caustic Condition Geometry

Figure 3-5 shows cross section of the earth with a concave surface on it and an isotropic source at height r_1 from the centre of the concave circle. It is desired to compare the density of a small cone reflected from the concave surface near the principal point of reflection with the density of the rays of the same cone would have if they were reflected from a plane reflector at the same point. The field strength is proportional to the square root of the ray density. More specifically, Convergent factor is the square root of the ratio of cross section of the cone after reflection by a plane to reflection from concave surface.

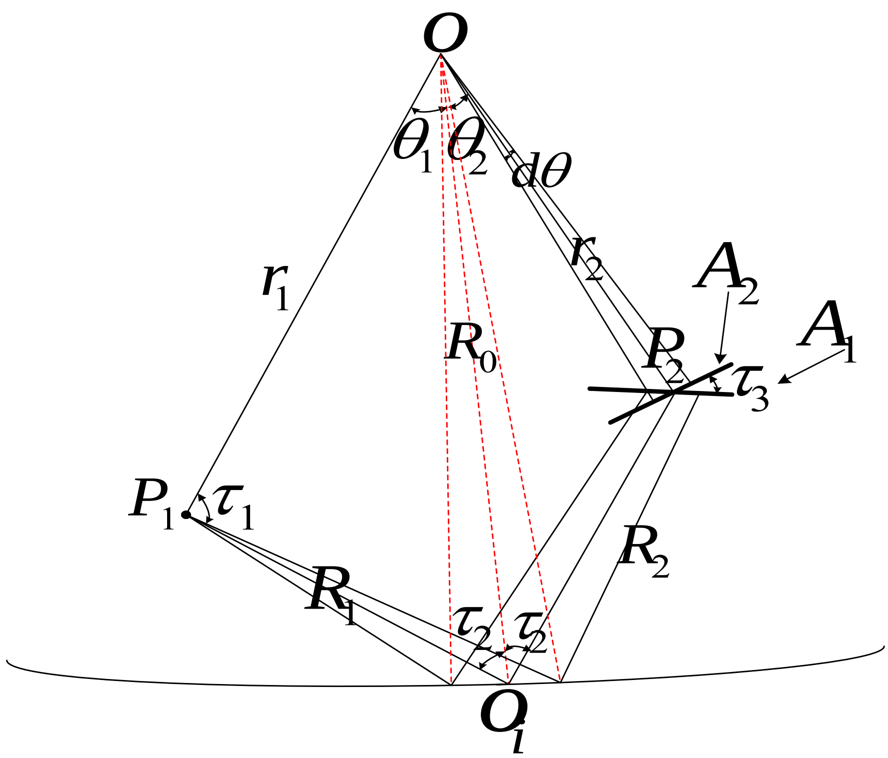

Figure 3-5 : Reflection from a Concave Surface

The cross section of the bundle of the rays leaving the source is $R^2.Sin\ \tau_1.d\tau_1.d\phi$ where ϕ measured perpendicular to the plane of the paper is and R is slant range. After reflection from a plane its cross section would be $(R_1 + R_2)^2.Sin\tau_1.d\tau_1.d\phi$, as the rays appear to have traveled a distance $R_1 + R_2$ from the image of the source below the plane tangent at the point of reflection (See Figure 3-6).

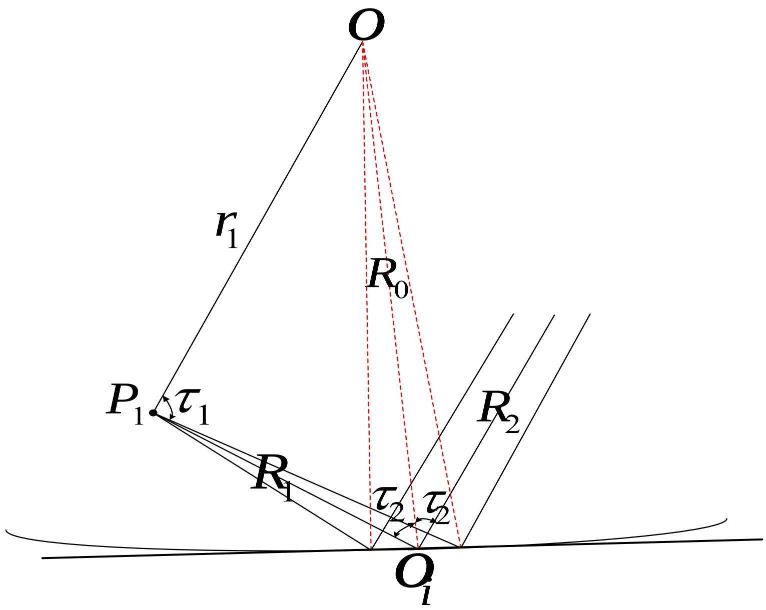

Figure 3-6 :. Reflection from a Plane Surface

After reflection from the concave surface the cross section is A_1 of the Figure 3-5. It is also equal to the $A_2.Cos\,\tau_3$, where $A_2 = r_2.Sin\ \theta.d\theta.d\phi$. The convergence factor is then given by

$$C = \sqrt{\frac{(R_1 + R_2)^2.Sin\ \tau_1.d\tau_1.d\phi}{r_2{}^2.Sin\ \theta.Cos\ \tau_3.d\theta.d\phi}}$$

$$C = \frac{R_1 + R_2}{r_2}\sqrt{\frac{Sin\ \tau_1}{Sin\ \theta.Cos\ \tau_3.\dfrac{d\theta}{d\tau_1}}} \tag{3.16}$$

In order to obtain $d\theta / d\tau_1$, we require several relations that can be obtained from inspection of Figure 3-6:

$$R_0.Sin\ \tau_2 = r_1.Sin\ \tau_1 = r_2.Sin\ \tau_3 \tag{3.17}$$

$$R_1.Sin\tau_1 = R_0.Sin\theta_1 \qquad R_2.Sin\tau_3 = R_0.Sin\theta_2 \tag{3.18}$$

$$R_1 = r_1.Cos\tau_1 + R_0.Cos\tau_2 \tag{3.19}$$

$$R_2 = r_2.Cos\tau_3 + R_0.Cos\tau_2 \tag{3.20}$$

$$R_1{}^2 = R_0^2 + r_1^2 - 2.R_0.r_1.Cos\theta_1 \tag{3.21}$$

$$R_2{}^2 = R_0^2 + r_2^2 - 2.R_0.r_2.Cos\theta_2 \tag{3.22}$$

By manipulation of (3.17) to (3.22) it is easy to show θ can be expressed in terms of $a, r_1, r_2(z_1 \;\&\; z_2)$ and τ_1. As τ_1 is the only variable quantity, we can write $d\theta = \frac{\partial\theta}{\partial\tau_1} d\tau_1$ where $\frac{\partial\theta}{\partial\tau_1}$ can be evaluated by differentiation of (3.21) and (3.22) wrt. τ_1 and use (3.18)

$$\frac{\partial(R_1)^2}{\partial\tau_1} = 2.R_1.\frac{\partial R_1}{\partial\tau_1} = 2.R_1.r_1.Sin\tau_1.\frac{\partial\theta_1}{\partial\tau_1} \tag{3.23}$$

$$\frac{\partial(R_2)^2}{\partial\tau_1} = 2.R_2.\frac{\partial R_2}{\partial\tau_1} = 2.R_2.r_2.Sin\tau_3.\frac{\partial\theta_2}{\partial\tau_1} \tag{3.24}$$

Then $\frac{\partial\theta}{\partial\tau_1}$ becomes

$$\frac{\partial\theta_1}{\partial\tau_1} + \frac{\partial\theta_2}{\partial\tau_1} = \frac{\partial\theta}{\partial\tau_1} = \frac{1}{r_1.Sin\tau_1}.\frac{\partial R_1}{\partial\tau_1} + \frac{1}{r_2.Sin\tau_3}.\frac{\partial R_2}{\partial\tau_2} \tag{3.24}$$

From (3.17) to (3.22) one can obtain $\frac{\partial R_1}{\partial\tau_1}$ and $\frac{\partial R_2}{\partial\tau_2}$

$$\frac{\partial R_1}{\partial\tau_1} = \frac{Sin\tau_2}{Cos\tau_2}.R_1 = R_1.Tan\tau_2 \tag{3.25}$$

$$\frac{\partial R_2}{\partial\tau_1} = R_2.Cot\tau_1.Tan\tau_2.Tan\tau_3 \tag{3.26}$$

Combination of (3.25) and (3.26) into (3.24) then $\frac{\partial\theta}{\partial\tau_1}$ becomes

$$\frac{\partial\theta}{\partial\tau_1} = \frac{r_2.R_1.Cos\tau_3 + r_1.R_2.Cos\tau_1}{R_0.r_2.Cos\tau_2.Cos\tau_3} \tag{3.27}$$

With the aid of (15) the expression Convergence Factor can be calculated as;

$$C = R_0.(R_1 + R_2).\sqrt{\frac{Sin\tau_2.Cos\tau_2}{r_1.r_2.Sin\theta.[2.R_1.R_2 - (R_1 + R_2).R_0.Cos\tau_2]}} \tag{3.28}$$

Kerr's Approximation!

Same as above the angle τ_2 is the complement of the grazing angle ψ_2, which is always very small in the region where Convergence Factor has an appreciable effect. Hence we write $Sin\tau_2 = Cos\psi_2 \approx 1$ and $Cos\tau_2 = Sin\psi_2$. Then if we make some simplification in (3.28) and assuming ranges are so small that $R_0.Sin\theta = R_0.\theta = R_1 + R_2$ Convergence Factor becomes;

$$C \approx \frac{1}{\sqrt{\frac{2.R_1.R_2}{R_0.(R_1 + R_2).Sin\tau_2} - 1}} \tag{3.29}$$

Comparing equation (3.28) and (3.9) with Equation (3.14) and (3.15), we notice the sign change as only the diffrences between the Divergence and Convergence Factor.

When the radius R_0 is large and the source point is sufficiently away from the surface the caustic occurs very close to the surface and rays diverge again, similar to convex surface.

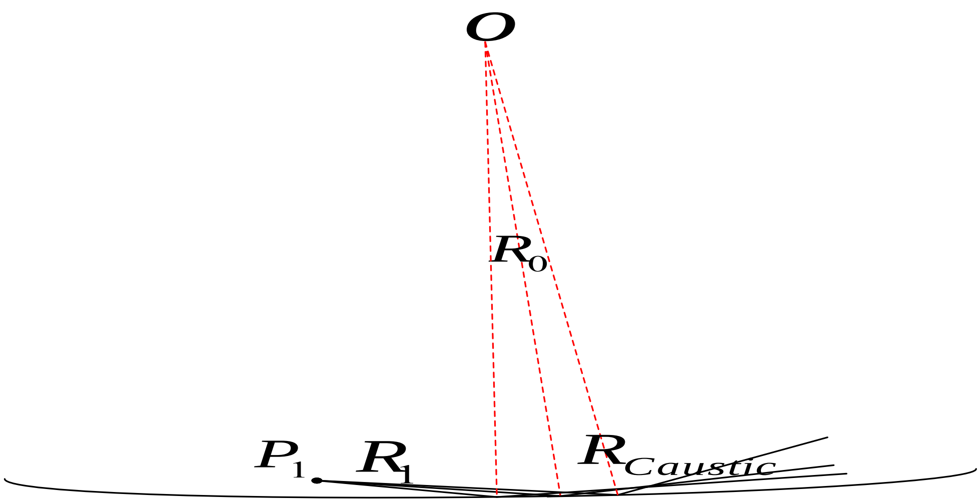

Figure-3.7 : Reflection from Convex Surface

3.5 Reflection from Convex Slant Plateau

We must find the specular reflection points Q 's between radar and target and their first order contributions to calculate reflection coefficient, which is required to calculate the path propagation factor. For convex plateaus it is difficult to calculate the specular reflection points Q 's directly due to the complexity of equation. We use Bisection Method and geometrical optics principle for finding the specular reflection points on convex surface.

Derivation of algorithms by using Figure 3.8 are as follows;

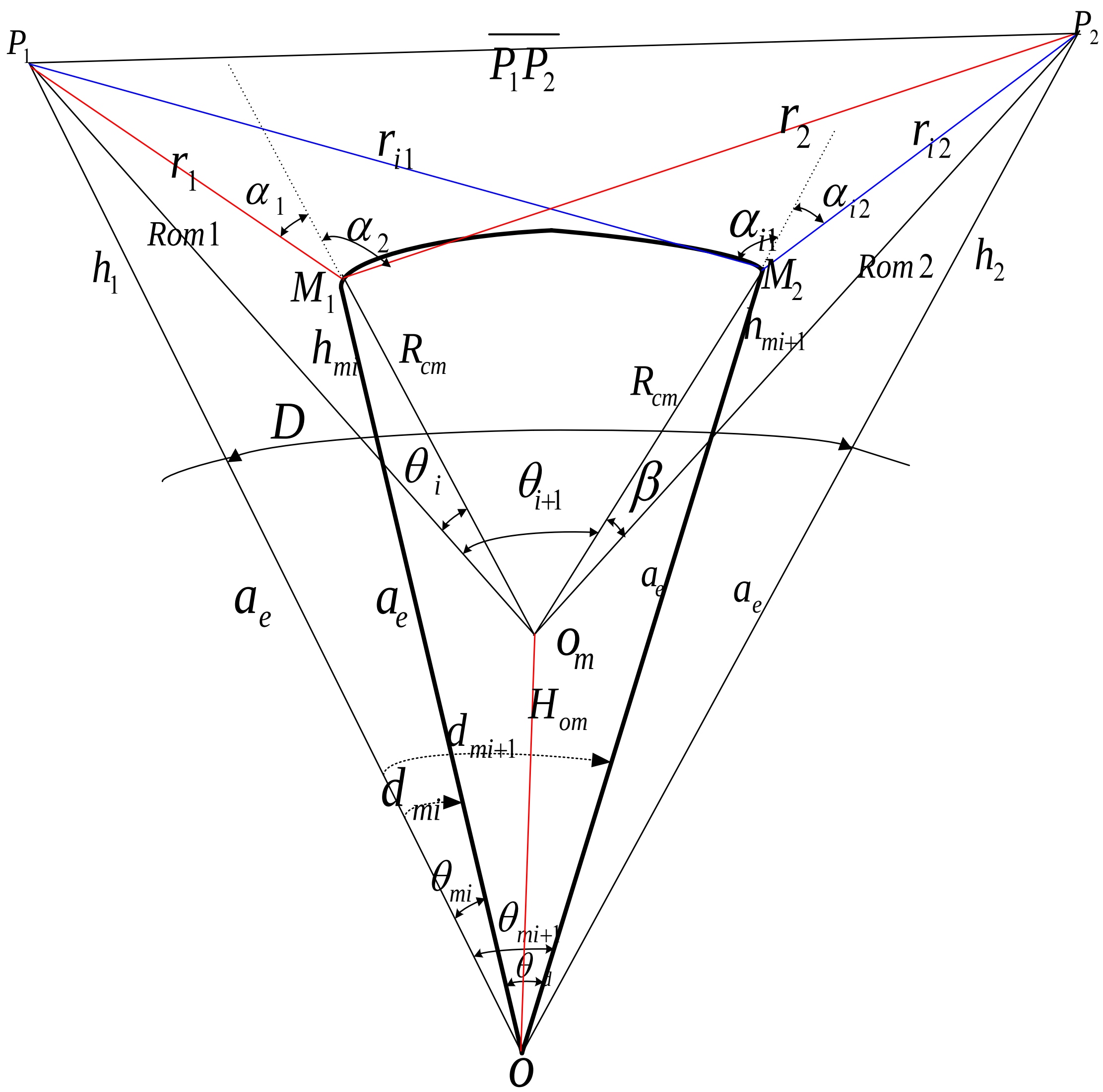

Figure-3.8 : Reflection from Convex Surface

In this figure, radius of the convex surface R_{cm} is input parameter, a_e is effective earth radius, θ_{om} ($P_1\hat{O}O_m$ angle) and the distance H_{om} ($\overline{OO_m}$) are calculated in the program.

$$R_{om1}{}^2 = (a_e + h_1)^2 + (H_{om})^2 - 2.(a_e + h_1).H_{om}.Cos(\theta_{om}) \quad (3.30)$$

$$R_{om2}{}^2 = (a_e + h_2)^2 + (H_{om})^2 - 2.(a_e + h_2).H_{om}.Cos(\theta_d - \theta_{om}) \quad (3.31)$$

$$r_1{}^2 = (a_e + h_1)^2 + (a_e + h_{m,i})^2 - 2.(a_e + h_1).(a_e + h_{m,i}).Cos(\theta_{m,i}) \quad (3.32)$$

$$r_1^2 = R_{cm}{}^2 + R_{om1}{}^2 - 2.R_{cm}.R_{0m1}.Cos\theta_i \quad (3.33)$$

$$\theta_i = Cos^{-1}\left(\frac{r_1{}^2 + R_{cm}{}^2 - R_{om1}{}^2}{2.R_{cm}.R_{om1}}\right) \quad (3.34)$$

At triangle $P_1M_1O_m$ the angle $P_1\hat{M}_1O_m$

$$\alpha_1 = \pi - Cos^{-1}\left(\frac{r_1{}^2 + R_{cm}{}^2 - R_{om1}{}^2}{2.r_1.R_{cm}}\right) \quad (3.35)$$

At triangle $O_m\overset{\Delta}{M}_1P_2$

$$\alpha_2 = \pi - Cos^{-1}\left(\frac{r_2{}^2 + R_{cm}{}^2 - R_{om2}{}^2}{2.r_2.R_{cm}}\right) \quad (3.36)$$

By similar process r_{i1} from triangle P_1OM_1

$$r_{i1}{}^2 = (a_e + h_1)^2 + (a_e + h_{m,i+1})^2 - 2.(a_e + h_1).(a_e + h_{m,i+1}).Cos(\theta_{m,i+1}) \quad (3.37)$$

At triangle $P_1M_2O_m$

$$r_{i1}{}^2 = R_{om1}{}^2 + R_{cm}{}^2 - 2.R_{om1}.R_{cm}.Cos(\theta_{i+1}) \quad (3.38)$$

$$\theta_{i+1} = Cos^{-1}\left(\frac{R_{om1}{}^2 + R_{cm}{}^2 - r_{i1}{}^2}{2.R_{om1}.R_{cm}}\right) \quad (3.40)$$

At triangle $P_1\overset{\Delta}{M}_2O_m$

$$\alpha_{i1} = \pi - Cos^{-1}\left(\frac{r_{i1}^{\ 2} + R_{cm}^{\ 2} - R_{om1}^{\ 2}}{2.r_{i1}.R_{cm}}\right) \tag{3.41}$$

At triangle $O_m\overset{\Delta}{M}_2P_2$

$$\alpha_{i2} = \pi - Cos^{-1}\left(\frac{r_{i2}^{\ 2} + R_{cm}^{\ 2} - R_{om2}^{\ 2}}{2.r_{i2}.R_{cm}}\right) \tag{3.42}$$

At $O_m\overset{\Delta}{P_2}M_2$ triangle

$$\beta = Cos^{-1}\left(\frac{R_{cm}^{\ 2} + R_{om2}^{\ 2} - r_{i2}^{\ 2}}{2.R_{cm}.R_{om2}}\right) \tag{3.43}$$

After this derivation we calculates α_1 and α_2 along the convex surface arc. If we can find any point where α_1 and α_2 are equal then this point is our specular reflection point Q.

3.6 Reflection from Concave Surface

We must find the specular reflection points Q 's between radar and target and their first order contributions to calculate reflection coefficient which is required to calculate the path propagation factor. For concave plateaus it is difficult to calculate the specular reflection points Q 's directly due to the complexity of equation. We use Bisection Method and geometrical optics principle for finding the specular reflection points on concave surface.

Derivation of algorithms by using Figure 3.9 are as follows;

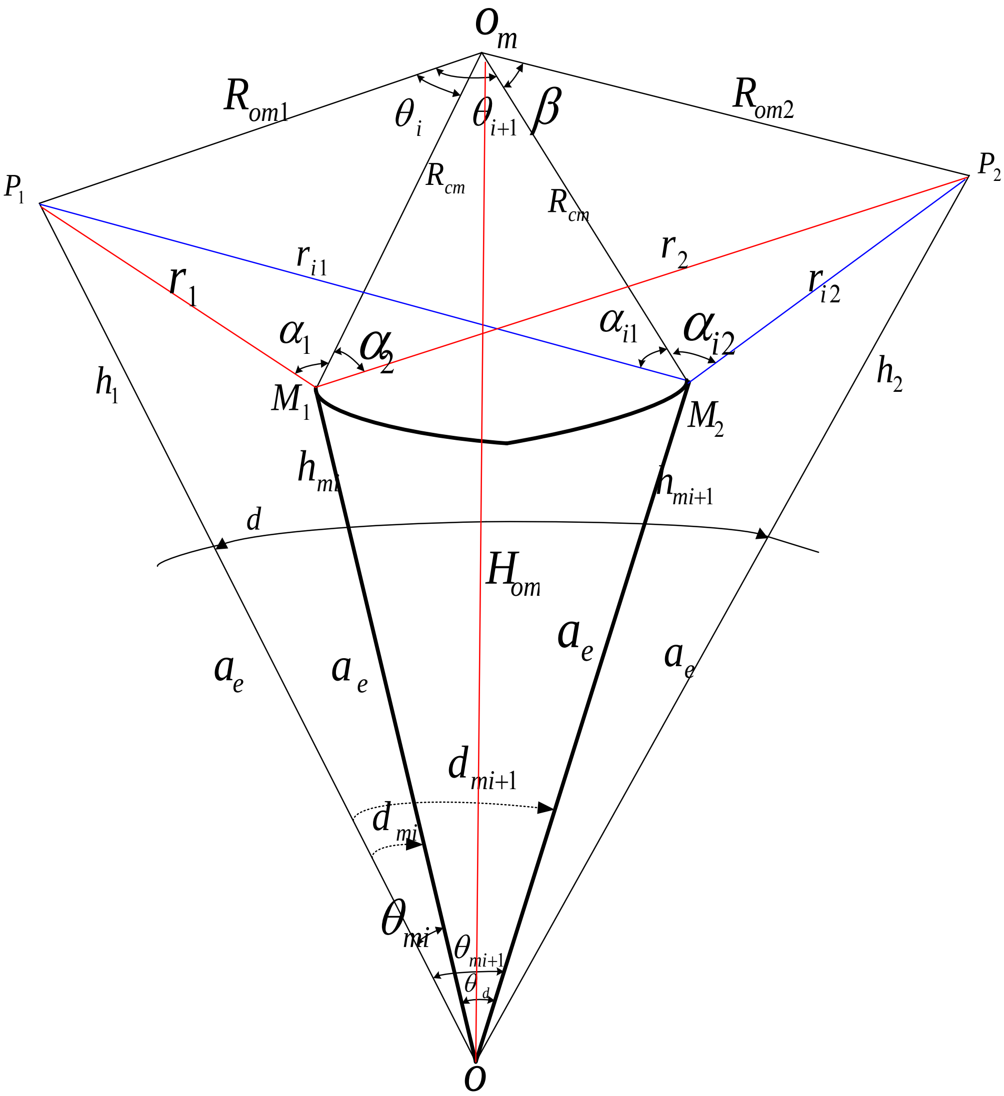

Figure-3.9 : Reflection from Concave Surface

In this figure, radius of the concave surface R_{cm} is input parameter, a_e is effective earth radius, θ_{om} ($P_1\hat{O}O_m$ angle) and the distance H_{om} ($\overline{OO_m}$) are calculated in the program.

$$R_{om1}{}^2 = (a_e + h_1)^2 + (H_{om})^2 - 2.(a_e + h_1).H_{om}.Cos(\theta_{om}) \tag{3.44}$$

$$R_{om2}{}^2 = (a_e + h_2)^2 + (H_{om})^2 - 2.(a_e + h_2).H_{om}.Cos(\theta_d - \theta_{om}) \tag{3.45}$$

$$r_1{}^2 = (a_e + h_1)^2 + (a_e + h_{m,i})^2 - 2.(a_e + h_1).(a_e + h_{m,i}).Cos(\theta_{m,i}) \tag{3.46}$$

$$r_1{}^2 = R_{cm}{}^2 + R_{om1}{}^2 - 2.R_{cm}.R_{om1}.Cos\theta_i \tag{3.47}$$

$$\theta_i = Cos^{-1}\left(\frac{r_1{}^2 + R_{cm}{}^2 - R_{om1}{}^2}{2.R_{cm}.R_{om1}}\right) \tag{3.48}$$

At triangle $P_1M_1O_m$ the angle $P_1\hat{M}_1O_m$

$$\alpha_1 = Cos^{-1}\left(\frac{r_1{}^2 + R_{cm}{}^2 - R_{om1}{}^2}{2.r_1.R_{cm}}\right) \tag{3.49}$$

At triangle $O_m\overset{\Delta}{M}_1P_2$

$$\alpha_2 = Cos^{-1}\left(\frac{r_2{}^2 + R_{cm}{}^2 - R_{om2}{}^2}{2.r_2.R_{cm}}\right) \tag{3.50}$$

By similar process r_{i1} from triangle P_1OM_1

$$r_{i1}{}^2 = (a_e + h_1)^2 + (a_e + h_{m,i+1})^2 - 2.(a_e + h_1).(a_e + h_{m,i+1}).Cos(\theta_{m,i+1}) \tag{3.51}$$

At triangle $P_1M_2O_m$

$$r_{i1}{}^2 = R_{om1}{}^2 + R_{cm}{}^2 - 2.R_{om1}.R_{cm}.Cos(\theta_{i+1}) \tag{3.52}$$

$$\theta_{i+1} = Cos^{-1}\left(\frac{R_{om1}{}^2 + R_{cm}{}^2 - r_{i1}{}^2}{2.R_{om1}.R_{cm}}\right) \tag{3.53}$$

At triangle $P_1\overset{\Delta}{M}_2O_m$

$$\alpha_{i1} = Cos^{-1}\left(\frac{r_{i1}^{\;2} + R_{cm}^{\;2} - R_{om1}^{\;2}}{2.r_{i1}.R_{cm}}\right) \tag{3.54}$$

At triangle $O_m\overset{\Delta}{M}_2P_2$

$$\alpha_{i2} = Cos^{-1}\left(\frac{r_{i2}^{\;2} + R_{cm}^{\;2} - R_{om2}^{\;2}}{2.r_{i2}.R_{cm}}\right) \tag{3.55}$$

At $O_m\overset{\Delta}{P}_2M_2$ triangle

$$\beta = Cos^{-1}\left(\frac{R_{cm}^{\;2} + R_{om2}^{\;2} - r_{i2}^{\;2}}{2.R_{cm}.R_{om2}}\right) \tag{3.56}$$

As you can see we derive same algorithms in reflection from convex surface. After this derivation we calculate α_1 and α_2 along the concave surface arc. If we can find any point where α_1 and α_2 are equal then this point is our specular reflection point Q.

CHAPTER 4

VERIFICATION OF PRESENT METHOD

4.1 Introduction

In chapter 3, we have presented an irregular terrain propagation model based on ray optics. In this chapter, numerical and geometrical verification of the present method is given.

4.2 Geometrical Verification of Methods

4.2.1 Divergence Factor

Divergence Factor derived in this paper is in exact agreement with the results of Keller's formula [5] which is based upon GO expansion of the exact solution of the Kerr. Keller applied a cylindrical wave to smooth conducting convex surface. When the medium is homogeneous, the incident rays are straight lines emanating from the source P of the incident cylindrical wave. Each incident ray which hits the cylinder gives rise to a reflected ray according to the law of reflection.

He used the optical form of the principle of conservation of energy which states that the flux of energy is proportional to the square of the field amplitude multiplied by the cross-sectional area of the tube in a steady-state condition. The field associated with an incident ray at a point with co-ordinate p is,

$$u_{inc} \approx \frac{A_0}{\sqrt{p}} e^{jkp} \tag{4.1}$$

In order to determine the field associated with a reflected ray, it is necessary to know the field on the incident ray and the conditions to be satisfied at the reflecting surface. We must now impose the boundary condition that the field vanishes at the surface. Then at the surface, the reflected field is the negative of the incident field. Therefore, at the surface the amplitudes of the reflected and incident fields are the same. However, the phase of the reflected field differs from that of the incident field by π. The amplitude of the reflected field $A(s)$ at a distance s from the surface along a reflected ray can be found as (See Figure 4-1)

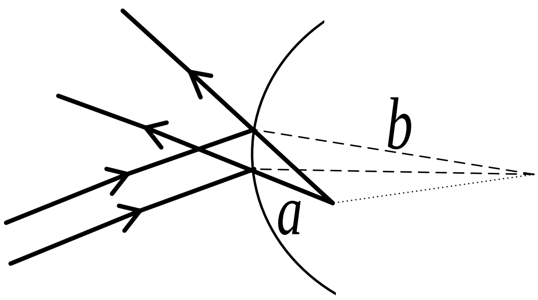

Figure 4-1 : The Reflected Rays from Convex Surface

$$A(s) = \frac{A_0}{\sqrt{p'}}(1 + a^{-1}s)^{-1/2} \tag{4.2}$$

In (4.2) p' is the distance from the source to the point of reflection and A_0 denotes the amplitude on the ray at unit distance from the source, b is radius of curvature of the cylinder at reflection point.

Before (4.2) can be used, the distance a must be determined. To find a we note that neighboring normal to the reflecting surface meet at a distance b from the surface, and b is called the radius of curvature of the surface at the point under consideration. For an incident plane wave any two neighboring incident rays are parallel. If they make the angle ϕ with the two neighbouring normal, then $a = \frac{b}{2}Cos\phi$ (See Figure 4-2). This value of 'a' is the focal length of the reflector for the particular point and angle of incidence considered. Now for an incident cylindrical wave we have from the mirror law of optics [37].

$$\frac{1}{a} = \frac{1}{p'} + \frac{2}{bCos\,\phi} \tag{4.3}$$

The reflected field can now be obtained as;

$$u_{ref} \approx \frac{A_0}{\sqrt{p'}}(1+\frac{2s}{b.\cos\phi}+\frac{s}{p'})^{-1/2} e^{jk(p'+s)} \tag{4.4}$$

where ϕ is the angle of incident on the cylinder. Then by using the same analogy in Section 3.3, the Divergence factor can be expressed as;

$$D = \frac{\text{Reflected Field from Flat Surface}}{\text{Reflected Field from Convex Surface}} = \frac{U_{ref\ /\ flat}}{U_{ref}} \tag{4.5}$$

where the reflected field from flat surface can be expressed as

$$u_{ref\ /\ flat} = \frac{A_0}{\sqrt{p'+s}} e^{jk(p'+s)} \tag{4.6}$$

Finally Divergence Factor D is

$$D = \frac{\sqrt{p'}}{\sqrt{p'+s}}(1+\frac{2s}{b.\cos\phi}+\frac{s}{p'})^{1/2} \tag{4.7}$$

4.2.2 Convergence Factor

From the symmetry of the Divergence Factor found by Keller for convex surface we can define a Convergent Factor for concave surface as follows(See Figure 4-2);

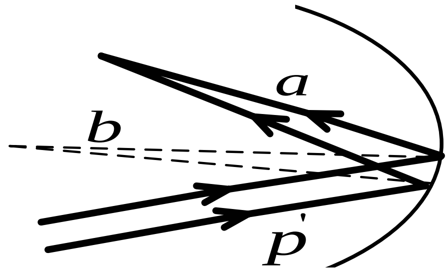

Figure 4-2 : The Reflected Rays from Concave Surface

$$C = \frac{\text{Reflected Field from Flat Surface}}{\text{Reflected Field from Concave Surface}} = \frac{U_{ref/flat}}{U_{ref}} \tag{4.8}$$

The amplitude of the reflected field at reflection point by using the energy principle

$$A(s) = \frac{A_0}{\sqrt{p'}}(1 + a^{-1}s)^{-1/2} \tag{4.9}$$

We know that the Law of Optics for the convex surface is;

$$\begin{matrix}\text{The reciprocal of} \\ \text{the image distance}\end{matrix} = \begin{matrix}\text{The reciprocal of} \\ \text{the object distance}\end{matrix} + \begin{matrix}\text{The reciprocal of} \\ \text{the focal length}\end{matrix}$$

or

$$\frac{1}{a} = \frac{1}{p'} + \frac{1}{f} \quad \text{where} \quad f = \frac{b}{2}Cos\phi \tag{4.10}$$

The focal length and object must be in the same plane so we multiply $\frac{b}{2}$ by $Cos\phi$.

In spherical surface, focal length is equal to the half of the radius of the curvature. Moreover, focal length and image length are negative for convex surface.

$$-\frac{1}{f}=-\frac{1}{a}+\frac{1}{p'} \quad \text{then} \quad \frac{1}{a}=\frac{1}{f}+\frac{1}{p'} \tag{4.11}$$

Keller used this equation for smooth convex surface. However, for concave surface both focal length and image distance are positive then (4.10) becomes

$$\frac{1}{f}=\frac{1}{a}+\frac{1}{p'} \quad \text{then} \quad \frac{1}{a}=\frac{1}{f}-\frac{1}{p'} \quad \text{where} \quad f=\frac{b}{2}Cos\phi \tag{4.12}$$

The amplitude of the reflected field at point S becomes

$$A(s)=\frac{A_0}{\sqrt{p'}}(1+\frac{2s}{b.\cos\phi}-\frac{s}{p'})^{-1/2} \tag{4.13}$$

So that reflected field from concave surface is

$$u_{ref} \approx \frac{A_0}{\sqrt{p'}}(1+\frac{2s}{b.\cos\phi}-\frac{s}{p'})^{-1/2}e^{jk(p'+s)} \tag{4.14}$$

Finally, Convergent Factor is

$$C=\frac{\sqrt{p'}}{\sqrt{p'+s}}(1+\frac{2s}{b.\cos\phi}-\frac{s}{p'})^{1/2} \tag{4.15}$$

For the present application we generalize the Keller techniques for the imperfect ground by weighting the reflected field from a perfect conductor by the Fresnel coefficient for an imperfect conductor.

4.3 Numerical Verification of Methods

We put the numerical values for parameter in the equation of Divergent Factor and Convergent Factor both in sections 4.2.1 and 4.2.2 with in section 3.3 and 3.4. We compare the results. They are nearly equal to each other.

In order to verify the formulation, we have inserted the Divergence Factor and Convergence Factor into the RADCAL program. We choose terrains which have convex or concave plateaus in them. Then we compared the output of the RADCAL with measured values and another propagation program spectrally accelerated forward-backward (FBSA).

In order to assess the accuracy of the RADCAL as well as to demonstrate its consistency with measurements, comparisons of RADCAL results with measurements are shown in Figures 4.3 to 4.12. The terrain profiles are from Denmark with lengths up to 8 km. The height variations are of the order 20–50 m. Measured data were obtained by Hviid et al. [46] using a dipole with a transmitted power of 10 W and a gain of 8 dBi. The transmitter height is 10.4 m. The receiver antenna is $\lambda/4$ a monopole on top of a van with a height of 2.4 m. Having no exact information about the vegetation and electrical properties of terrains, the surface impedances are taken as $\eta_s = 20.2 + j8.1\Omega$ in order to handle some small forests and other land cover data along the profiles [46]. This method neglects the backscattering for the terrain profiles in Figures. 4.3 and 4.8. A study concerning the effects of fine details of terrain is also studied. This work reveals the significant features of a terrain and suggest ways of smoothing a very detailed terrain profile.Smoothed Hadsund and Jerslev terrain profiles are in Figure 4.4 and Figure 4.9 respectively.

In Figure 4.5, the results for 435 MHz operating frequency are presented over Hadsund terrain profile, while the comparisons over Jerslev profile for 970 MHz are shown in Figure 4.10. Both figures show the very good agreement of the RADCAL results with the measurements. Therefore, the RADCAL can safely be used as a reference solution to test the accuracy of the prediction of various propagation models.

In these examples we don’t know the structure of the reflection surface exactly. So we predict rough surface coefficient and vegetation coefficient for these terrain profile roughly and use them in our calculation. Consequently, in some examples RADCAL results are at most 5 dB higher then the measured values. We explain this shift by our overestimate of the

Fresnel Reflection Ceofficient and the hill-top diffraction coefficient for the real terrain. So we make normalization to compare the RADCAL results with other. In RADCAL we use Ament's Formula to calculate the reflection coefficient and we also consider the vegetation effect. Rough surface scattering and diffraction formulas overestimate the actual values and consequently they provide rather optimistic path loss values. They shold be lower by empirical formulas for various terrain surfaces.

Then the RADCAL results have compared with another propagation program (IE method) which use the spectrally accelerated forward-backward (FBSA) method as a benchmark solution[45]. FBSA results are obtained from C. A. Tunç, A. Altintaş and V.B. Ertürk from Bilkent University. Propagation over large scale terrain profiles (Jerslev and Hudsand Terrain Profiles) are investigated and the results are compared in Figure 4.6 to Figure 4.9 and Figure 4.11 to Figure 4.12.

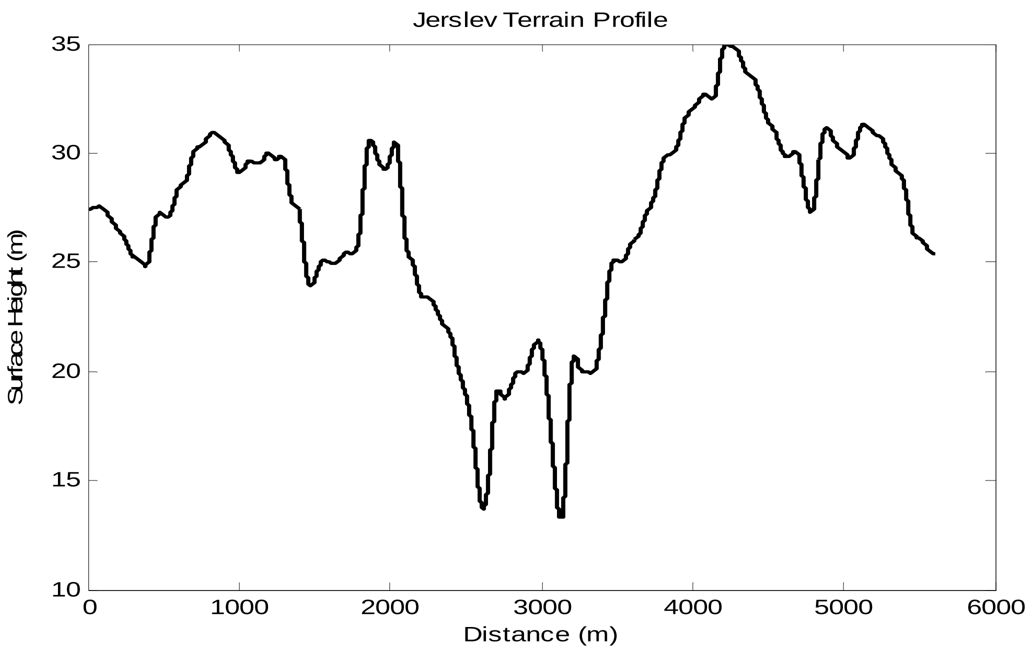

Figure 4-3 : Jerslev Terrain Profile

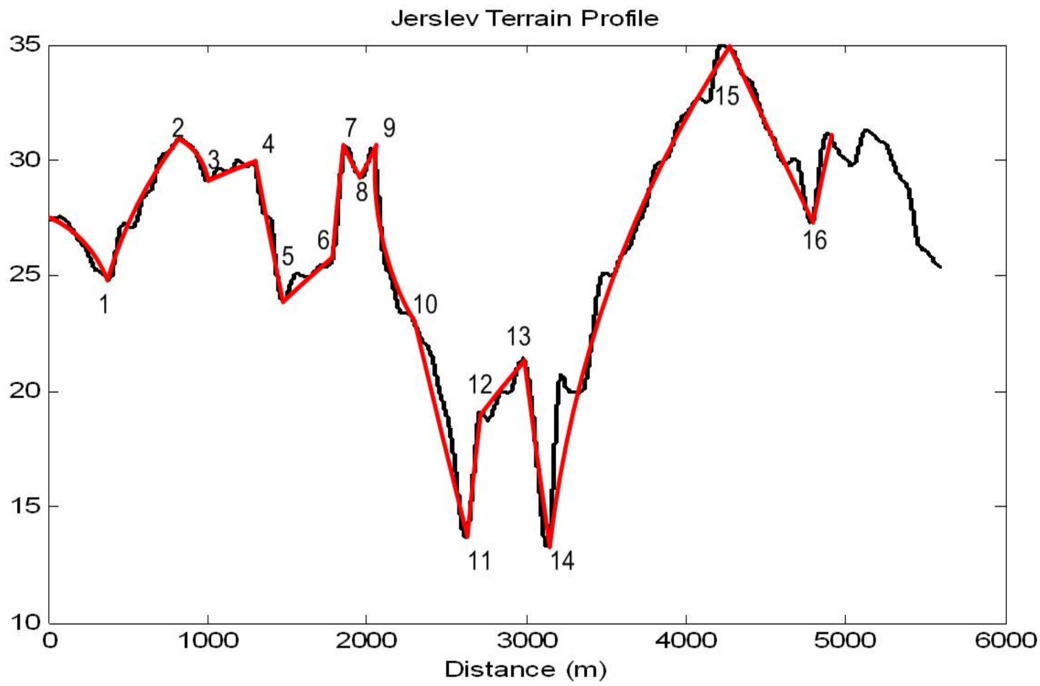

Figure 4-4 : Smoothed Jerslev Terrain Profile

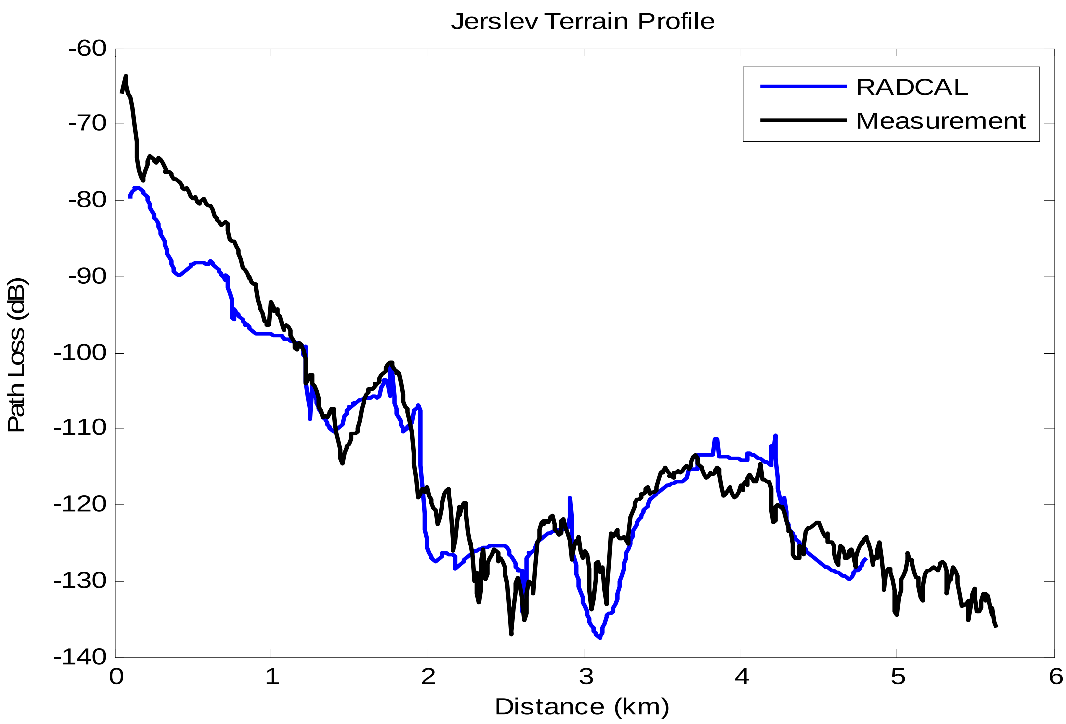

Figure 4-5 : Comparasion of RADCAL Result and Measurement Data

Figure 4-6 : Comparasion of RADCAL and FBSA Results

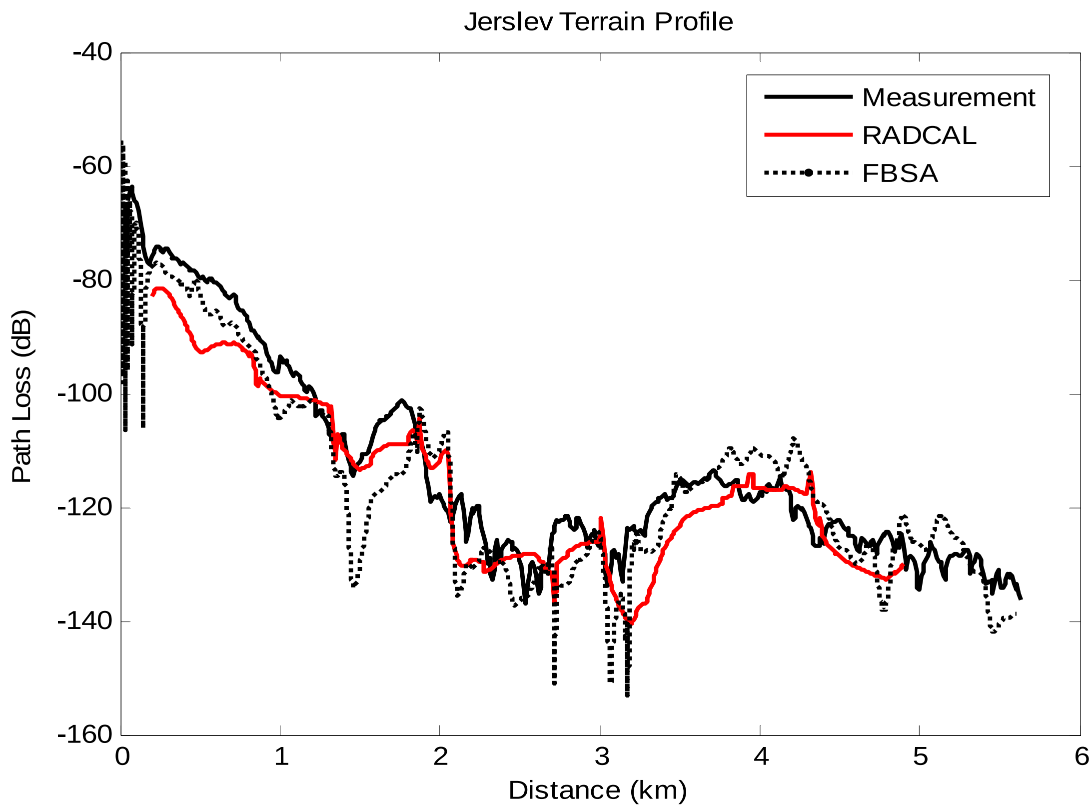

Figure 4.7 : Comparasion of RADCAL, FBSA Results and Measurement Data

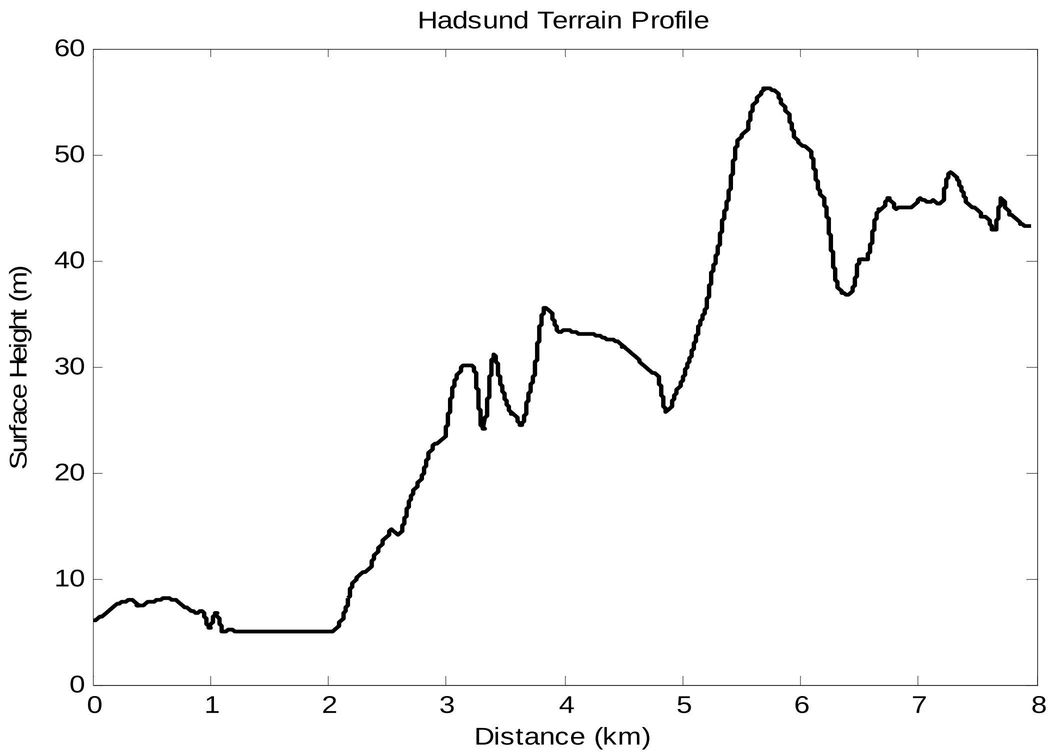

Figure 4.8 : Hadsund Terrain Profile

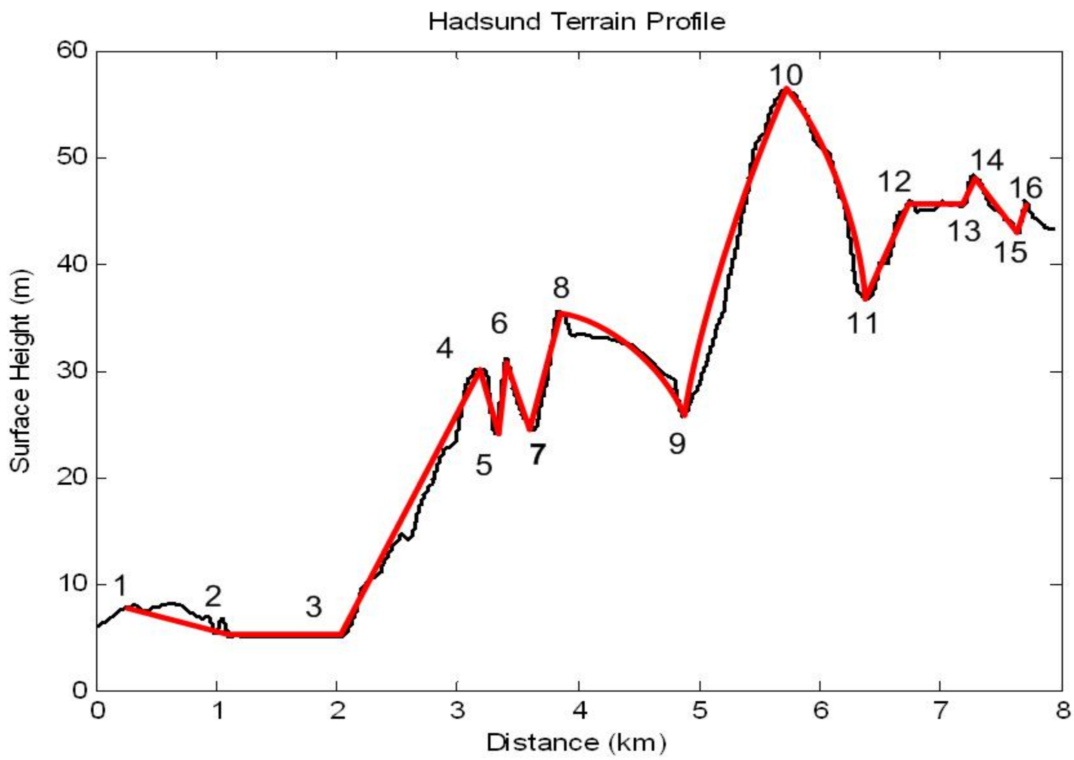

Figure 4-9 : Smoothed Jerslev Terrain Profile

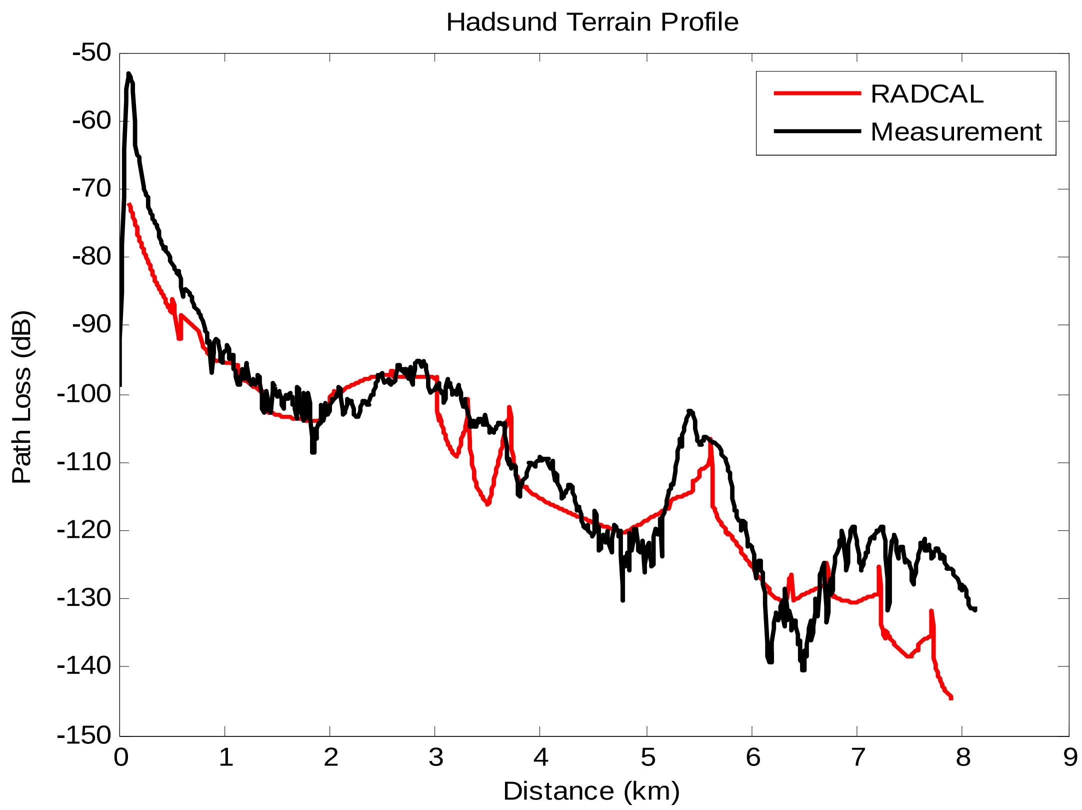

Figure 4.10 : Comparasion of RADCAL Result and Measurement Data

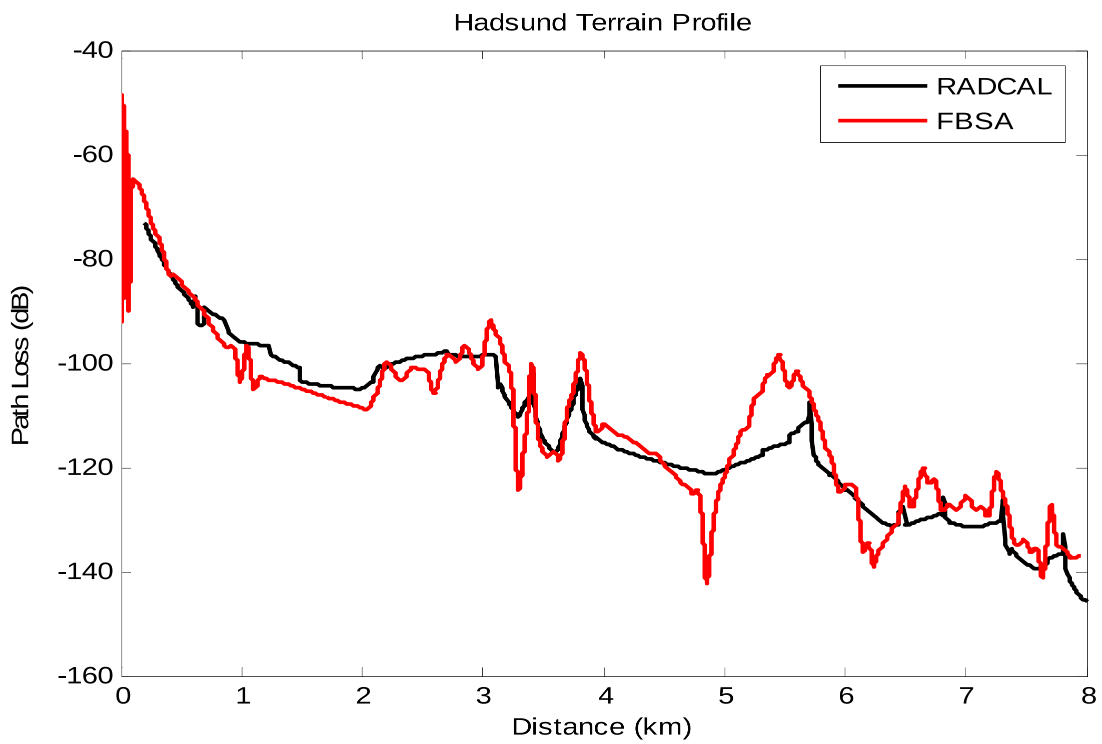

Figure 4.11 : Comparasion of RADCAL and FBSA Results

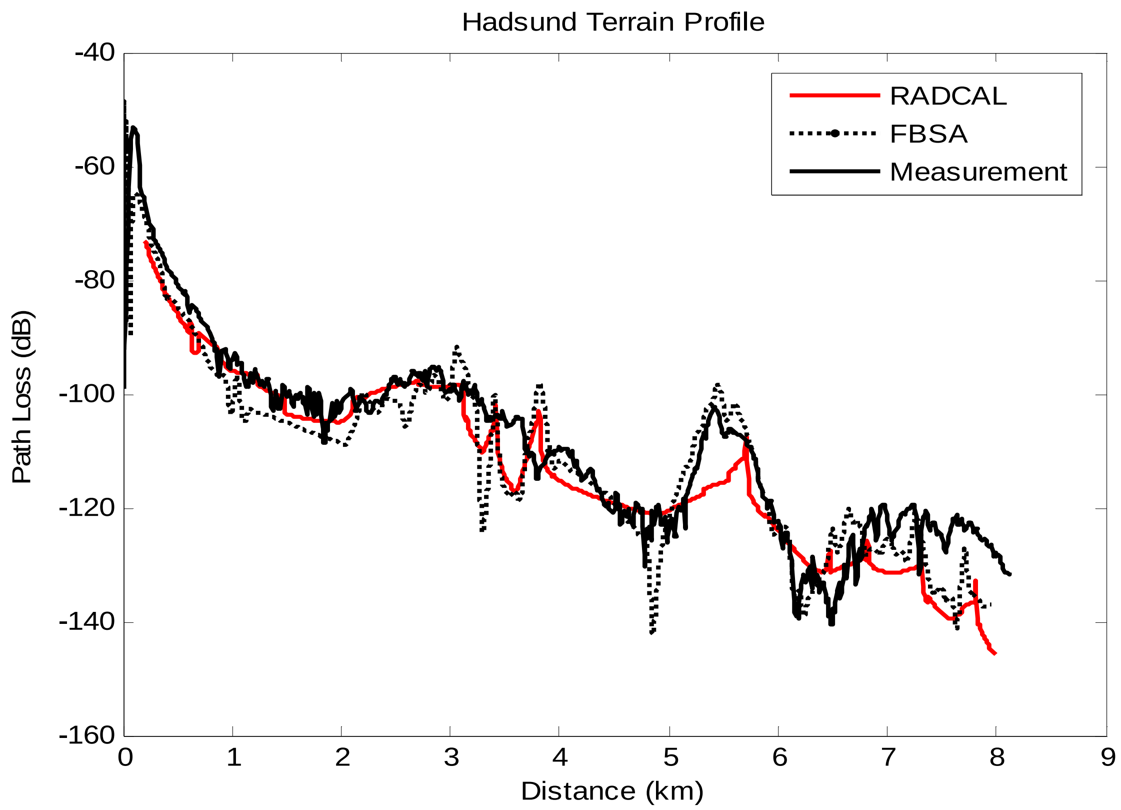

Figure 4.12 : Comparasion of RADCAL, FBSA Results and Measurement Data

RADCAL is based on GTD so it is meaningfull to compare the RADCAL results with another GTD based propagation model. For this purpose SEKE propagation model's results was used [4]. SEKE model has been used to compute path loss for different types of terrain as a function of receiving antenna height over a range of 12 m, and for diffraction paths over 700 m range of antenna heights. Its results have excellent agreement with measurements. For Actual Beiseker Terrain profile given in Figure 4.13 the results of RADCAL, SEKE results and measurements are demonstrated in Figure 4.14 to Figure 4.16 for the frequencies of 167MHz(VHF), 435MHz(UHF), and 1230 MHz(L Band).

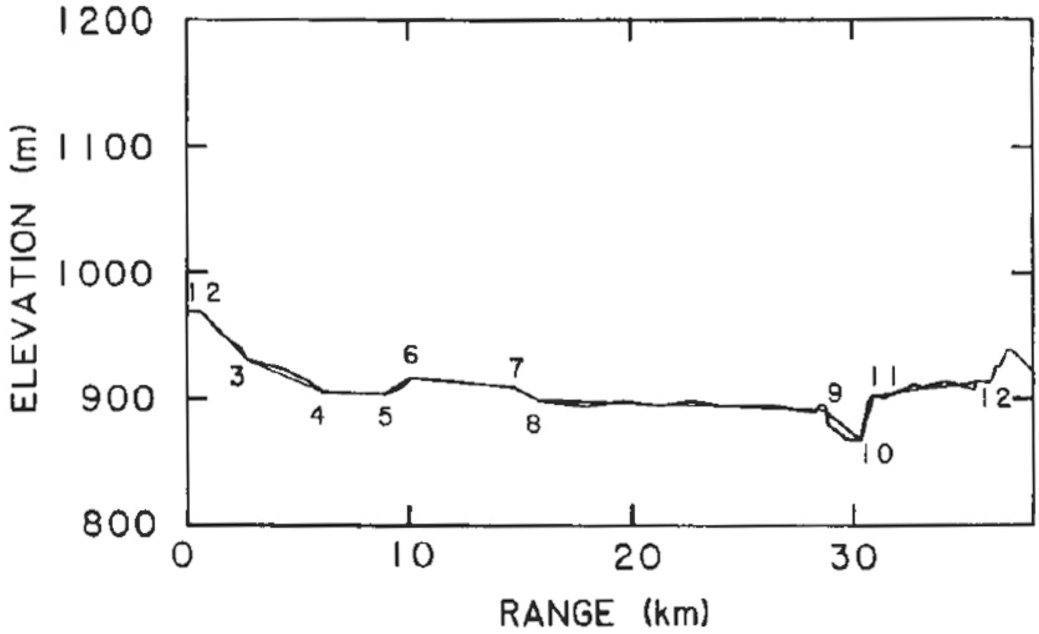

Figure 4.13 : Actual Beiseker W35 Terrain Profile

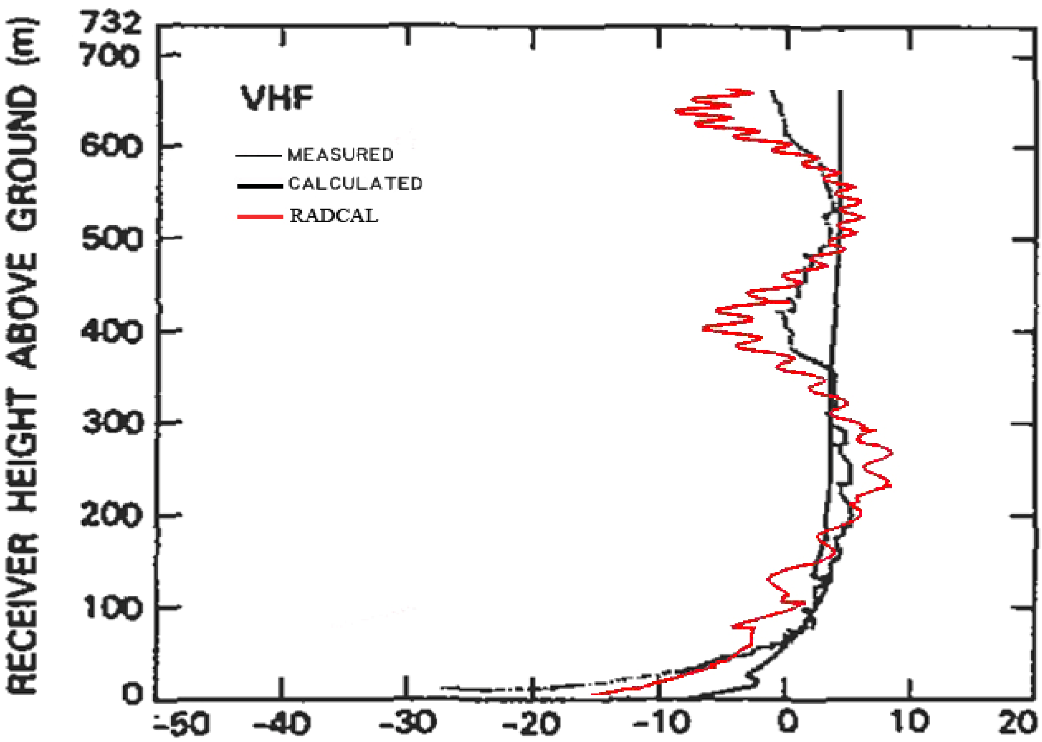

Figure 4.14 : Path loss in excess of free space versus receiver altitude for Beiseker W35 Terrain Profile for VHF.

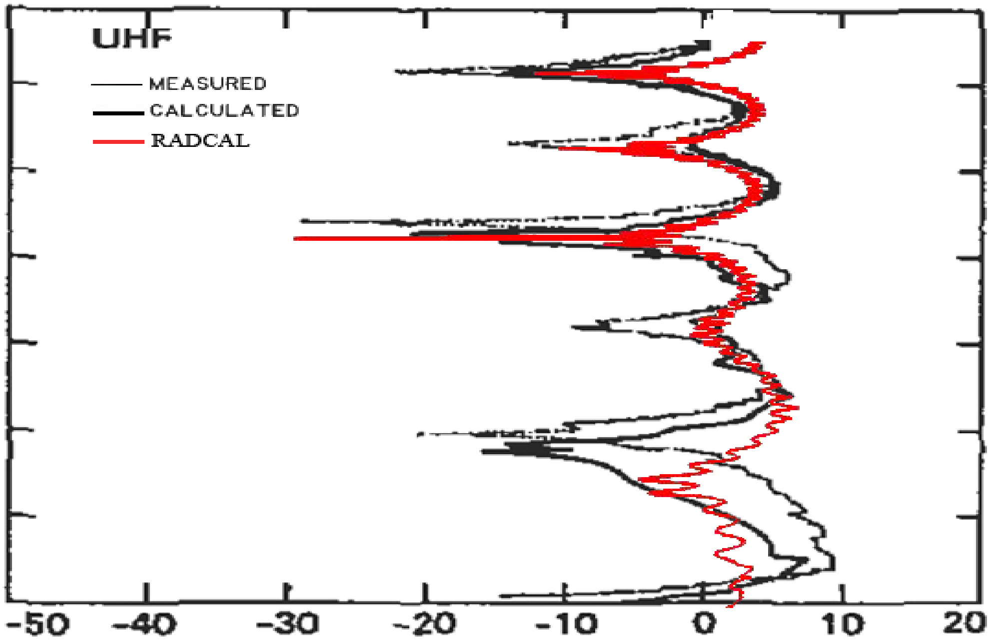

Figure 4.15 : Path loss in excess of free space versus receiver altitude for Beiseker W35 Terrain Profile for UHF

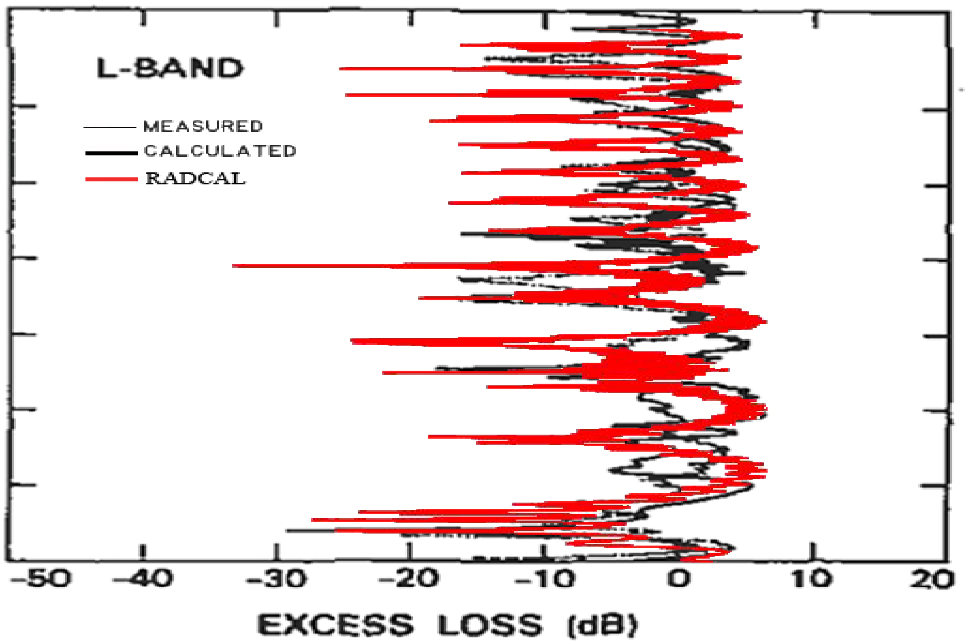

Figure 4.16 : Path loss in excess of free space versus receiver altitude for Beiseker W35 Terrain Profile for L-Band.

R. J LUEBBERS developed another GTD based propagation model [61]. Similar to SEKE model, LUEBBERS has been used to compute path loss for different types of terrain as a function of receiving antenna height. For actual Magrath NE54 terrain profile given in Figure 4.17 the results of RADCAL, LUEBBERS results and measurements are demonstrated in Figure 4.18.

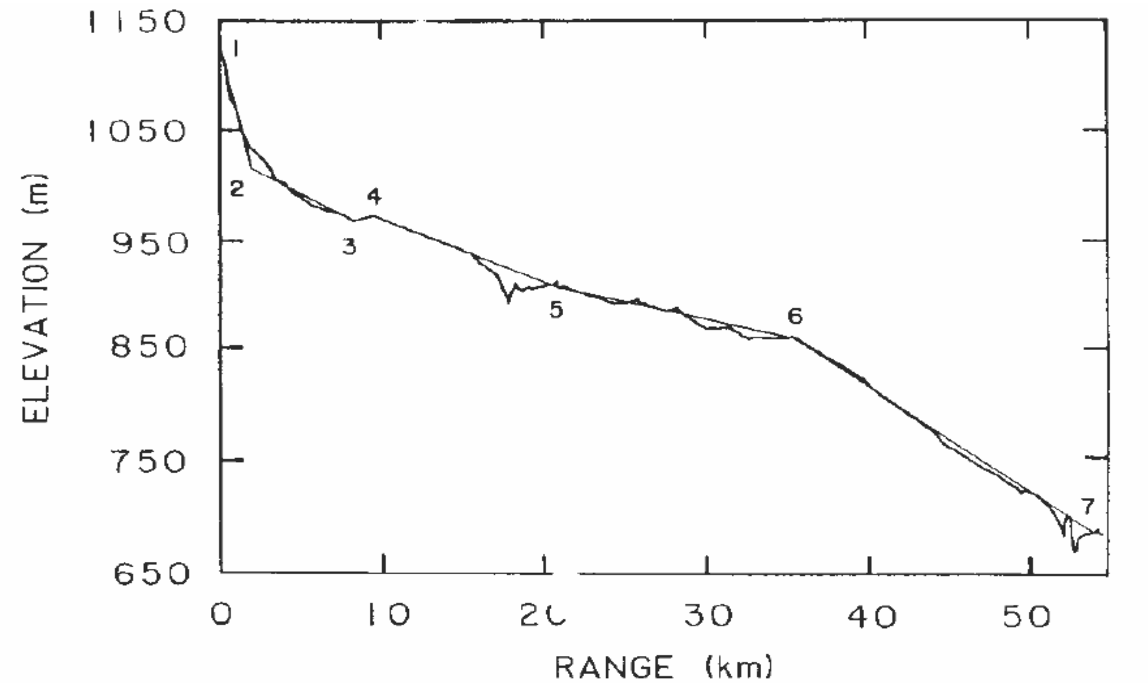

Figure 4.17 : Actual Magrath NE54 terrain profile (corrected for 4/3 earth curvature) and piecewise linear approximation used bt the GTD model. The transmitting antenna is located at 0 km and elevated at 18.3 m. The receiving antenna located at 54 km from the transmitting antenna.

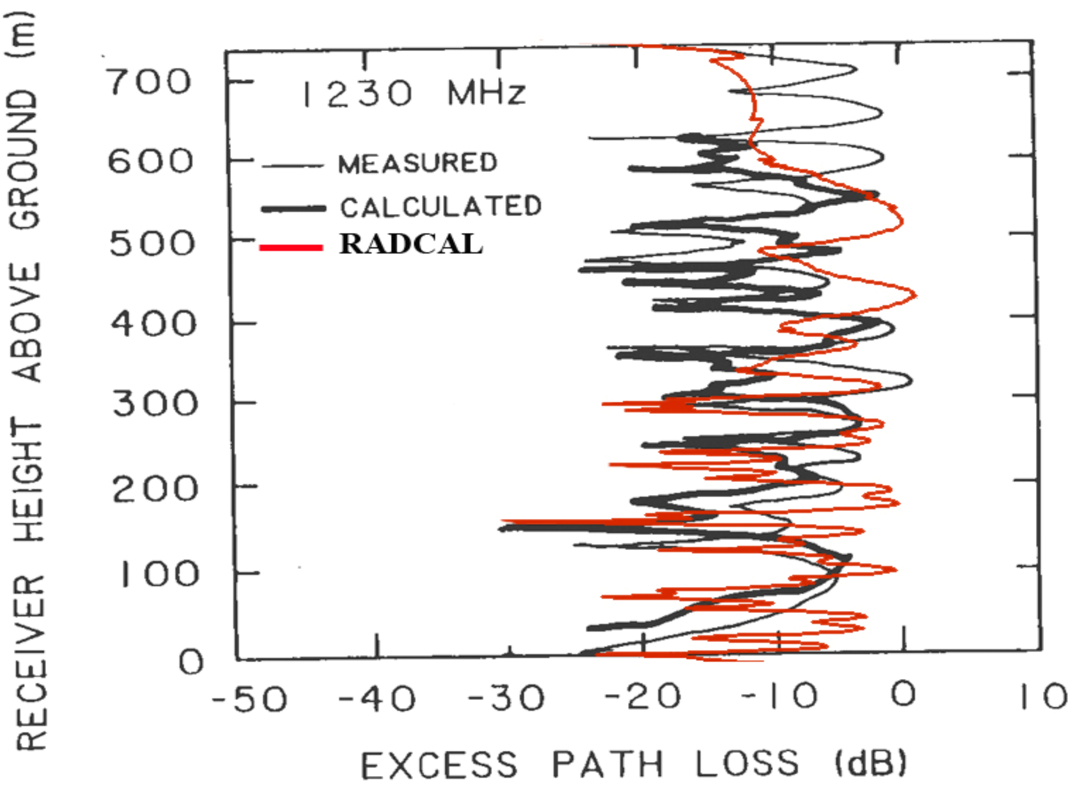

Figure 4.18 : Terrain profile for Actual Magrath NE54 path with height-gain plot showing LUEBBERS, RADCAL and measured signal at 1230 MHz.

For Actual Magrath NE54 terrain profile plateaus and hills extracted from the graph and given in Table 4.1.

Table 4.1: Distance and Height Values for Actual Magrath NE54 terrain profile

ID	Dmi (km)	Hmi (m)
1	2	1030
2	2.6	1000
3	8	968
4	10	970
5	15.5	930
6	18	890
7	21	910
8	35.5	860
9	50	725
10	52	690
11	52.5	710
12	53	670
13	54	690

The plot of the RAYS for this terrain is given in Figure 4.19 and Path propagation Factors for each RAY is given in Table 4.2.

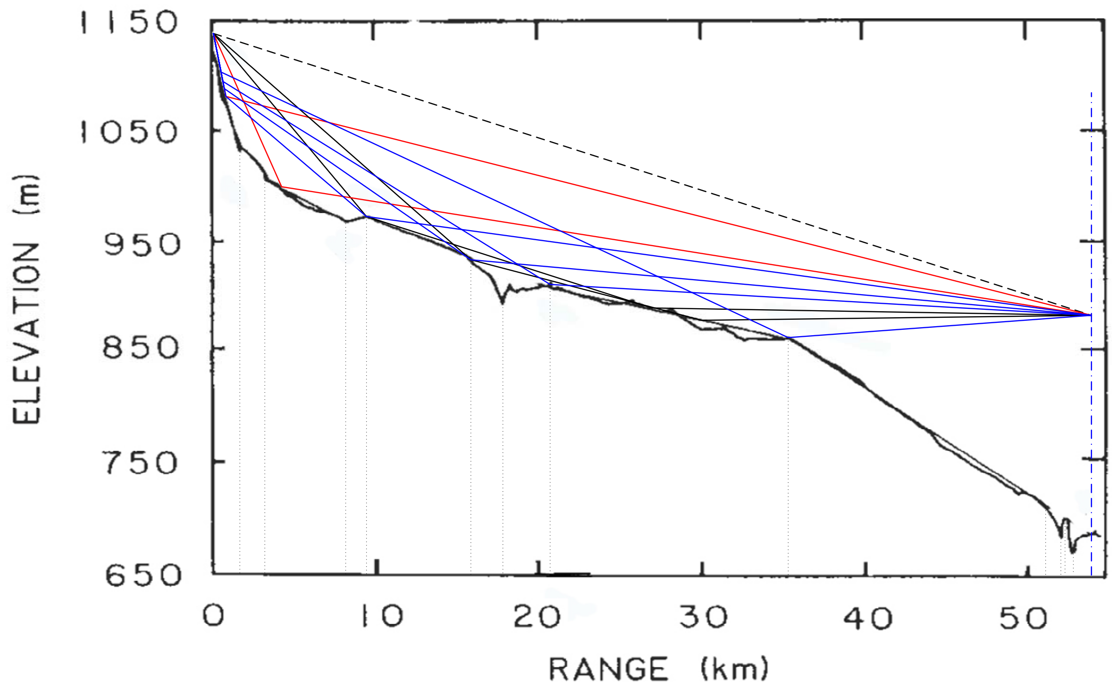

Figure 4.19 : RAYS for Actual Magrath NE54 terrain profile (**a** is RAY_1(Black dashed Line), **b** is RAY_2 (Red Lines), **c** is RAY_3 (Black Lines) and d is RAY_4 (Blue Lines))

Table 4.2 : RAYS Propagation Factors for Actual Magrath NE54 terrain profile

Direct Ray (Ray-1)→ Amplitude= 0.9354 Phase = 4.7123
Reflected Ray (Ray-2)→ Amplitude= 0.6522 Phase = -39.9496 (Reflect from plateau 0) Amplitude= 0.7005 Phase = -80.7527 (Reflect from plateau 2) **Complex Summmation is** Amplitude= 0.05453 Phase = 1.3952
Diffracted-Reflected (Ray-3)→ Amplitude= 0.2741 Phase = -1.5945 (Diffracted from Hill 4 and Reflected from plateau 7) Amplitude= 0.4547 Phase = 1.6539 (Diffracted from Hill 5 and Reflected from plateau 7) **Complex Summmation is** Amplitude= 0.1844 Phase = 1.8131
Reflected-Diffracted (Ray-4)→ Amplitude= 0.8363 Phase = -1.2318 (Reflected from plateau 0 and Diffracted from Hill 4) Amplitude= 0.8267 Phase = 1.1880 (Reflected from plateau 0 and Diffracted from Hill 5) Amplitude= 0.7980 Phase = -1.7215 (Reflected from plateau 0 and Diffracted from Hill 7) Amplitude= 0.6227 Phase = 1.8314 (Reflected from plateau 0 and Diffracted from Hill 8) **Complex Summmation is** Amplitude= 0.3673 Phase = -0.5898

Another model is the Terrain Parabolic Equation Model (TPEM) [14], based on the split-step Fourier algorithm to solve the parabolic wave equation, which has been shown to be numerically efficient. Comparisons of RADCAL, TPEM, and SEKE are given below.

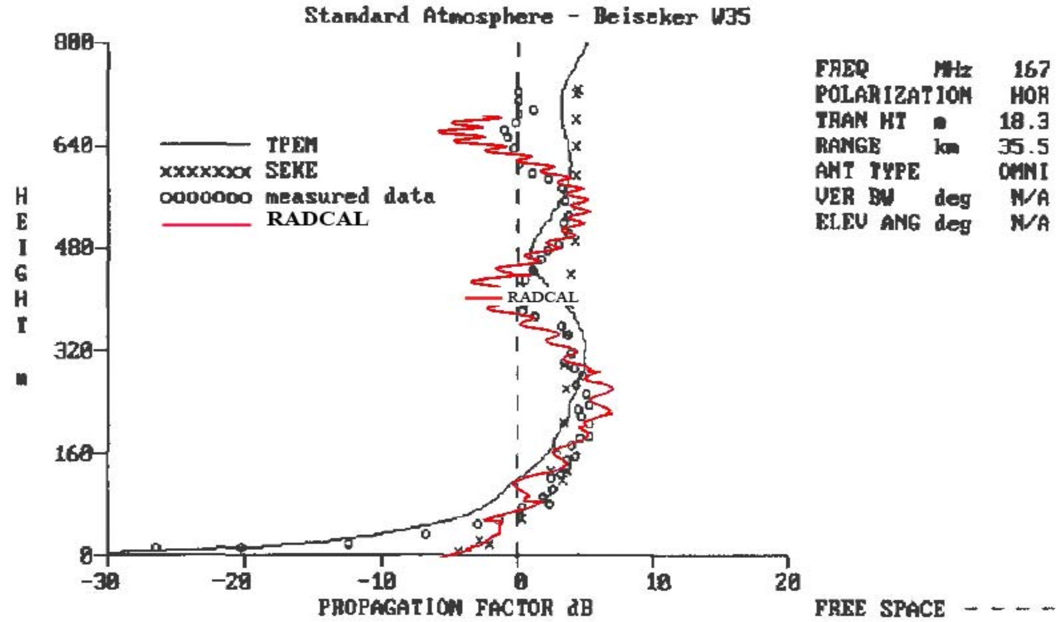

Figure 4.20 : Terrain profile for west (35 h) Beiseker path with height-gain plot showing TPEM, SEKE, RADCAL and measured signal.

An irregular terrain propagation model based on ray optics is developed. The model consist of modeling the terrain by round earth plateaus, slant flat plateaus, convex and concave plateaus between hills and depression. To show the effect of including convex and concave slant plateaus into the model, so that the calculation of a simple example is given below.

When the plateaus after 10th hill in Hadsund Terrain Profile is modeled by convex plateaus (See Figure 4.21) instead of the slant flat plateaus; the results of the RADCAL approaches the measurement results better (See Figure 4.22 and Figure 4.23).

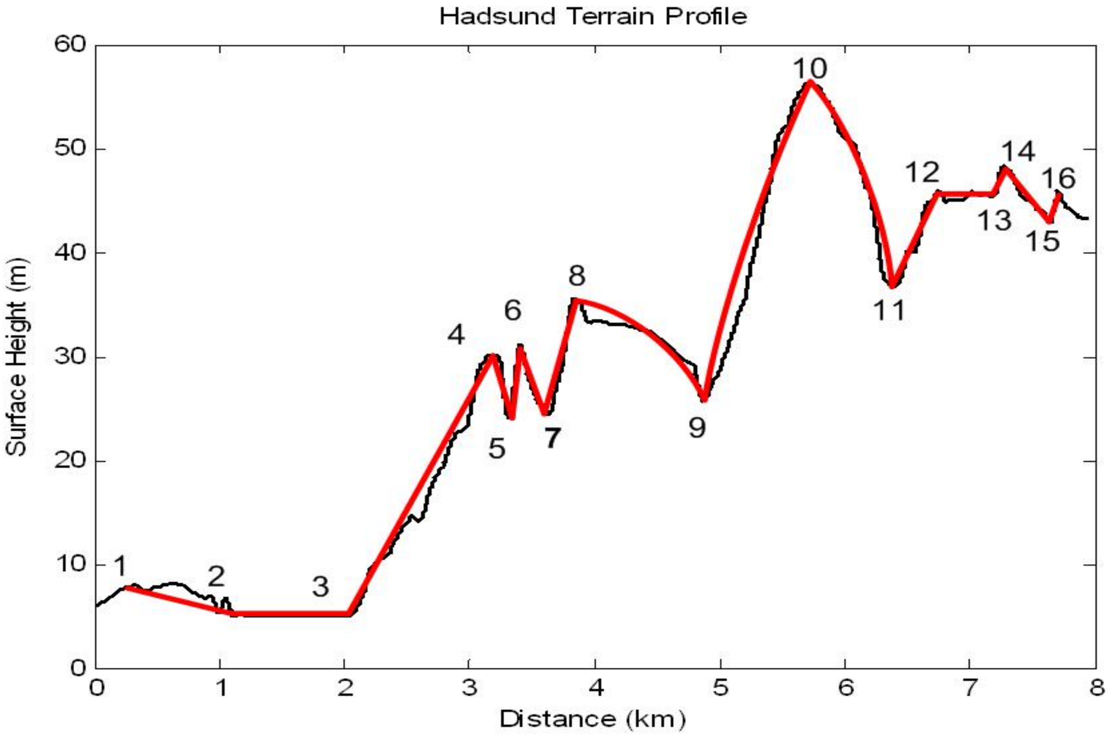

Figure 4-21 : Smoothed Hadsund Terrain Profile

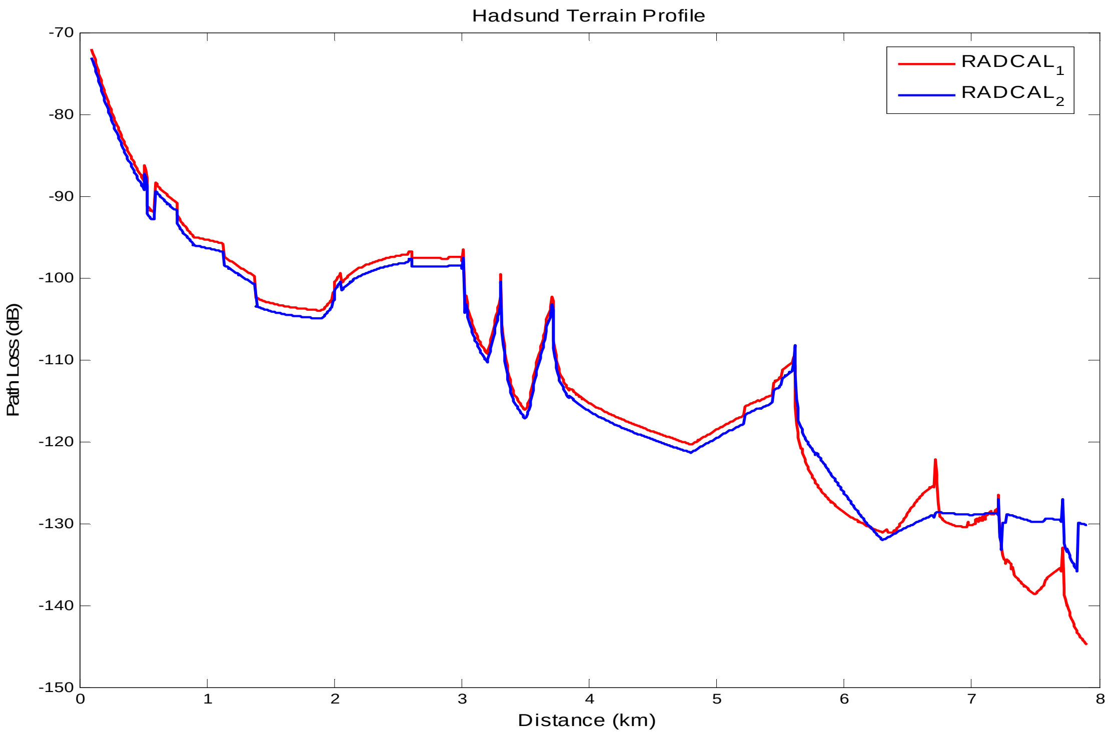

Figure 4.22 : Comparison of RADCAL Results when radius of curvature of the plateaus after 10 th hill is taken as slant flat plateaus (Red) and convex plateaus (Blue)

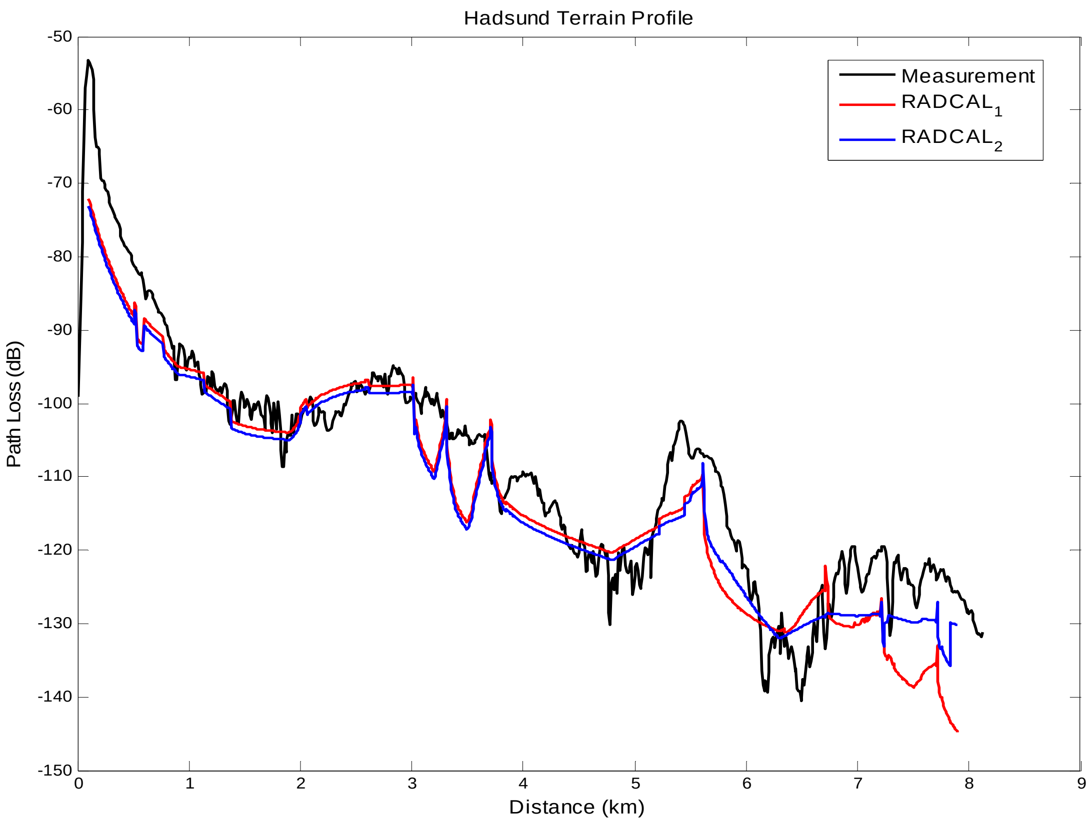

Figure 4.23 : Comparison of RADCAL Results when radius of curvature of the plateaus after 10 th hill is taken as slant flat plateaus (Red) and convex plateaus (Blue) with Measurements (Black)

When the plateaus after 9th hill in Jerslev Terrain Profile is modeled by convcave plateaus (See Figure 4.24) instead of the slant flat plateaus; the results of the RADCAL approaches the measurement results better (See Figure 4.25 and Figure 4.26).

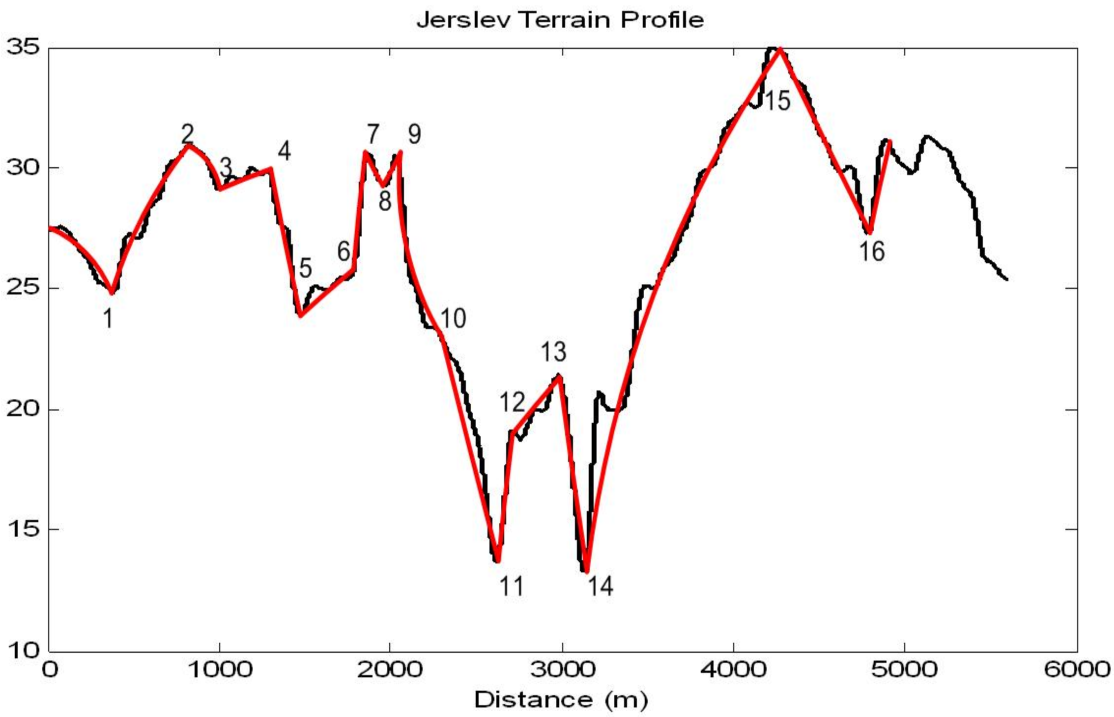

Figure 4-24 : Smoothed Jerslev Terrain Profile

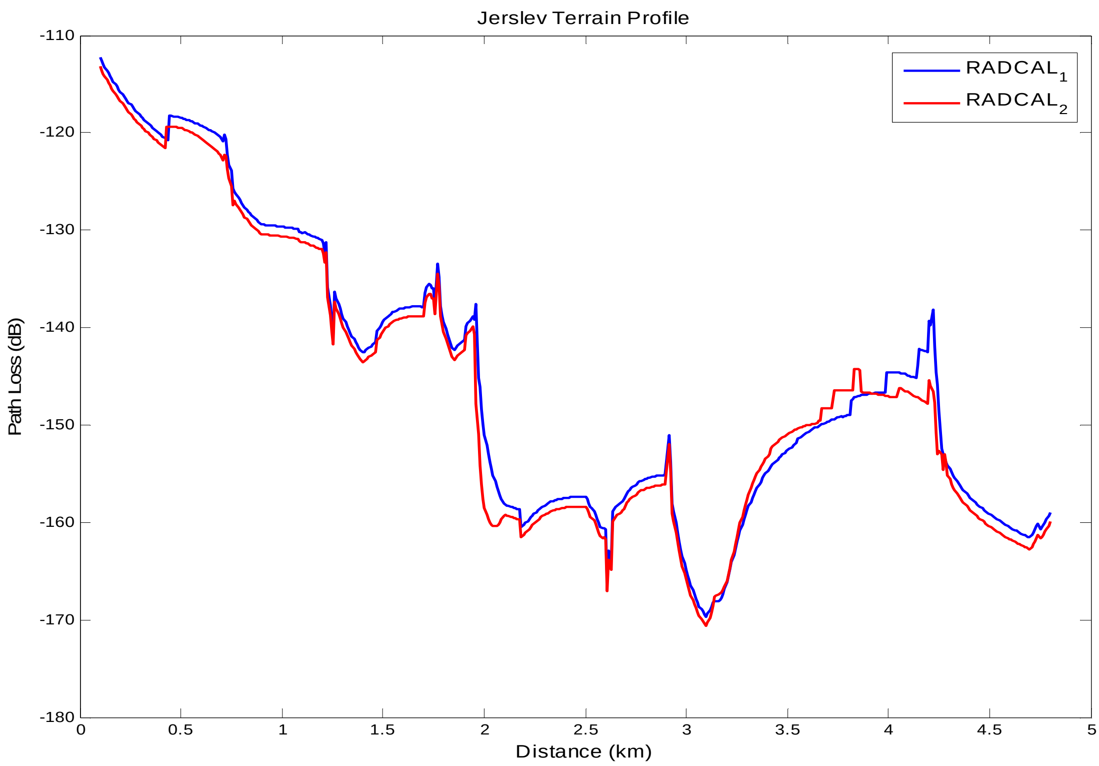

Figure 4.25 : Comparison of RADCAL Results when radius of curvature of the plateaus after 9 th hill is taken as slant flat plateaus (Blue) and concave plateaus (Red)

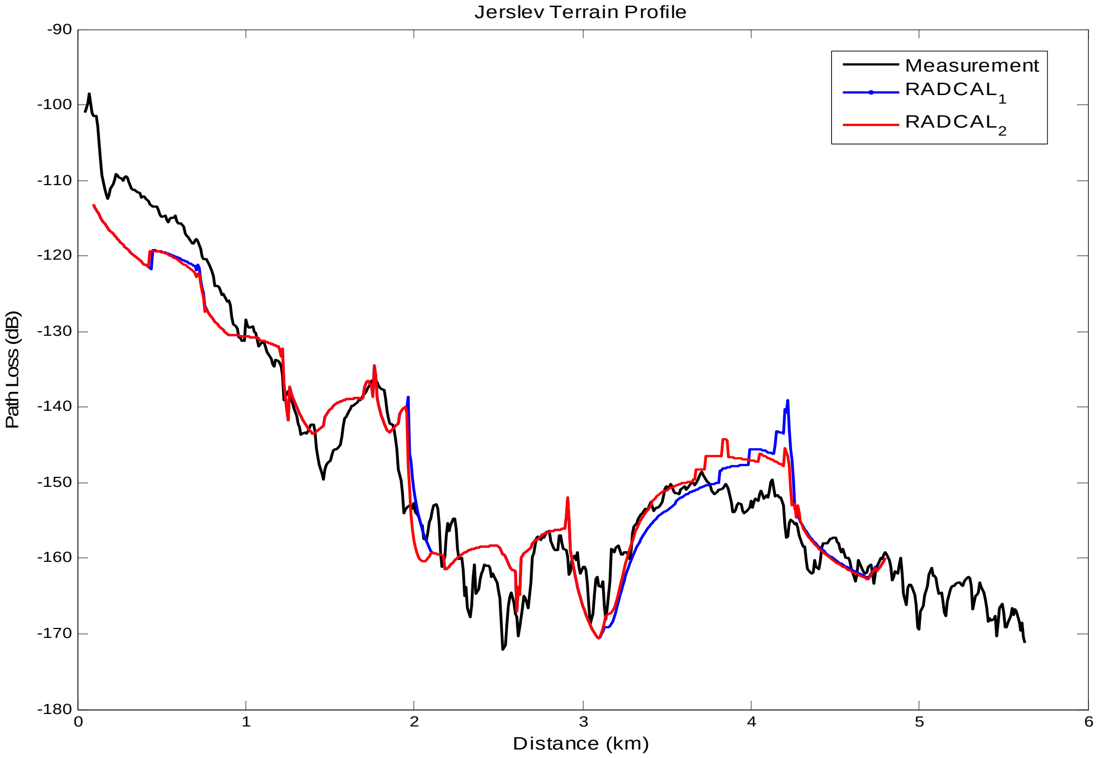

Figure 4.26 : Comparison of RADCAL Results when radius of curvature of the plateaus after 9 th hill is taken as slant flat plateaus (Blue) and concave plateaus (Red) with Measurements (Black)

CHAPTER 5

CONCLUSION

5.1 Introduction

As previously discussed, the ability to predict the propagation of radio waves are essential in the performance analysis and optimal design of a radar system. Without a propagation model, system issues such as coherency, field variations, multipath, and path delay effects cannot be properly addressed. With that in mind it was decided that the concentration of this work would be on predicting propagation in an irregular terrain, in the frequency range of UHF and above.

Propagation aspects of low altitude radar performance have been modeled using geometrical optics. Both the path propagation factor and the radar clutter have been modeled. In the proposed model we have considered an extension to RADCAL's terrain model to include convex and concave slant plateaus between hills and depressions (troughs). This propagation model uses a reflection model based on the Geometrical Theory of Reflection for the convex and concave surfaces. The effects of the features of the terrain profile on the path propagation factor have been investigated. A real terrain data have been smoothed on the basis of the above study. In this chapter this work will be summarized as well as a discussion of future work presented.

5.2 Conclusion

A robust technique for the prediction of field strengths over irregular terrain profiles must be polarization and frequency dependent, and must take electrical properties, and details of the terrain profile into account.

An efficient method has been presented to model groundwave propagation over irregular terrain in the presence of range-dependent nonstandard environmental conditions. The results from this model were compared against measured data and other existing models and were shown to give predominantly excellent agreement. The final objective in model were shown to give good agreement. The final objective in model development is to produce a real-time capability for predicting signal levels for operational assessment, whether it be for military or civilian requirements.

We have presented a ray optics based method to estimate the path propagation factor of an irregular terrain. Explicit expressions are obtained for the Divergence and Convergence factors for the convex and concave spherically shaped slant plateaus joining the hills and depression. The algorithm developed is very fast and provides good estimates of the propagation factor. Numerical predictions are compared with other full wave and GO methods and also measurements.

It is observed that very fine terraın features have insignificant effect on the path propagation factor for most terrain in VHF to microwave frequency. In order to verify the formulation, the Divergence and Convergence Factors associated with the convex and concave plateaus, respectively are inserted into the RADCAL program. The chosen terrains have convex or concave plateaus in the model. The output of the RADCAL is compared with measured values and other propagation algorithms such as Forward-Backward Spectrally Accelerated (FBSA) and Parabolic Equation Method. Moreover, as the RADCAL Propagation model is based on the ray optics, the results are also compared with another ray optics based propagation model. For this purpose the results of SEKE [Lincoln Lab.] propagation model are used. SEKE model has been used to compute path loss for different types of terrain as a function of receiving antenna height at a fixed distance between transmit and receive antennas. For Beiseker W35 Terrain profile, the results of RADCAL, SEKE and measurements are compared. All results are found to be in good agreement with those obtained by RADCAL.

5.3 Future Work

There are several issues that still need to be addressed in further development of the model described in this thesis and that will be discussed in the sections that follow.

During this thesis a new version of RADCAL is developed. This new version primarily modifies the terrain propagation model. It considers contributions of specular reflections from flat and slant plateaus between diffracting hills. Obstructions of incident and reflected rays by flat plateaus are checked. Knife-edge diffraction from rounded hilltops at oblique incidence is considered. Effects of convex slant plateaus are twofold. First it may curve reflections, second it may cause incident and diffracted field obstructions.

As stated in the previous section, the structure of the program is open to improvements. Also the documentation of the RADCAL program is completed. All functions in the program are documented in Appendix E and all procedures in program are documented in Appendix G. The document "Notes on RADCAL Radar Calculation Software" written by A.Hızal and O.Sengul completes the documentation of program.

- Some of the input parameters can be extracted from database as a function of the radar, target and terrain geometry. These are surface reflectivity, terrain profile, surface roughness and electrical parameters of the surface.
- Geometry can be extended to 3 dimensional (3D) geometry. As the radar beams scans the 3D space, the geometry thus the relevant position, terrain, rain and target parameters change. The required input data can be extracted from the database as a function of time.
- The input parameters concerning the radar and the target can be provided graphically by assigning a specific radar and a specific target to scenario based, time-variable positions.
- The output can be displayed in a 3D to 2D projection format, the time being a parameter. The projection can be displaced as a simulated radar screen by intensity modulation of the screen by noise, clutter and the signal. Alternatively, contours of equal probability of detection can be calculated and a 3D-coverage surface can be displayed.

BIBLIOGRAPHY

[1]. Hızal, A., "Notes on Radar Calculation Software, RADCAL, Low Altitude Radar Performance Prediction", Part I, Middle East Technical University/Department of Electric and Electronics Engineering and ASELSAN/Military Electronics Industries, Inc. 1988-2000.

[2]. Hızal, A. and Sengul O., " Propagation Aspects of Communication and Radar Systems Lecture Notes", Middle East Technical University/Department of Electric and Electronics Engineering., 1993-2006.

[3]. Şengül, O., “Low Altitude Radar Simulation Program RADCAL”, M.S. Thesis, The Department of Electrical and Electronic Engineering, Middle East Technical University. 2001.

[4]. Ayaslı, S.,"SEKE: A computer Model for Low Altitude Radar Propagation Over Irregular Terrain,IEEE Transactions on Antennas and Propagation, Vol. Ap-34, No.8, 1986.

[5]. Keller, J., "Diffraction by a Convex Cylinder*, Electromagnetic Wave Theory Symposium, pp-312-322, 1953.

[6]. Skolnik, M. I., Introduction to Radar Systems, McGraw-Hill Book Company, Taiwan, 1980.

[7]. Kerr, D.E., “Propagation of Short Waves, Dover Publishing”, New York, 1965.

[8]. Barton, D. K., Modern Radar System Analysis, Artech House, 1988.

[9]. Barton, D. K., Modern Radar System Analysis Software and User’s Manual, Artech House, 1990.

[10]. Barton, D. K., Radars, Vol.2, Artech House, 1977.

[11]. Huizing, A. G. and Theil, A., CARPET Computer-Aided Radar Performance Evaluation Tool, Artech House, 1993.

[12]. Weill, T A., Aerospace and Electrical Systems, IEEE Transaction, Vol. AES-9, No.1, 1973.

[13]. Beckmann, B., and Spizzichino, A., The Scattering of Electromagnetic Waves from Rough Surfaces, Mac Millan, New York, 1963.

[14]. Warner, C., "Calculations of Scattering from Water Drops of Radar Reflectivity and Attenuation at Frequencies from 2.9 to 110 GHz", Department Memo, No.449, Department of EE., University of Birmingham, U.K., 1973.

[15]. Dougherty, H. T., and Moloney, L. J., “Application of Diffractions by Convex Surfaces”, Radio Science, 68 D., 1964.

[16]. Millington, G., (Ground Wave Propagation over Inhomogeneous Smooth Earth, Proc. IEE, pt.III, Vol.96.

[17]. Millington, G., and Hewitt, R., and Immirzi, F. S., “Double Knife-Edge Diffraction in Field Strength Predictions”, Proc. IEE, 109C. 1962.

[18]. Deygout, J., “Multiple Knife-Edge Diffraction of Microwaves”,IEEE, AP-14., 1966.

[19]. Dolukhanov, M., “Propagation of Radio Waves”, Mir Publishers, 1971.

[20]. Long, M. W., Radar Reflectivity of Land and Sea, Lexington Books D.C. Health & Company, 1975.

[21]. Di Franco, J. V., and Rubin, W. L., Radar Detection, Englewood Cliffs, Prentice-Hall, N.J., 1968.

[22]. Hall, W. M., Antenna Beam Shape Factor in Scanning Radars, IEEE, AES-4, #3., 1968.

[23]. Blake, L. V., Radar Range Performance Analysis, Artech House, 1986.

[24]. Trunk, G.V. and George, S.F., “Detection of Targets in Non-Gaussian Sea Clutter”, IEEE Vol. AES-6, No. 5., 1970.

[25]. Trunk, G. V., “Further Results on the Detection of Targets in Non-Gaussian Sea Clutter”, IEEE Vol. AES-9, No. 1., 1971.

[26]. Goldstein, G. B., “False Alarm Regulation in Log-Normal and Weibull Clutter”, IEEE Vol. AES-9, No. 1., 1973.

[27]. Nathanson F.E., Radar Design Principles, McGraw-Hill Book Company, NewYork, 1969.

[28]. Meyer, B., Object-Oriented Software Construction, 2nd Edition, Prentice Hall, 2000.

[29]. A uniform GTD analysis of the diffraction of electromagnetic waves by a smooth convex surface Pathak, P. Burnside, W.; Marhefka, R.; Antennas and Propagation, IEEE Transactions on [legacy, pre - 1988] Vol. 28, Issue 5, pp:631 – 642, Sep 1980

[30]. A uniform GTD treatment of surface diffraction by impedance and coated cylinders Hussar, P.E.; Antennas and Propagation, IEEE Transactions on Vol. 46, Issue 7, pp:998 – 1008, July 1998

[31]. A uniform GTD solution for the far-field scattering by polygonal cylinders and strips Michaeli, A.; Antennas and Propagation, IEEE Transactions on [legacy, pre - 1988] Vol. 35, Issue 8, pp: 983 – 986, Aug 1987

[32]. Akıncı, Y. 2003. ” Integrating A Radar Model Into Synthetic Environment”, M.S. Thesis, The Department of Computer Engineering, Middle East Technical University.

[33]. VOGLER, L.E.: 'An attenuation function for multiple knife-edge diffraction', Radio Sci., 17, pp. 1541-1546, 1982

[34]. SAUNDERS, S.R., and BONAR, F.R.: 'Prediction Of mobile radio wave propagation over buildings of irregular heights and spacing', IEEE Trans., Ap-42, (2), pp. 137-144, 1994

[35]. WALFISCH, J., and BERTONI, H.L., "A theoretical model of UHF propagation in urban environments", IEEE Trans., Ap-36, (12), pp. 1788-1796, 1988,

[36]. SAVOV, S.V., and ANDERSEN, J.B.: "Efficient method for calculation of Fresnel double integral", Electron. Lett., 1995, 31, (6), pp. 435437

[37]. BORN, M., and WOLF, E.: "Principles of optics"(Pergamon Press, Oxford, 1980), 6th Edn.2

[38]. TZARAS C., SAUNDERS, S.R., "Rapid, Uniform computation of multiple knife edge diffraction", Electronic Letters 4th Feb., Vol.35 No.3, pp. 237-239, 1999

[39]. Shatz M.P. and Polychronopoulos G.H., "An algorithm for the evaluation of radar propagation in the spherical earth diffraction region", Antennas and Propagation, IEEE Trans. on Vol. 38, No. 8, pp: 1249 – 1252, Aug 1990

[40]. Van der Pol and Bremmer, "Further note on the Propagation of Radio Waves over a Finitely Conducting Spherical Earth", Phil. Mag.,27,Ser. 7,No. 182, March 1930

[41]. Ott R. E., "An alternative integral equation for Propagation over irregular terrain." Radio Sci., Vol. 6. pp. 429-435, Apr. 1971.

[42]. Levy, M.F. " Parabolic equation modelling of propagation over irregular terrain. Electronics Letters Vol. 26, Issue 15, 19 pp:1153 – 1155, July 1990

[43]. Monteath, G.D., "Application of electromagnetic Reciprocity Principle", Pergaman Press p:115, 1973

[44]. Hufford, G.A., "An integral equation approach to the problem of wave propagation over an irregular surface", Q.Applical Math. Vol.9, pp:391-1952

[45]. N Geng, W Wiesbeck: "Parabolic Equation Method Simulations Compared To Measurements", Antennas and Propagation, 4-7, April 1995

[46]. C.A. Tunc, A. Altintas, V.B. Ertürk, "Examination of Existent Propagation Models over Large Inhomogeneous Terrain Profiles Using Fast Integral Equation Solution", Trans. on Antennas & Prop., Vol. 53, Issue 9, pp:3080 – 3083, Sept. 2005

[47]. J. T. Hviid, J. B. Anderson, J. Toftgard, and J. Bojer, "Terrain based propagation model for rural area–An integral equations approach," IEEE Trans. Antennas Prop., Vol. 43, No.1, pp: 41–46, Jan. 1995.

[48]. R. Janaswamy, “A fredholm integral equation method for propagation over small terrain irregularities,” IEEE Trans. Antennas Propag., Vol. 40, No. 9, pp: 1416–1422, Sep. 1994.

[49]. J. T. Johnson, R. T. Shin, J. C. Eidson, L. Tsang, and J. A. Kong, “A method of moments model for vhf propagation,” IEEE Trans. Antennas Propag., Vol. 45, No. 1, pp. 115–125, Jan. 1997.

[50]. C. Brennan and P. J. Cullen, “Application of the fast far-field approximation to the computation of uhf pathloss over irregular terrain,” IEEE Trans. Antennas Propag., Vol. 46, No. 6, pp. 881–890, Jun. 1998.

[51]. C. Brennan and P. J. Cullen “Tabulated interaction method for uhf terrain propagation problems” IEEE Trans.Antennas Propag.,Vol.46, No.5, pp.738–739, May 1998.

[52]. C. L. Rino and H. D. Ngo, “Forward propagation in a half-space with an irregular boundary,” IEEE Trans. Antennas Propag., Vol. 45, No. 9, pp. 1340–1347, Sep. 1997.

[53]. C. L. Rino and V. R. Kruger, “A comparison of forward-boundary-integral and parabolic-wave-equation propagation models,” IEEE Trans. Antennas Propag., Vol. 49, No. 4, pp. 574–582, Apr. 2001.

[54]. F. K. Akorli and E. Costa, “An efficient solution of an integral equation applicable to simulation of propagation along irregular terrain,” IEEE Trans. Antennas Propag., Vol. 49, No. 7, pp. 1033–1036, Jul. 2001.

[55]. T. B. A. Senior, “Impedance boundaryconditions for imperfectlyconducting surfaces,” Appl. Sci. Res., Vol. 8, pp. 418–436, 1961.

[56]. T. S. Rappaport, Wireless Communications: Principles and Practice, 2nd ed. Englewood Cliffs, NJ: Prentice Hall, 2001.

[57]. J. A. López, M. R. Pino, F. Obelleiro, and J. L. Rodríguez, “Application of the spectral acceleration forward-backward method to coverage analysis over terrain profiles,” J. Electromagn. Waves Appl., Vol. 15, pp. 1049–1074, Aug. 2001.

[58]. A. Beilis and F. D. Tappert, “Coupled mode analysis of multiple rough surface scattering,” J. Acout. Soc. Am., Vol. 66, No. 3, pp. 811-826, Sept. 1979.

[59]. V. A. Fnck, Electromagnetic and Propagation Problems. New York: Pergamon, 1965, ch. 11-14.

[60]. A. E. Barrios, “ A Terrain Parabolic Equation Model for Propagation in the Troposphere”, IEEE Trans. Antennas Propag., Vol. 42, No. 1, pp. 90–98, Jan. 1994.

[61]. R. J. Luebbers, “ A Semiblind Test of the GTD Propagation Model for Reflective Rolling Terrain”, IEEE Trans. Antennas Propag., vol. 38, no. 3, pp. 403–405, March 1990.

APPENDIX A

PATH PROPAGATION FACTOR

A.1 Knife Edge Diffraction (Fresnel Diffraction)

If the LOS propagation path has its First Fresnel zone free of any obstacles such as hills and ridges, the field in the receiving site can be approximately calculated as if LOS path is in free space. However if a hill or ridge enters into the First Fresnel zone ellipsoids, it is necessary to account for the signal loss or gain due to obstruction. Also, due to the diffraction, a field exists in the geometrical shadow region, which makes radio communication and radar target detection possible within these zones.

Hills and ridges obstructing the propagation path can be modeled by knife edges if their widths perpendicular to the plane of incidence is greater than the width of the first Fresnel zone; i.e. $w > 2b_1$, where b_1 is the radius of the first Fresnel Zone and can be calculated from the equation of the radius of the Fresnel zones, given in Eqn.(A.1). The effect of rounded hilltops can also be taken into account.

$$b_n = \sqrt{\frac{d_1 d_2 \lambda}{d_1 + d_2} n} \qquad n = 1,2,.... \qquad \lambda = wavelength \tag{A.1}$$

In practice knife-edges [16,17] in UHF and microwave frequencies can approximate most hills and ridges. The knife edge diffraction problem was first solved by Sommerfeld in 1896,

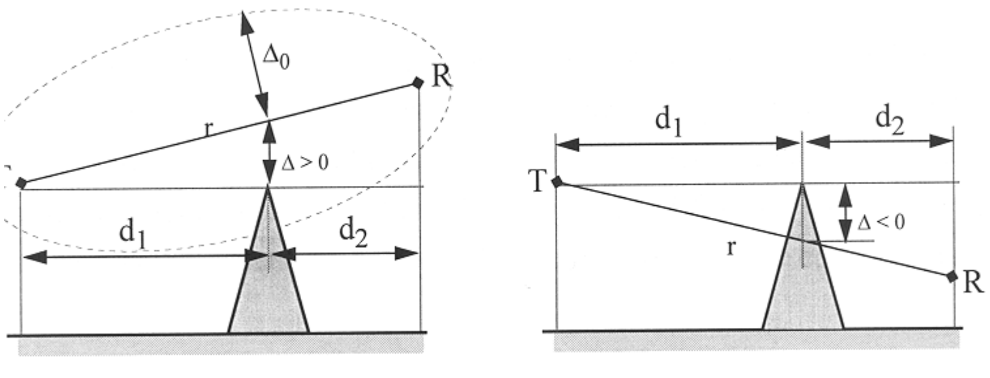

Figure A.1. Illustration of Cases in Knife-Edge Diffraction Phenomena

Referring to Fig.A.1., if a wave of unit amplitude is incident along TR path, the total field for either polarization should be multiplied by:

$$F_{KE}(d_1, d_2, \Delta) = \frac{e^{j\frac{\pi}{4}}}{\sqrt{2}}\left[\frac{1}{2} + C(v) - j\left(\frac{1}{2} + S(v)\right)\right] = \frac{1}{2} + \left(\frac{1+j}{2}\right)C(v) + \left(\frac{1-j}{2}\right)S(v) \quad \text{(A.2)}$$

where F_{KE} is for the field strength. $C(v)$ and $S(v)$ are the Cosine and Sine type Fresnel integrals defined by,

$$C(v) = \int_0^v \cos\frac{\pi x^2}{2} \cdot dx \ , \qquad S(v) = \int_0^v \sin\frac{\pi x^2}{2} \cdot dx \quad \text{(A.3)}$$

$$v = \sqrt{2} \cdot \frac{\Delta}{\Delta_0} \qquad \text{where} \qquad \Delta_0 = b_1 = \sqrt{\frac{d_1 d_2 \lambda}{d_1 + d_2}} \quad \text{(A.4)}$$

Δ is the Fresnel clearance and Δ_0 is the first Fresnel zone radius at the position of mask. The limits of above expressions are:

$$\Delta \to \infty: \qquad v \to \infty \quad C(v) = S(v) = \frac{1}{2} \qquad F_{KE} = 1 \quad \text{no blockage(no hill)} \quad \text{(A.5)}$$

$$\Delta \to -\infty: \qquad C(-v) = -C(v) = -\frac{1}{2}, \quad S(-v) = -S(v) = -\frac{1}{2} \qquad F_{KE} = 0 \quad \text{complete blockage} \quad \text{(A.6)}$$

$|F_{KE}|^2$ should be used for power calculations. The radar equation should be multiplied by $|F_{KE}|^4$ then there is a single knife edge obstruction on the propagation path. The 4^{th} power comes from the twice traverse of the radar waves between the radar and target.

A.1.1 Round Edged Obstructions

In some cases roundness of the hills and ridges should be taken into account. For this purpose the results of Dougherty and Moloney [14] may be used. A dimensionless parameter ρ is defined to characterize the effect of the finite radius of curvature of the hilltops:

$$\rho = \left(\frac{\lambda r_c^{\ 2}}{\pi} \right)^{1/6} \cdot \sqrt{\frac{d_1 + d_2}{d_1 d_2}} \qquad \text{(A.7)}$$

where r_c is the radius of curvature of the cylindrical hilltop as shown in Fig.A.2.

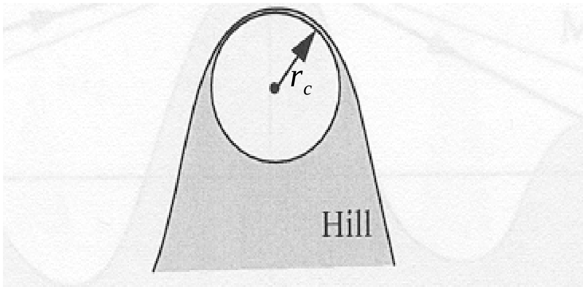

Figure A.2. Rounded Hill-Top Representation

Fig.A.3. below shows the path propagation factor (here it is the diffraction loss) as a function of Δ/Δ_0 with various values of ρ. The value $\rho = 0$ corresponds to that in for the knife edge diffraction. For example at $f = 300MHz$ ($\lambda = 1m$), and for a hill with $r_c = 500m$, $d_1 = d_2 = 5km$, we find that $\rho = 0.131$. For $\Delta/\Delta_0 = -0.5 |F_{KE}| = -14\,dB$. However for the pure knife edge model $|F_{KE}| = -12dB$.

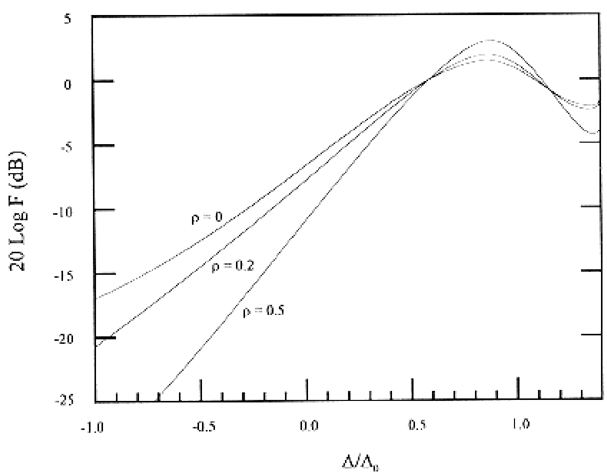

Figure A.3. Diffraction Loss For the rounded Hill-Tops

A.1.2 Multiple Knife Edge Diffraction

Radio waves propagating near the surface of earth may encounter more than one hill or ridge. Millington [16] had studied the problem for double knife-edges. For multiple knife-edges the method suggested by Deygout [17], which is based on successive application of Millington's technique for double knife-edges, is widely used. Deygout method is described below with the aid of Fig.A.4. for three hills or ridges simply called masks.

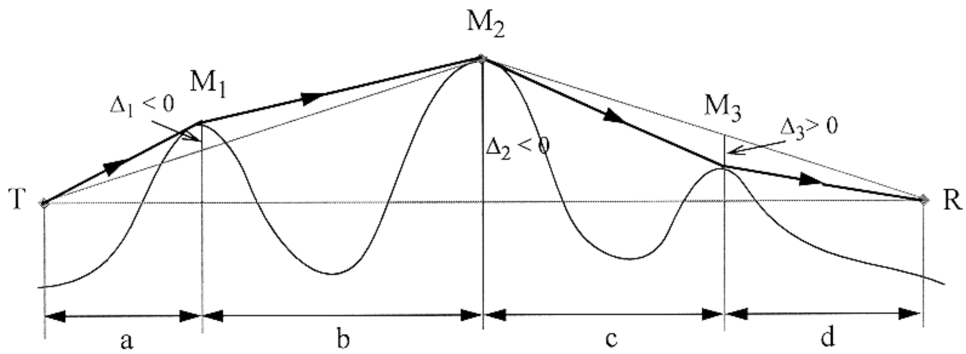

Figure A.4. Deygout Method For Three Hills

The principle mask is determined by dividing the clearance Δ of each by its first Fresnel zone Clearance Δ_0 for the path TR and by selecting the most negative Fresnel clearance Δ/Δ_0 . In Fig.A.3. M_2 is the principle mask. Next we draw the paths to the top of the principle mask, TM_2 and M_2R and record Δ_2 as the clearance for the principle mask. Finally we draw the paths TM_1, M_1M_2 and paths M_3R. Appropriate clearances for path TM_2 is Δ_1 and for path M_2R is Δ_3. The corresponding diffraction losses for the three paths are calculated using Eqn.(A.2) and multiplied to obtain the resultant F_{KE}. The parameters d_1, d_2, and Δ for F_{KE} defined in Eqn.(A.2) are given in table below.

Table A.1. Calculated Δ values in F_{KE} for Three Hills

Parameters	M_1	M_2	M_3
d_1	a	$a+b$	c
d_2	b	$c+d$	d
Δ	Δ_1	Δ_2	Δ_3

Then the total F_{KE} is given by:

$$F_{KE} = F_{KE}(a,b,\Delta_1)\cdot F_{KE}(a+b,c+d,\Delta_2)\cdot F_{KE}(c,d,\Delta_3) \tag{A.8}$$

For five masks as shown in Fig.A.5., we have the parameters listed in Table A.2..

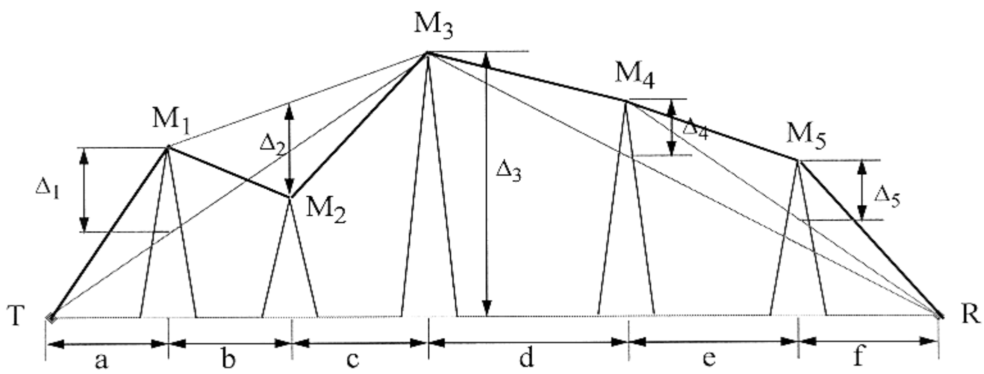

Figure A.5. Deygout Method For Five Hills

M_3 : Main mask between T and R : Main (T , R)

M_1 : Main mask between T and M_3 : Main (T , M_3)

M_2 : Main mask between M_1 and M_3 : Main (M_1, M_3)

M_4 : Main mask between M_3 and R : Main (M_3, R)

M_5 : Main mask between M_4 and R : Main (M_4, R)

Table A.2. Calculated Δ values in F_{KE} for Five Hills

Parameters	M_1	M_2	M_3	M_4	M_5
d_1	a	b	$a+b+c$	d	e
d_2	$b+c$	c	$d+e+f$	$e+f$	f
Δ	Δ_1	Δ_2	Δ_3	Δ_4	Δ_5

The total F_{KE} is given by:

$$F_{KE} = F_{KE}(a,b+c,\Delta_1)\cdot F_{KE}(b,c,\Delta_2)\cdot F_{KE}(a+b+c,d+e+f,\Delta_3)$$

$$\cdot F_{KE}(d,e+f,\Delta_4)\cdot F_{KE}(e,f,\Delta_5) \tag{A.9}$$

Experimental observations and theoretical verifications show that, Deygout method rapidly looses its accuracy when the number of hills exceeds 5. The value of knife-edge diffraction factor is calculated by using the procedure $Knifedge(X_{ref}, H_1, H_2, D, D_m, H_m, R_m, A_m, E_m, N_m, \lambda, Afk, Pfk)$.

A.2 The Width of the Specular Reflection Point

In order that the ground reflection to take place on a terrain of earth, sufficiently large area should exist in the vicinity of the specular reflection point. The size of the area required is determined by the Fresnel ellipsoid constructed as shown in Fig.A.9.

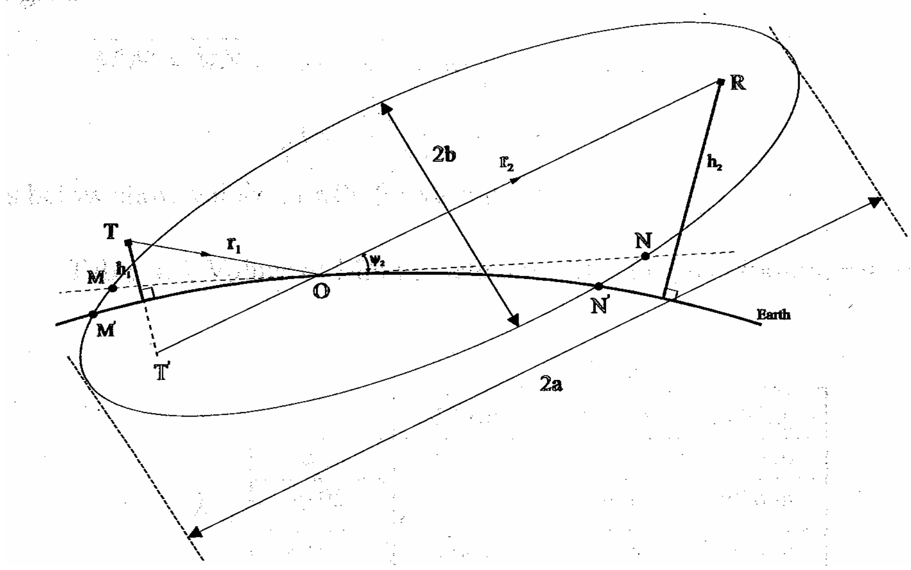

Figure A.6 : Geometry for Determining the Area Available in Specular Reflection

$$\overline{MN} = \frac{2ab}{\sqrt{b^2 + a^2 \tan^2 \psi}} \tag{A.10}$$

where

$$b = \sqrt{\frac{d_1 d_2 \lambda}{d_1 + d_2}} \qquad d_1 = d_2 = \frac{r_1 + r_2}{2} \qquad d_1 + d_2 = r_1 + r_2 \tag{A.11}$$

$$b = \frac{1}{2}\sqrt{(r_1 + r_2)\lambda} \qquad 2a \approx r_1 + r_2 \tag{A.12}$$

Substituting these values in Eqn.(A.42) we obtain,

$$\overline{M'N''} \approx \overline{MN} \approx \frac{r_1 + r_2}{\sqrt{1 + \left(\frac{r_1 + r_2}{\lambda}\right)\tan^2 \psi}} \tag{A.13}$$

$$Znr = \frac{\overline{MN}}{Radius\_Plain} \tag{A.14}$$

$$Znra = \frac{\sqrt{\dfrac{r_1 \cdot r_2 \cdot \lambda}{r_1 + r_2}}}{Radius\_Plain} \tag{A.15}$$

where $Radius\_Plain$ is existing longitudinal reflection area and value of it is calculated in $Specular(\ )$ procedure. Then the Ratio of lateral extension of the specular reflection point to the radius plain length is expressed as:

$$Wr = \begin{cases} 1 & \text{Znr} \le 1 \\ 1/Znr & \text{Znr} > 1 \end{cases} \tag{A.16}$$

and the ratio of longitudinal extension of the specular reflection point to the radius plain length is expressed as:

$$Wra = \begin{cases} 1 & \text{Znra} \le 1 \\ 1/Znra & \text{Znra} > 1 \end{cases} \tag{A.17}$$

A.3 Calculation of Reflection Coefficient

- Reflection coefficient at the specular reflection point is expressed as $\Gamma = \rho e^{j\theta}$ and

can be calculated from the following formulas:

For vertical polarization:

$$\Gamma_v = \frac{\varepsilon_c \sin\psi - \sqrt{\varepsilon_c - \cos^2\psi}}{\varepsilon_c \sin\psi + \sqrt{\varepsilon_c - \cos^2\psi}} = \rho e^{j\theta} \tag{A.18}$$

For horizontal polarization:

$$\Gamma_h = \frac{\sin\psi - \sqrt{\varepsilon_c - \cos^2\psi}}{\sin\psi + \sqrt{\varepsilon_c - \cos^2\psi}} = \rho e^{j\theta} \tag{A.19}$$

The complex relative dielectric constant ε_c is defined by

$$\varepsilon_c = \varepsilon - j60\sigma\lambda = \varepsilon - j\frac{18\sigma_{mho/m}}{f_{GHz}} \tag{A.20}$$

where ε is the relative dielectric constant, σ is the conductivity in $mhos/m$ (or $Siemens/m$) and λ is the wavelength in meters.

When the incident wave is circularly polarized having an E field

$$\vec{E}_i = \hat{h} - j\hat{v}_i \quad \text{(L.H.C.P.)} \tag{A.21}$$

as shown in Fig.A.10., the reflected wave can be expressed by:

$$\vec{E}_r = \Gamma_h \hat{h} - j\Gamma_v \hat{v}_r \quad \text{elliptically polarized} \tag{A.22}$$

$$\vec{E}_r = \underbrace{\frac{1}{2}(\Gamma_h + \Gamma_v)\hat{h} - j\frac{1}{2}(\Gamma_h + \Gamma_v)\hat{v}_r}_{\substack{\text{L.H.C.P.} \\ \text{Cross-Polar component}}} + \underbrace{\frac{1}{2}(\Gamma_h - \Gamma_v)\hat{h} + j\frac{1}{2}(\Gamma_h - \Gamma_v)\hat{v}_r}_{\substack{\text{R.H.C.P.} \\ \text{Co-Polar component}}} \tag{A.23}$$

What we need for circular polarization is:

$$\Gamma_c = \frac{(L.H.C.P.)_r}{(L.H.C.P.)_i} = \frac{1}{2}(\Gamma_h - \Gamma_v) \tag{A.24}$$

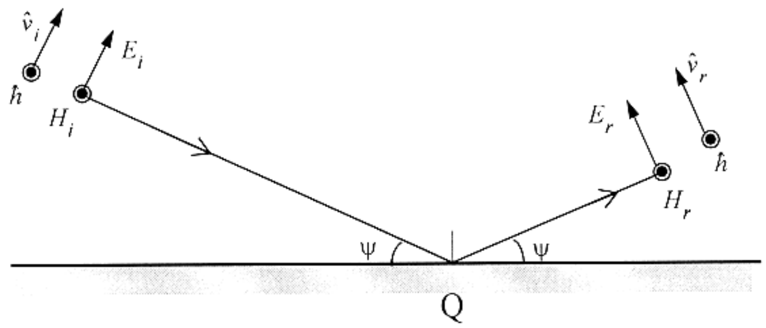

Figure A.10. Circularly Polarized E-Field Reflection

- Rough surface specular reflection coefficient ρ_s should be taken into account if there is diffusion of the specularly reflected wave due to the surface roughness. For example rough sea surface or rough ground causes the reflected wave to be decreased due to the scattering effects. A surface is optically rough if the height of the surface roughness is comparable with wavelength. This is expressed in so-called Rayleigh's criteria. Referring to Fig.A.11., the rays I and II will be out of phase by the amount

$$\Delta\varphi = \frac{2\pi}{\lambda}\overline{BAC} = \frac{2\pi}{\lambda}2h\sin\psi = \frac{4\pi h}{\lambda}\sin\psi \tag{A.25}$$

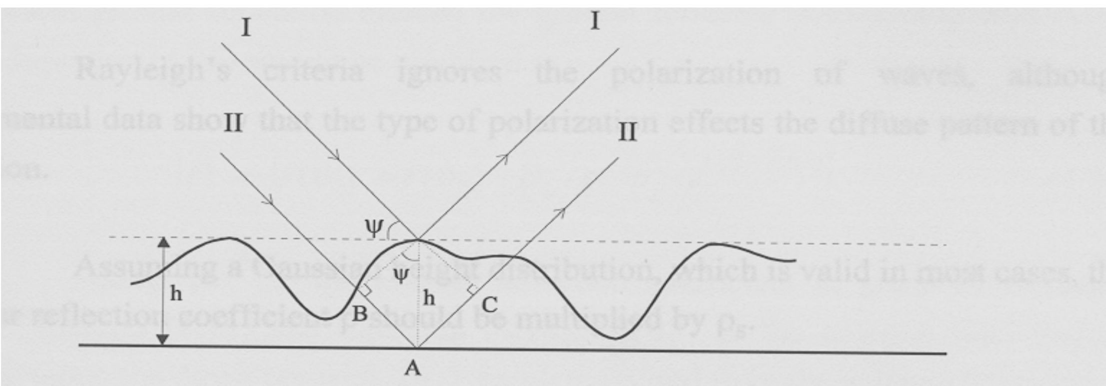

Figure A.11. Obtaining the Rayleigh's Criteria for Specular Reflection

If $\Delta\varphi < \pi/2$, then the reflection may be considered specular, otherwise diffuse. In other words, the sum of the fields of rays I and II will tend to cancel for $\Delta\varphi > \pi/2$. Thus, a surface may be considered as smooth if

$$\frac{4\pi h}{\lambda}\sin\psi < \pi/2 \tag{A.26}$$

The above equation can be expressed in a more meaningful way as:

$$h > h_R = \frac{\lambda}{8\sin\psi} \tag{A.27}$$

which is the Rayleigh's criteria. Rayleigh's criteria ignores the polarization of waves, although experimental data show that the type of polarization effects the diffuse pattern of the reflection.

Assuming a Gaussian height distribution, which is valid in most cases, the specular reflection coefficient p should be multiplied by ρ_s.

$$\Gamma = \rho e^{j\theta} \rightarrow \rho \cdot \rho_s \cdot e^{j\theta} \tag{A.28}$$

ρ_s takes account the surface roughness.

$$\rho_s = \exp\left[-2\left(\frac{2\pi\sigma_h \sin\psi}{\lambda}\right)^2\right] \quad \text{Ament's Formula} \tag{A.29}$$

where ψ is the grazing angle at the reflection point for a smooth surface of mean height $\bar{h}$; and σ_h is the standard deviation of h from $\bar{h}$.

Vegetation reflection coefficient, ρ_v, should be considered when surface of the ground is covered by vegetation. It can be expressed by Eqn.A.30.

$$\rho_v = \exp\left(-Veg\_c \cdot \frac{\sin\psi}{\lambda}\right) \tag{A.30}$$

where Veg_c is vegetation reflection coefficient and ψ is the grazing angle.

A.4 Phase Correction Terms

- Phase Correction for RAY-3

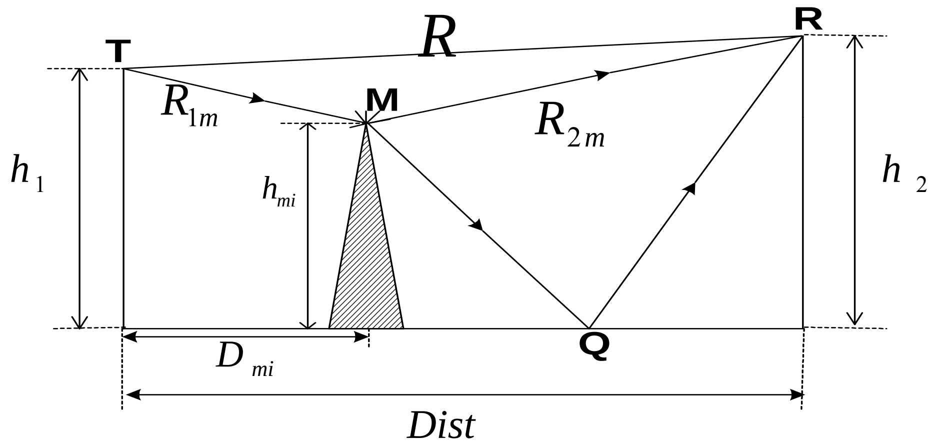

Figure A.12 Geometry for Phase Correction of RAY-3

From the Fig.A.12 path phase of RAY-4 with respect to direct ray path is

$$-k\left(\overline{TM} + \overline{MQ} + \overline{QR} - \overline{TR}\right) \tag{A.31}$$

and specular reflection path phase is considered as

$$-k\left(\overline{MQ} + \overline{QR} - \overline{MR}\right) \tag{A.32}$$

Thus we need to add a phase correlation

$$\Phi_3 = -k\left(\overline{TM} - \overline{TR}\right) - k\overline{MR} = -k\left(\overline{TM} + \overline{MR} - \overline{TR}\right) \tag{A.33}$$

$$\Phi_3 = -k\left(R_{1m} + R_{2m} - R\right) \tag{A.34}$$

- Phase Correction for RAY-4

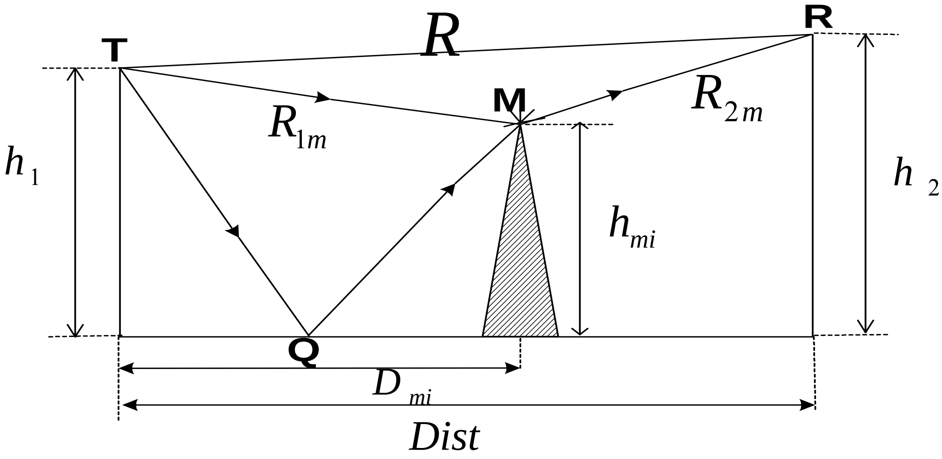

Figure A.13 Geometry for Phase Correction of RAY-4

From the Fig.A.13 path phase of RAY-4 with respect to direct ray path is

$$-k\left(\overline{TQ}+\overline{QM}+\overline{MR}-\overline{TR}\right) \tag{A.35}$$

and specular reflection path phase is considered as

$$-k\left(\overline{TQ}+\overline{QM}-\overline{TM}\right) \tag{A.36}$$

Thus we need to add a phase correlation

$$\Phi_4=-k\left(\overline{MR}-\overline{TR}\right)-k\overline{TM}=-k\left(\overline{MR}+\overline{TM}-\overline{TR}\right) \tag{A.37}$$

$$\Phi_4=-k\left(R_{1m}+R_{2m}-R\right) \tag{A.38}$$

- Phase Correction for RAY-5

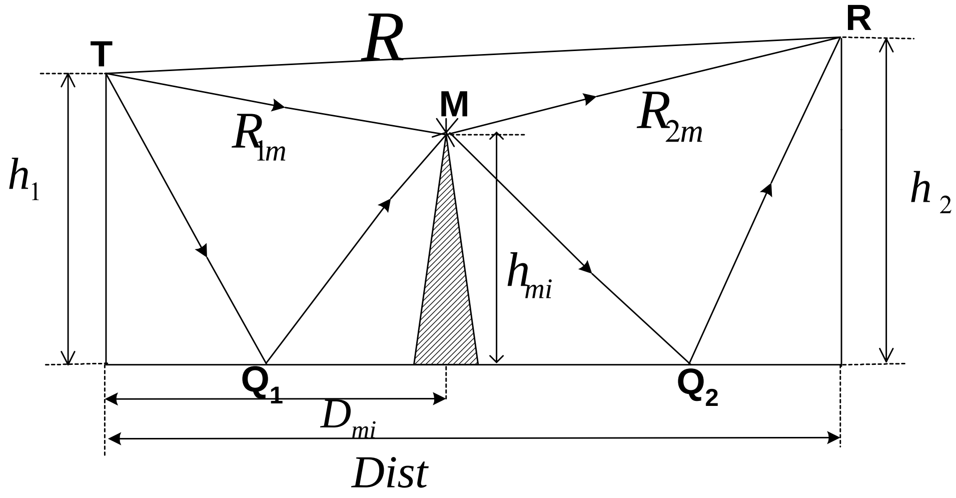

Figure A.14 Geometry for Phase Correction of RAY-5

From the Fig.A.14 path phase of RAY-5 with respect to direct ray path is

$$-k\left(\overline{TQ_1}+\overline{Q_1M}+\overline{MQ_2}+\overline{Q_2R}-\overline{TR}\right) \tag{A.39}$$

and specular reflection path phase is considered as

$$-k\left(\overline{TQ_1}+\overline{Q_1M}-\overline{TM}+\overline{MQ_2}+\overline{Q_2R}-\overline{MR}\right) \tag{A.40}$$

Thus we need to add a phase correlation

$$\Phi_5=-k\left(-\overline{TR}\right)-k\overline{TM}-k\overline{MR}=-k\left(\overline{TM}+\overline{MR}-\overline{TR}\right) \tag{A.41}$$

$$\Phi_5=-k\left(R_{1m}+R_{2m}-R\right) \tag{A.42}$$

As a result phase correction term for RAY-3, RAY-4 and RAY-5 are same and can be expressed as follow.

$$P_{cor}=-\left(2\cdot\frac{\pi}{\lambda}\right)\cdot\left(R_{1m}+R_{2m}-R\right) \tag{A.43}$$

$$R_{1m} = \sqrt{(a_e + h_1)^2 + (a_e + h_{mi})^2 - 2 \cdot (a_e + h_1) \cdot (a_e + h_{mi}) \cdot \cos\left(\frac{D_{mi}}{a_e}\right)} \quad \text{(A.44)}$$

$$R_{2m} = \sqrt{(a_e + h_2)^2 + (a_e + h_{mi})^2 - 2 \cdot (a_e + h_2) \cdot (a_e + h_{mi}) \cdot \cos\left(\frac{Dist - D_{mi}}{a_e}\right)} \quad \text{(A.45)}$$